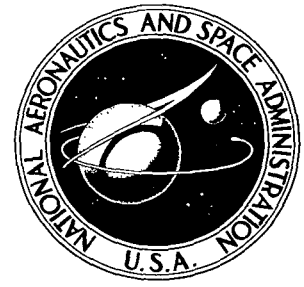

SHOCK WAVES IN AN ANISOTROPIC PLASMA

by F. M. Neubauer

Braunschweig Technical University
Braunschweig, 1969

NATIONAL AERONAUTICS AND SPACE ADMINISTRATION • WASHINGTON, D. C. • JUNE 1972

NASA TT F-709

SHOCK WAVES IN AN ANISOTROPIC PLASMA

By F. M. Neubauer

Translation of "Stosswellen in einem anisotropen Plasma." Doctoral Dissertation, Braunschweig Technical University, Braunschweig, March 1969

NATIONAL AERONAUTICS AND SPACE ADMINISTRATION

For sale by the National Technical Information Service, Springfield, Virginia 22151
$3.00

This dissertation was prepared at the Geophysics and Meteorology Institute of Braunschweig Technical University.

The author is obliged to Professor Dr. W. Kertz for the opportunity of implementing these studies at his institute.

The numerical evaluation of the jump functions for Figures 10 through 23 was made at the Computer Center of Braunschweig Technical University and at the German Computer Center in Darmstadt, Germany. The author is obliged to Dr. Siemann for preparing the plotting program.

TABLE OF CONTENTS

Page

1. Introduction

/5*

The plan to prepare this paper evolved from a paper presented at the Pioneer 6 Symposium in Washington [Wolfe et al., 1966], and a paper presented at the Inter-Union Symposium on Solar-Terrestrial Physics in Belgrade in 1966 [Hundhausen et al., 1966]. These papers reported on observations of solar wind plasma by the Pioneer 6 space probes and by the satellites of the Vela 3 series. One important result of these experiments was the observation that the distribution functions of the solar wind ions, primarily protons, are anisotropic. The Vela 3 observations yielded data for T_{max}/T_{mean} ranging from 1.0 to more than 2.5, with a frequency maximum near 1.4. The significance of the temperature in this ratio will become evident immediately if we consider the definition which states that the temperature in a certain direction is determined by the variance of the velocities of all the particles moving in this direction in the reference system of mean particle velocity. The Pioneer measurements yielded even greater values of anisotropy. Moreover, it was observed that the direction of maximum temperature agrees with the direction of the magnetic field [Hundhausen et al., 1967]. More recent measurements made with the aid of the Vela 4 satellites have shown that the electrons, too, show some anisotropy, although to a lesser degree [Montgomery et al., 1968]. However, according to personal information received from J. Wolfe, these results indicating electron anisotropy must be considered with some degree of caution because of the experimental difficulties involved in their acquisition. Additional information on measured parameters and solar wind magnitudes close to the earth's orbit that were computed from them, is presented in Tables 1 and 2. Here it applies that

$$\hat{s}_0 = \frac{5}{6} \frac{1/2\ (P_{\parallel} + P_{\perp})}{\text{magnetic field pressure}}$$

where $P_{\parallel}$ and $P_{\perp}$ represent the parallel and the vertical component of total pressure. /6 Parker's solar wind theory was used to compute the curves plotted in Figure 1. The solid curves were based on a stipulated corona temperature of 10^6°K = T_{ion} = $T_{electron}$ and a stipulated polytropic index of $\alpha = 1$, that is, a constant temperature. In addition, we find a dotted curve $\hat{s}_0$ which corresponds to $T \sim n^{0.1}$, that is, $\alpha = 1.1$, where n is the ion number density. The other

---

* Numbers in the margin indicate pagination in the foreign text.

magnitudes hardly deviate from the values for T = const, provided that the distance of the sun is not too great. In the case where α = 1.1, the corona temperature was selected so that a value of $T_{electron} = T_{ion} = 10^6$°K will result in proximity of the earth. Since Parker's theory requires only the sum of $T_{electron} + T_{ion}$ the temperatures of, for instance, T_{ion} = 500,000°K and $T_{electron} = 1.5 \times 10^6$°K in the vicinity of earth will correspond to this corona temperature. The curves provide a first impression of the mean profile of these magnitudes that must be expected.

The solar wind plasma is the medium in which the perturbations propagate which frequently produce magnetic storms on earth after solar flares. Since our present-day concepts state that the propagation of these perturbations is associated with the formation of shock waves, the observations of plasma anisotropy which were mentioned above will immediately pose the question as to the type of changes in the well-known shock waves in isotropic plasma that will result from anisotropy. MHD shock waves of isotropic pressure were first treated in theory by de Hoffmann and Teller [1950]. Later, it was primarily two problem areas that became the subject of investigation. The first of these involved the problem of the behavior of the characteristics of the plasma and of the magnetic field behind the shock wave as a function of one shock wave intensity parameter such as the shock wave velocity, referred to the nonperturbed medium, or as a function of the change of the magnetic field across the shock wave, when the corresponding magnitudes in the area in front of the shock wave are known, that is, in the nonperturbed medium. Moreover, the problem as to the stability of the /10
shock waves has been investigated. The second problem area includes all the questions as to the structure of the shock wave, that is, to the functions which describe the spatial dependence of the physical magnitudes during the transition from the area in front of the shock wave to the area behind the shock wave. The treatment of this second problem area is much more difficult than that of the first, and it is far from being resolved, while the first-named problem area can be considered completed in its major aspects. The most important papers on the interdependence of the plasma states on either side of the shock wave include the paper by de Hoffmann and Teller [1950], a paper by Helfer [1953], Lüst [1955], and Bazer and Ericson [1958]. The problem of the stability of the shock waves

waves has been solved by Russian authors. A summary is found in the paper by Anderson [1963].

TABLE 1. COMPILATION OF SOME CHARACTERISTICS OF THE INTERPLANETARY MEDIUM, ACCORDING TO NESS [1967]. THESE DATA ORIGINATED FROM OBSERVATIONS MADE IN THE VICINITY OF THE EARTH ORBIT DURING THE PERIOD FROM 1962 THROUGH 1966. /7

	Minimum	Maximum	Mean
Velocity, km/sec	280	900	400 to 500
Flux direction	±10°		-1.5° against the solar radius vector (+ indicates an originating direction west of the sun's center)
Numerical ion density, cm^{-3}	0.4	80	5
Helium concentration in percent of proton concentration	0	15	4
Proton temperature, °K	6×10^3	1×10^6	2×10^5
Ion anisotropy T_{max}/T_{mean}	1.0	25	1.4
Magnitude of the magnetic field, $\gamma(1\gamma = 10^{-5}$Oe)	0.25	40	6
Magnetic field direction	in the ecliptic, with frequency maxima near 135° or 315° against the sun's radius vector		
Alfvén velocity, km/sec	30	150	60

TABLE 2. PLASMA DATA FOR SELECTED INTERVALS DURING MARCH AND APRIL, 1967, ACCORDING TO MONTGOMERY ET AL. [1968]

/8

Electron temperature, °K	7×10^4	to	2×10^5 °K
Electron anisotropy, T_{max}/T_{mean}	1.1	to	1.2
Ratio of electron temperature to mean proton temperature	1.5	to	5
Proton anisotropy	1.0	to	5 (!)
Velocity, km/sec	400		
Numerical proton density, cm^{-3}	4	to	10
$\hat{s}_0$ with $\|\underline{H}\| = 6\ \gamma$	0.9	to	1.5

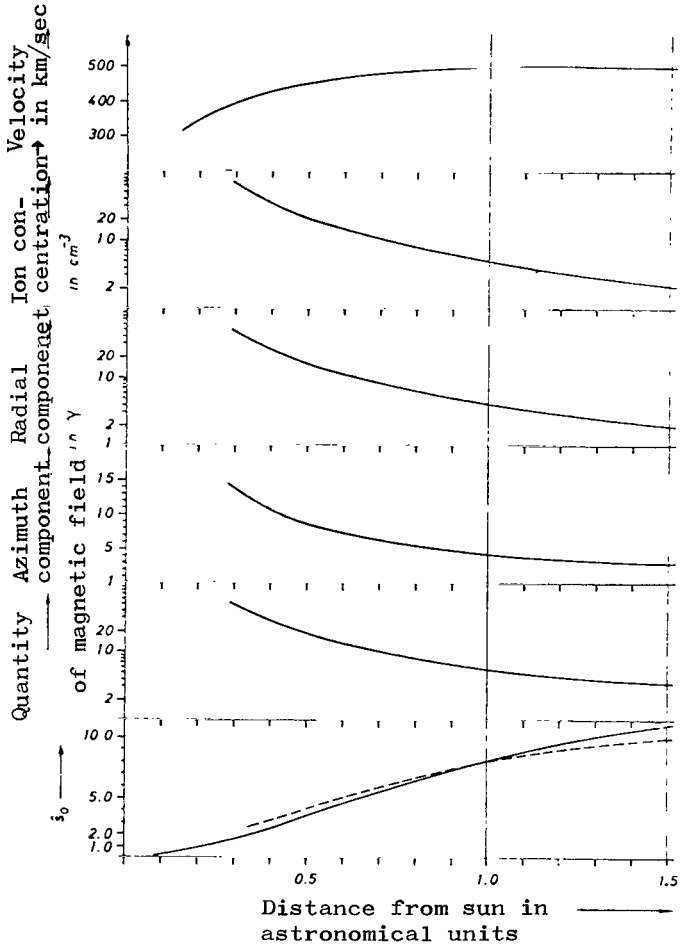

Figure 1. Some important solar wind parameters, according to Parker's theory. The solid lines correspond to the polytropic index α = 1, the dotted lines to α = 1.1.

This paper does not propose to deal with the stability problem in conjunction with shock waves in an anisotropic plasma. Only the relationships existing between the magnitudes on either side of the shock wave shall be derived. The denotations and the classification system of possible solutions represent an expansion of the paper by Bazer and Ericson [1958] which includes a very clearly stated classification system acquired exclusively via analytic methods. Consequently, this paper will be structured as follows. /10

The step functions for the discontinuities under consideration shall be derived in Chapter 2, starting out from the basic equations of kinetic plasma theory stated by Dupree [1963]. The justification of the stipulations made for this purpose shall be discussed, including comparison with other authors. Moreover, the H-theorem shall be used to introduce a generalized entropy condition, and some consequences shall be discussed briefly. The step functions shall be discussed and classified with respect to their dependence on several shock wave parameters in Chapter 3. Finally, a summary of the results shall be provided, discussing the possibilities for testing the theory. /11

2. Derivation of the Shock Relationships /12

2.1. Derivation of the Basic Equations

2.1.1. Klimontovich-Dupree Formulas

We shall start out by deriving the basic plasma equations. After several intermediate steps these will yield the basis for the computation of the shock wave jump functions in Section 2.5. First, we stipulate that we shall use the electromagnetic dimensional system. Moreover, a nonrelativistic calculation procedure shall be used.

Let us stipulate a completely ionized plasma consisting of M_μ particles of type μ. Under certain initial conditions, let the trajectory of the particle numbered i in the hexadimensional space $\underline{x}$, $\underline{v}$, be described by the position vector $\underline{x}_{\mu,i}(t)$ and by the velocity vector $\underline{v}_{\mu,i}(t)$. In that case, we will obtain the following for the particle densities in the hexadimensional space $\underline{x}$, $\underline{v}$, according to Klimontovich [1957] and Dupree [1963]:

$$N_\mu = \sum_{i=1}^{M_\mu} \delta(\underline{x} - \underline{x}_{\mu,i}(t))\ \delta(\underline{v} - \underline{v}_{\mu,i}(t)) \qquad (1)$$

where $\mu = 1, 2, 3 \ldots$ number of particle types. Integration over the entire permissible space $\underline{x}$, $\underline{v}$ will yield

$$\int\int N_\mu\ d\underline{x}\ d\underline{v} = M_\mu$$

where $d\underline{x}$ is the volume element in position space, and $d\underline{v}$ in velocity space. Now the density N_μ satisfies the equation

$$\frac{\partial N_\mu}{\partial t} + \underline{v}\frac{\partial N_\mu}{\partial \underline{x}} + \frac{e_\mu}{m_\mu}(\tilde{\underline{E}} + \underline{v} \times \tilde{\underline{B}})\frac{\partial N_\mu}{\partial \underline{v}} = 0 \qquad (2a)$$

where e_μ and m_μ, successively, represent the charge and the mass of a particle of type μ. $\tilde{\underline{E}}$ is the electrical field vector and $\tilde{\underline{B}}$ the vector of magnetic induction which in this case is always equal to the vector of magnetic field strength, $\tilde{\underline{H}}$. The fields $\tilde{\underline{E}}$ and $\tilde{\underline{H}}$ satisfy the following equations: /13

$$\text{rot}\ \tilde{\underline{E}} = -\frac{\partial \tilde{\underline{H}}}{\partial t}$$

$$\text{rot}\ \tilde{\underline{H}} = 4\pi \sum_\mu e_\mu \int \underline{v} N_\mu\ d\underline{v} + \frac{1}{c^2}\frac{\partial \tilde{\underline{E}}}{\partial t} \qquad (2b)$$

$$\text{div}\ \tilde{\underline{E}} = 4\pi c^2 \sum_\mu e_\mu \int N_\mu\ d\underline{v}$$

$$\text{div}\ \tilde{\underline{H}} = 0$$

c = velocity of light in a vacuum

This equation system describes the behavior of the stipulated plasma. As a rule, its exact solution will be extremely difficult. However, in many cases, this solution will not be required because the objective in most cases is to compute merely statistical quantities from these solutions. Certain ensemble

means are such quantities. An ensemble in statistical mechanics is represented by a large number of similar systems. Similarity in this case means that all systems consisting of $\sum_\mu M_\mu$ particles have the same Hamiltonian. The ensemble is characterized at any point of time by the probability distribution of the $6\sum_\mu M_\mu$ position and velocity coordinates and of the electromagnetic field components at any point in space. This probability density is defined so that it will be compatible with the initial boundary conditions of the problem under consideration [Tolman, 1950, Chapter III]. We shall return to this point in Sections 2.2. and 2.4. /14

We shall now determine an equation system for the ensemble means $\langle\ \rangle$ of N_μ and $\tilde{\underline{E}}$, as well as $\tilde{\underline{H}}$. Using the definitions for the fluctuations $\delta N_\mu = N_\mu - \langle N_\mu \rangle$, $\delta \underline{E} = \tilde{\underline{E}} - \langle \tilde{\underline{E}} \rangle$, $\delta \underline{H} = \tilde{\underline{H}} - \langle \tilde{\underline{H}} \rangle$, and the definitions $\langle N_\mu \rangle = f_\mu$ for the single-particle distribution function of particle type μ, in addition to $\underline{E} = \langle \tilde{\underline{E}} \rangle$ and $\underline{H} = \langle \tilde{\underline{H}} \rangle$, we obtain the following by forming the ensemble mean of Eq. (2a):

$$\frac{\partial f_\mu}{\partial t} + \underline{v} \frac{\partial f_\mu}{\partial \underline{x}} + \frac{e_\mu}{m_\mu} (\underline{E} + \underline{v} \times \underline{H}) \frac{\partial f_\mu}{\partial \underline{v}} = \tag{3a}$$

$$= - \frac{e_\mu}{m_\mu} \left\langle \frac{\partial \delta N_\mu}{\partial \underline{v}} (\delta \underline{E} + \underline{v} \times \delta \underline{H}) \right\rangle = C_\mu$$

Since the Maxwellian equations are linear in N_μ, $\tilde{\underline{E}}$, and $\tilde{\underline{H}}$, it is merely necessary to replace N_μ by $\langle N_\mu \rangle = f_\mu$ and $\tilde{\underline{E}}$ by $\langle \tilde{\underline{E}} \rangle = \underline{E}$, and so on, after forming the ensemble mean:

$$\text{rot}\ \underline{E} = - \frac{\partial \underline{H}}{\partial t}$$

$$\text{rot}\ \underline{H} = 4\pi \sum_\mu e_\mu \int \underline{v} f_\mu \, d\underline{v} + \frac{1}{c^2} \frac{\partial \underline{E}}{\partial t} \tag{3b}$$

$$\text{div}\ \underline{E} = 4\pi c^2 \sum_\mu e_\mu \int f_\mu \, d\underline{v} \qquad /15$$

$$\text{div}\ \underline{H} = 0$$

As a rule, the equation system (3) will not be closed because of the term on the right-hand side of (3a), so that it will not be adequate to compute f_μ, $\underline{E}$ and $\underline{H}$. In fact, the equation system (3) is merely the first element in an infinite hierarchy of equations that are coupled to each other [Dupree, 1963].

Therefore, the transition from the equation system (2) to the mentioned hierarchy of equations will not usually yield any advantage. However, this hierarchy will become valuable if it can be closed, for instance, through development by the smallness parameter ε which is discontinued when a certain order is reached. Disregarding the term on the right-hand side of (3a) will lead to the Vlasov equation which, consequently, can be well distinguished from Eq. (2a).

We progress one step further when we derive the Balescu-Lenard equation where we allow only for Coulombian forces, stipulate homogeneity of the medium, and disregard correlations between three or more particles. Stipulating adiabatic conditions we will then obtain an expression for $-\frac{e_\mu}{m_\mu}\left\langle \frac{\partial \delta N_\mu}{\partial \underline{v}}\, \delta \underline{E} \right\rangle$ which is a functional of f_μ. The second component is small of higher order. Under certain prerequisites this correlation term will yield the Rosenbluth-MacDonald-Judd form [1957] which can also be obtained as a development of Boltzmann's shock integral. Henceforth, we shall use the general form of the term $-\frac{e_\mu}{m_\mu}\frac{\partial}{\partial \underline{v}}\left\langle \delta N_\mu \left(\delta \underline{E} + \underline{v} \times \delta \underline{H}\right)\right\rangle$ which was designated C_μ. We shall revert to the specific forms of the correlation term, or with reservations, of the shock term C_μ only in some exceptional instances.

2.1.2. Formation of Velocity Moments

The next step shall be to determine the continuity equation, the impulse equation, and the energy equation from Eqs. (3a) by forming the velocity moments via the usual procedure. First, we shall define as follows:

$$n_\mu = \int f_\mu \, d\underline{v} \qquad = \text{concentration of particle type } \mu$$

$$\rho_\mu = m_\mu n_\mu \qquad = \text{density} \qquad (4)$$

$$\underline{u}_\mu = \frac{1}{n_\mu} \int f_\mu \underline{v} \, d\underline{v} \qquad \underline{u} \text{ mass velocity}$$

$$\underline{\underline{P}}_\mu = m_\mu \int (\underline{v} - \underline{u}_\mu)(\underline{v} - \underline{u}_\mu)\, f_\mu \, d\underline{v} = \text{pressure tensor}$$

$$\hat{e}_\mu = \frac{1}{2 n_\mu} \int (\underline{v} - \underline{u}_\mu)^2 \, f_\mu \, d\underline{v} = \text{internal energy per unit mass}$$

$$\underline{q}_\mu = \frac{m_\mu}{2} \int (\underline{v} - \underline{u}_\mu)^2 (\underline{v} - \underline{u}_\mu) f_\mu \, d\underline{v} = \text{thermal flux vector}$$

Now, we integrate the Eq. (3a) over the velocity space, and using the relationship /17

$$(\underline{E} + \underline{v} \times \underline{H}) \frac{\partial f_\mu}{\partial \underline{v}} = \frac{\partial}{\partial \underline{v}} ((\underline{E} + \underline{v} \times \underline{H}) f_\mu) ,$$

obtain:

$$\int \frac{\partial f_\mu}{\partial t} \, d\underline{v} = \frac{\partial n_\mu}{\partial t}$$

$$\int \underline{v} \frac{\partial f_\mu}{\partial \underline{x}} \, d\underline{v} = \frac{\partial (n_\mu \underline{u}_\mu)}{\partial \underline{x}}$$

$$\int \frac{e_\mu}{m_\mu} \frac{\partial}{\partial \underline{v}} ((\underline{E} + \underline{v} \times \underline{H}) f_\mu) \, d\underline{v} = 0$$

$$-\int \frac{e_\mu}{m_\mu} \frac{\partial}{\partial \underline{v}} \langle (\delta \underline{E} + \underline{v} \times \delta \underline{H}) \delta N_\mu \rangle \, d\underline{v} = 0$$

and hence, the continuity equation

$$\frac{\partial n_\mu}{\partial t} + \frac{\partial (n_\mu \underline{u}_\mu)}{\partial \underline{x}} = 0 \qquad (5)$$

or

$$\frac{\partial \rho_\mu}{\partial t} + \frac{\partial (\rho_\mu \underline{u}_\mu)}{\partial \underline{x}} = 0$$

Multiplication of (3a) by $\underline{v}\, m_\mu$ and integration over the velocity space will yield

$$m_\mu \int v_\kappa \frac{\partial f_\mu}{\partial t} \, d\underline{v} = \frac{\partial (m_\mu n_\mu u_{\mu\kappa})}{\partial t}$$

$$m_\mu \int v_\kappa \left(\frac{\partial f_\mu}{\partial \underline{x}} \cdot \underline{v}\right) d\underline{v} = \frac{\partial P_{\mu,\kappa\ell}}{\partial x_\ell} + \frac{\partial (m_\mu n_\mu u_{\mu,\kappa} u_{\mu,\ell})}{\partial x_\ell}$$

/ 18

$$e_\mu \int v_\kappa \left((\underline{E} + \underline{v} \times \underline{H}) \frac{\partial f_\mu}{\partial \underline{v}} \right) d\underline{v} = - e_\mu n_\mu (\underline{E} + \underline{u}_\mu \times \underline{H})_\kappa$$

and

$$- e_\mu \int v_\kappa \left\langle (\delta \underline{E} + \underline{v} \times \delta \underline{H}) \frac{\partial \delta N_\mu}{\partial \underline{v}} \right\rangle d\underline{v} = e_\mu \langle \delta n_\mu (\delta \underline{E} + \delta \underline{u}_\mu \times \underline{H})_\kappa \rangle$$

$$= F_{\mu,\kappa}$$

This will result in the impulse equation for particle type μ:

$$\frac{\partial (\rho_\mu u_{\mu,\kappa})}{\partial t} + \frac{\partial}{\partial x_\ell} \left(P_{\mu,\kappa\ell} + \rho_\mu u_{\mu,\kappa} u_{\mu,\ell} \right) = e_\mu n_\mu (\underline{E} + \underline{u}_\mu \times \underline{H})_\kappa + F_{\mu,\kappa} \qquad (6)$$

Here we used component writing with summation convention for some of the vectors and tensors. The fluctuations δn_μ, $\delta \underline{U}_\mu$ etc. are obtained through replacement of f_μ by δN_μ in the definition equation system 4. The vector $\underline{F}_\mu$ represents a generalized friction force.

Finally, we must determine the energy equation. For this purpose we multiply by $\frac{m_\mu}{2} \underline{v}^2$ and integrate over the velocity space:

$$\frac{m_\mu}{2} \int v^2 \frac{\partial f_\mu}{\partial t} d\underline{v} = \frac{\partial}{\partial t} \left(\frac{\rho_\mu}{2} u_\mu^2 \right) + \frac{\partial (\hat{e}_\mu \rho_\mu)}{\partial t}$$

$$\frac{m_\mu}{2} \int v^2 \left(\underline{v} \cdot \frac{\partial f_\mu}{\partial \underline{x}} \right) d\underline{v} = \frac{\partial}{\partial \underline{x}} \left(\underline{u}_\mu \left(\frac{\rho_\mu u_\mu^2}{2} + \hat{e}_\mu \rho_\mu \right) + \underline{q}_\mu + \underline{u}_\mu \cdot \underline{\underline{P}}_\mu \right)$$

/ 19

$$\frac{e_\mu}{2} \int \left((\underline{v} \times \underline{H}) \frac{\partial f_\mu}{\partial \underline{v}} \right) v^2 \, d\underline{v} = 0$$

$$\frac{e_\mu}{2}\int\left(\underline{E}\cdot\frac{\partial f_\mu}{\partial \underline{v}}\right)v^2\,d\underline{v} = -\,(\underline{u}_\mu\cdot\underline{E})\,n_\mu\,e_\mu$$

$$-\frac{e_\mu}{2}\int\langle(\delta\underline{E}+\underline{v}\times\delta\underline{H})\frac{\partial\,\delta N_\mu}{\partial\underline{v}}\rangle\,v^2\,d\underline{v} = +\,e_\mu\langle\delta n_\mu(\delta\underline{u}_\mu\cdot\delta\underline{E})\rangle = \varepsilon_\mu$$

We obtain the following:

$$\frac{\partial}{\partial t}\left(\frac{1}{2}\rho_\mu\,u_\mu^2+\hat{e}_\mu\,\rho_\mu\right)$$

$$+\frac{\partial}{\partial x}\left(u_\mu\,\rho_\mu\left(\frac{1}{2}u_\mu^2+\hat{e}_\mu\right)+\underline{u}_\mu\cdot\underline{\underline{P}}_\mu+\underline{q}_\mu\right)-e_\mu n_\mu(\underline{u}_\mu\cdot\underline{E})=\varepsilon_\mu \qquad (7)$$

Eqs. 5, 6, 7, and 3b are used in the next section where they serve as the basis for the derivation of the conservation equations for the shock wave transition.

2.2. Derivation of the Conservation Equations

/20

2.2.1. Introduction

The conservation equations for the shock wave transition shall be derived in this sub-section. Although this paper is concerned primarily with shock waves, we shall use these conservation equations for completeness in order to acquire statements on contact discontinuities and rotational discontinuities as well. A precise definition of these concepts shall be given later on. First we must clarify some problems with respect to the shock wave model under consideration. Shock waves, rotational discontinuities, and contact discontinuities arising in problems of gas dynamics, magnetohydrodynamics, and plasma dynamics represent areas of extremely great spatial gradients. Let L_s be the thickness of one shock wave transition and L the characteristic length for the remainder of the space: in that case, it will apply frequently that $L_s \ll L$. In conjunction with the further condition that the curvature of the shock front be $\ll 1/L_s$, we derive from this circumstance the justification for treating the investigation of the structure and of other characteristics of shock waves as a one-dimensional problem where only a segment is taken into consideration. Consequently, we allow only for the spatial variations located perpendicularly to the shock front.

Moreover, we assume the existence of a reference system B_s and, at rest within it, coordinate system K_s within which the shock wave is stationary. In the coordinate system K_s so defined the shock wave represents the area where the transition takes place from the medium on the one side of the shock front to the medium on the other side of the shock front. Beyond this area all the gradients will disappear in this model.

The one-dimensional configuration described above can be realized exactly in the classical case of shock waves in gas dynamics, but also in the case of magnetohydrodynamic shock waves where particle collisions are the predominant effect. We simply consider the uniform motion into the homogeneous propagation medium of a suitable selected, infinitely extended piston. In that case there /21 will be thermodynamic equilibrium on both sides at an adequate distance from the shock front, and all three gradients will disappear.

However, in our case we are dealing with shock waves that propagate in a generally anisotropic plasma. Such a plasma will not be in thermodynamic equilibrium, and it will not be possible to satisfy the stipulation $\frac{\partial}{\partial x} = \frac{\partial}{\partial y} = \frac{\partial}{\partial z} = 0$ and $\frac{\partial}{\partial t} = 0$ at some distance from the shock front. Shocks and plasma instabilities will tend to establish isotropy of the plasma. Anisotropy-producing phenomena can counteract these processes.

Let us consider the solar wind as an example. We have a plasma that is outflowing from the sun, expanding in the process, where the mass velocity varies only little from a point of about 0.2 to 0.4 astronomical units (cf. Figure 1). According to Parker's model of the interplanetary magnetic field [Parker, 1963], the strength of the magnetic field $|\underline{H}|$ initially decreases at a rate of $1/r^2$, and at the rate of $1/r$ at greater distance from the sun. If there were no collisions and instabilities the temperature in the direction parallel to the magnetic field would remain constant and the temperature perpendicular to the magnetic field would decrease in proportion to $|\underline{H}|$ with increasing distance from the sun, in accordance with the conservation of the first adiabatic invariant [Parker, 1963]. In reality, however, this process is opposed by collisions and instabilities which limit the anisotropy. Here the inhomogeneity of the medium is required to generate and maintain the anisotropy. This inhomogeneity of the medium can be expressed by a characteristic length $L \approx 1$ astronomical unit of

the solar wind, which is much greater than the length scale L_s of a shock wave which shall be discussed later on. Although this inhomogeneity is important as such, we can disregard it provided that we also disregard the anisotropy- / 22
destroying processes in the non-perturbed solar wind as being of a higher order. More exactly speaking, Scarf et al. [1967] stated that these are instable, low-frequency "whistler" waves whose amplitude will not involve any significant perturbation of the physical magnitudes of solar wind.

We deduce from this brief discussion that shock waves in an anisotropic plasma in general are collsion-free shock waves, that is shock waves where simple Coulombian two-body collisions play a subordinate role. For these

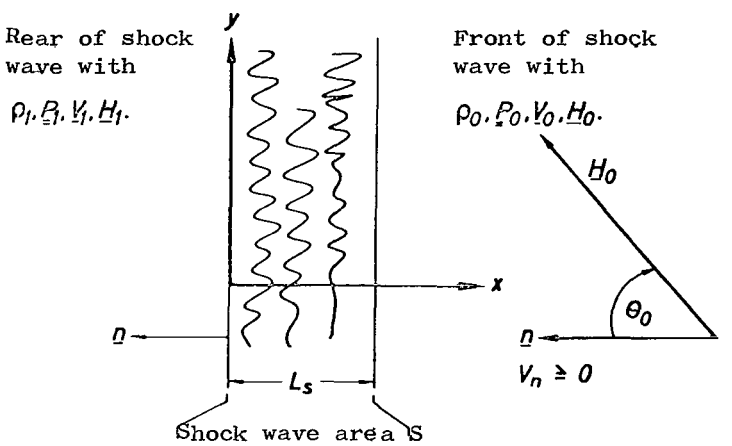

Figure 2. Sketch to orient the coordinate system K_0 within the reference system B_0 and to establish some frequently used denotations.

types of shock waves the assumption of a coordinate system K_s with $\frac{\partial}{\partial t} = 0$ for every point will be too restrictive, since non-steady state processes play an important role in considerations with respect to structure of these phenomena. We shall discuss this problem in some more detail later on. Here we shall make / 23
the much less restrictive assumption that a reference system B_0 exists,

with a coordinate system K_0 at rest within it, as shown in Figure 2, where it applies outside an adequately wide interval that $(0, L_s)$ $\frac{\partial}{\partial x} = \frac{\partial}{\partial y} = \frac{\partial}{\partial z} = 0$ and $\frac{\partial}{\partial t} = 0$ and where, moreover, we can assume the validity of Vlasov's equation. The statistical characteristics of the turbulence which must be expected within $(0, L_s)$ should not be dependent on y, z, and t. Up to this point we have not made a statement as to the statistical ensemble over which the mean is taken. This question is important with respect to a comparison with observations. We can use the statements just made in order to define an ensemble $\mathcal{E}$. Any realization of our problem, expressed by the functions N_μ $(\underline{x}, \underline{v}, t)$ and $\underline{\tilde{E}}(\underline{x}, t)$, as well as $\underline{\tilde{H}}(\underline{x}, t)$, shall belong to the ensemble $\mathcal{E}$, provided that it satisfies the following conditions.

Let a fictitious plasma analyzer located in the half-space $x > L_s$, that is on the front side of the shock wave, measure the same particle flux energy spectrum within a certain boundary about the spectrum resulting from the given f_μ, for any particle type, for any orientation of the normal of the inlet aperture located at any point, and for any initial point of time of the measuring cycle. Let the width of the boundary about the value in question decrease with increasing measuring time t, in accordance with the increasing statistical accuracy. In other words, as the measuring time increases, the measured distribution functions should be grouped ever more closely about the given distribution function which in the case of $x > L_s$ is not dependent on x, y, z, and t. Moreover, it is advantageous to suppose that the number of energy levels of the fictitious plasma analyzer increases with increasing measuring time $\tilde{t}$ so that the accuracy of the mean of the measured distribution function increases with increasing $\tilde{t}$. In addition, let the mean magnetic field vector which is measured by a fictitious magnetometer at any location where $x > L_s$ and for any position of the time interval /24
$(t, t + \tilde{t})$ converge on the given vector $\underline{H}_0$ as $\tilde{t}$ increases.

Second, homogeneity and steady state shall exist in the same sense behind the shock wave where $x < 0$ (cf. Figure 2). However, here the distribution functions f_μ and $\underline{H}_1$ shall not be prescribed.

Third, let the fluctuations of the ensemble $\mathcal{E}$ outside of $(0, L_s)$ be so small that they cannot cause changes of f_μ whose length is greater than $\geq L$ and

their contributions to pressure, energy flux and energy density are so small that they can be disregarded. All of these conditions should apply only to terms up to order L_s/L. Since any realization of the shock wave problem which satisfies the conditions explained above will be part of $\mathcal{E}$, we can see immediately that the ensemble means of ensemble $\mathcal{E}$ cannot be dependent on y, z, and t. Any realization which is part of $\mathcal{E}$ can be used to construct a new permissible realization by means of random displacement in the y and z direction or along the time axis.

The deviations from the ensemble means, that is, fluctuations of the ensemble $\mathcal{E}$, incorporate all the time variations and spatial variations in the y and z directions such as, for instance, standing waves, turbulence, and the like, and especially those fluctuations that result from the discrete character of matter. The latter fluctuation component can be separated from the other components by using another ensemble $\mathcal{E}_1$ which is a genuine fraction of ensemble $\mathcal{E}$ and is so defined that the fluctuations incorporate as few variations with t, y, and z as possible and that the ensemble means still represent smooth functions. Here the fluctuations include primarily the contributions of the discrete character of matter. The ensemble means depend not only on x but usually also on y, z, and t.

Since the statistical characteristics of the realization of the shock wave transition do not depend on y, z, and t, it applies that $\overline{\langle N_\mu, \tilde{E}, \tilde{H} \rangle_\mathcal{E}} = \langle N_\mu, \tilde{E}, \tilde{H} \rangle_\mathcal{E}$ where the crossbar indicates that a mean is taken over y, z, and t. Outside of $(0, L_s)$ it applies, of course, that $f_{\mu, \mathcal{E}_1} = f_{\mu, \mathcal{E}}$, $\langle \tilde{E} \rangle_{\mathcal{E}_1} = \langle \tilde{E} \rangle_\mathcal{E}$ and $\langle \tilde{H} \rangle_{\mathcal{E}_1} = \langle \tilde{H} \rangle_\mathcal{E}$. The physical magnitudes used below are based on ensemble means of $\mathcal{E}_1$, unless a deviation from this stipulation is expressly stated. /25

2.2.2. Taking the Means and Integrating Over the Basic Equations

The conservation equations for the shock wave transition or simply the shock wave relationships are now obtained with the aid of Eqs. (3b) and (5), (6), and (7). Some additional denotations are required for this purpose:

$$\rho = \sum_{\mu} \rho_{\mu} \quad = \text{total mass density}$$

$$\underline{u} = \frac{1}{\rho} \sum_{\mu} \rho_{\mu} \underline{u}_{\mu} \quad = \text{total mass velocity} \qquad (8)$$

$$\underline{\underline{P}} = \sum_{\mu} \underline{\underline{P}}_{\mu} \quad = \text{total pressure tensor}$$

$$\underline{q} = \sum_{\mu} \underline{q}_{\mu} \quad = \text{total thermal flux vector}$$

$$\rho \hat{e} = \sum_{\mu} \hat{e}_{\mu} \rho_{\mu} \quad = \text{internal energy per unit of volume}$$

/26

$$T_{k\ell} = \frac{1}{4\pi} \left(H_k H_\ell + \frac{E_k E_\ell}{c^2} \right) - \frac{1}{8\pi} \left(\underline{H}^2 + \frac{\underline{E}^2}{c^2} \right) \delta_{k\ell}$$

= Maxwellian stress tensor

$$\hat{\eta} = \sum_{\mu} n_{\mu} e_{\mu} \quad = \text{charge density}$$

$$\underline{j} = \sum_{\mu} e_{\mu} n_{\mu} \underline{u}_{\mu} \quad = \text{flux density}$$

$$\underline{S} = \frac{1}{4\pi} \left(\underline{E} \times \underline{H} \right) \quad = \text{Poynting vector}$$

In any desired reference system we define

$\underline{u}_0 = \underline{u}$ front side
$\underline{u}_1 = \underline{u}$ rear

The following definitions apply in the specific reference system B_0:

$$\underline{u}_0 = \underline{V}_0$$
$$\underline{u}_1 = \underline{V}_1$$

Moreover, in order to characterize any desired point outside the shock wave area within the system K_0, we introduce x_0 and x_1, where $x_0 > L_s$ and $x_1 < 0$. We integrate the Eq. (5) from + x_1 through x_0 over x, and take the mean over y, z and t. / 27

$$\overline{\int_{x_1}^{x_0} \frac{\partial \rho_\mu}{\partial t}\, dx = 0}$$

$$\overline{\int_{x_1}^{x_0} \frac{\partial (\rho_\mu u_{\mu,y})}{\partial y}\, dx = 0} \qquad (9)$$

$$\overline{\int_{x_1}^{x_0} \frac{\partial (\rho_\mu u_{\mu,z})}{\partial z}\, dx = 0}$$

$$\overline{\int_{x_1}^{x_0} \frac{\partial (\rho_\mu u_{\mu,x})}{\partial x}\, dx = \rho_{\mu,0}\, u_{\mu x,0} - \rho_{\mu,1}\, u_{\mu x,1} = -[\rho_\mu u_{\mu x}]}$$

Here we exploited the fact that it applies outside the shock wave area S that $\frac{\partial}{\partial t} = 0$ and $\frac{\partial}{\partial y} = 0$, $\frac{\partial}{\partial z} = 0$, and that $\overline{\rho}_\mu = \rho_\mu$, and so on. Moreover, we define $[A] = A_1 - A_0$.

Now, what is the interrelationship existing outside the area S between the velocity vectors of the different particle types? Measurements in solar wind [Hundhausen et al. 1967; Neugebauer and Snyder, 1966] have shown that $\underline{u} \approx \underline{u}_\mu$ applies outside of S. It follows for a two-component plasma with $\mu = 1$ and 2 outside of S, due to the absence of any spatial and time derivatives, that

$$\operatorname{div} \underline{E} = 4\pi c^2 \hat{\eta}$$

and

$$\underline{j} = \frac{1}{4\pi} \operatorname{rot} \underline{H} - \frac{1}{4\pi c^2} \frac{\partial \underline{E}}{\partial t}$$
$$= 0$$

$$\hat{\eta} = e_1 n_1 + e_2 n_2 = 0 \qquad (28$$

and

$$\underline{j} = e_1 n_1 \underline{u}_1 + e_2 n_2 \underline{u}_2 = 0$$

and hence, strictly speaking, that

$$\underline{u}_1 = \underline{u}_2$$

However, the solar wind plasma represents a two-component plasma of electrons and protons only in approximation. The next frequently occurring ions are H_e^{++}-ions with a mean of $n_\alpha/n_p = 0.04$, although this value can rise as high as 0.15 (cf. Table 1). The cited data originate from measurements performed by the satellites of the Vela series [Hundhausen, Asbridge, Bame, Gilbert, and Strong, 1967; Ness, 1967].

In the case of a general multicomponent plasma, we can argue as follows. It follows from Eq. (6) for an homogeneous, steady-state Vlasov plasma where $C_\mu = 0$, and consequently, where $\underline{F}_\mu = 0$, that

$$\underline{E} + \underline{u}_\mu \times \underline{H} = 0 \qquad (10a)$$

This means that the component of $\underline{u}_\mu$ which is oriented perpendicularly with respect to $\underline{H}$ is equal to the drift velocity $\underline{u}_D = \underline{E} \times \underline{H}/\underline{H}^2$ for all μ

$$\underline{u}_{\mu\perp} = \underline{u}_D = \frac{\underline{E} \times \underline{H}}{\underline{H}^2} \qquad (10b)$$

Consequently, in a steady-state, homogeneous Vlasov plasma, the velocity differences can occur only in the direction of the magnetic field. They are further limited by the occurrence of instabilities of the dual-flux instability type. These are encountered when exceeding critical velocity differences between distributions that are displaced with respect to each other in the $\underline{v}$ space. In addition, $\underline{j} = 0$ and $\hat{\eta} = 0$ must be satisfied in this case. The instable waves can be purely electrostatic or ion acoustical waves, but also electromagnetic waves such as "whistler waves" or Alfvén waves. However, important processes occur even below the critical velocity difference. /29

For illustration, let us consider a plasma whose magnetic field can be disregarded. The ion acoustical waves encountered in the plasma are damped at velocity differences below the stability limit, but their damping is reduced

as we approach the critical velocity difference. This will result in an increase of the fluctuations $\delta\underline{E}$ and hence of the correlation terms C_μ which in this case can be described by the Balescu-Lenard equation. The fluctuations cause the destruction of anisotropy and of the velocity differences, since the terminal state described by the Balescu-Lenard equation is a state of thermodynamic equilibrium [Montgomery and Tidman, 1964, Section 7.2]. Therefore, due to the requirement that $L \gg L_s$ the plasma must have a sufficient distance from the stability limit. In other words, excessive proximity to the stability limit and maintaining the anisotropy of the plasma are incompatibilities. However, a paper by Joyce et al., [1967] has shown that the effect of the fluctuations $\delta\underline{E}$ will decrease rapidly when we move away from the stability limit in the direction of greater stability. Here it is insignificant for our consideration that Joyce et al. [1967] assumed a plasma in flux.

From now on we shall stipulate that, outside of S, all $\underline{u}_\mu$ are equal to $\underline{u}_\mu = \underline{V}$. In that case, it follows from Eq. (9) that

$$[\rho V_n] = 0 \qquad \angle 30$$

or that

$$\rho_0 V_{n,0} = \rho_1 V_{n,1} = M \qquad (11)$$

where $V_n = \underline{n} \cdot \underline{V}$ while M represents the mass flow through the area S.

Now we determine the impulse conservation equation. For this purpose, we summate the Eqs. (6) for all particle types and make use of the definitions 8. We find that

$$\frac{\partial}{\partial t}(\rho u_\kappa) + \frac{\partial}{\partial x_\ell}\left(P_{k\ell} + \sum_\mu \rho_\mu u_{\mu,\kappa}\, u_{\mu,\ell}\right)$$

$$= \sum_\mu e_\mu n_\mu (\underline{E} + \underline{u}_\mu \times \underline{H})_\kappa + \sum_\mu F_{\mu,\kappa}$$

Moreover, it applies

$$\sum_\mu e_\mu n_\mu (\underline{E} + \underline{u}_\mu \times \underline{H}) = \hat{\eta}\,\underline{E} + \underline{j} \times \underline{H}$$

and consequently, that

$$(\hat{\eta}\,\underline{E} + \underline{j} \times \underline{H})_\kappa = + \frac{\partial T_{k\ell}}{\partial x_\ell} - \frac{1}{c^2}\frac{\partial S_\kappa}{\partial t}$$

Subsequently, integration over x from x_1 through x_0 and taking the mean over $\angle 31$

y, z, and t, together with $H_n = \underline{n} \cdot \underline{H}$ will yield

$$[M\underline{V} + \underline{\underline{P}} \cdot \underline{n} + \frac{H^2}{8\pi}\underline{n} - \frac{1}{4\pi}\underline{H}\,H_n] = \int_{x_1}^{x_2} \sum_\mu \overline{\underline{F}_\mu}\, dx$$

Because of $V/c \ll 1$ we disregard the contributions of the electrical field to the Maxwellian stress tensor, using Eq. (10a). Now we must determine the integral $\int_{x_1}^{x_2} \sum_\mu \overline{\underline{F}_\mu}$. It applies that

$$\int_{x_1}^{x_2} \sum_\mu \overline{\underline{F}_\mu}\, dx = \int_{x_1}^{x_2} \sum_\mu m_\mu \int d\underline{v}\, \underline{v}\overline{C_\mu}\, dx$$

The integral will not yield a quantity outside of area S, because of $C_\mu = 0$. As a rule, C_μ will differ from zero when inside the area S. In the case of shock waves that are controlled by collisions we can use Boltzmann's collision integral for C_μ which due to the conservation of the impulse will yield

$$\sum_\mu \int \underline{v}\, C_\mu\, m_\mu\, d\underline{v} = 0$$

upon collision. In our case, we are concerned with shock waves where collective interactions are important and where simple Coulombian collisions can be disregarded. Now we must also allow interactions of greater range. In that case, it will usually no longer apply that

$$\sum_\mu \int \underline{v}\, C_\mu\, m_\mu\, d\underline{v} = 0$$

but only that

$$\int_{x_1}^{x_2} \sum_\mu m_\mu \int \underline{v}\, \overline{C_\mu}\, d\underline{v}\, dx = 0$$

/32

which, however, is adequate for our purposes. Thus, we obtain:

$$[M\underline{V} + \underline{\underline{P}} \cdot \underline{n} + \frac{H^2}{8\pi}\underline{n} - \frac{1}{4\pi}\underline{H}\,H_n] = 0 \qquad (12)$$

Next, we consider Eq. (7), and as a first step, summate over all μ:

$$\frac{\partial}{\partial t}\left(\sum_\mu \tfrac{1}{2}\rho_\mu \underline{u}_\mu^2 + \sum_\mu \hat{e}_\mu \rho_\mu\right)$$

$$+\frac{\partial}{\partial \underline{x}}\left(\sum_\mu \underline{u}_\mu \rho_\mu \left(\tfrac{1}{2}\underline{u}_\mu^2 + \hat{e}_\mu\right) + \sum_\mu \underline{u}_\mu \cdot \underline{\underline{P}}_\mu + \underline{q}\right) - \underline{j}\cdot\underline{E} = \sum_\mu \varepsilon_\mu$$

In accordance with the energy equation of electrodynamics, we obtain the following for $\underline{j} \cdot \underline{E}$:

$$\underline{j}\cdot\underline{E} + \frac{\partial}{\partial t}\left(\frac{1}{8\pi c^2}\underline{E}^2 + \frac{1}{8\pi}\underline{H}^2\right) + \operatorname{div}\underline{S} = 0$$

Consequently, the usual integration over x and taking the mean will yield: /33

$$\left[M\left(\tfrac{1}{2}\underline{V}^2 + \hat{e}\right) + \underline{V}\cdot\underline{\underline{P}}\cdot\underline{n} + (\underline{q} + \underline{S})\cdot\underline{n}\right] = \int_{x_1}^{x_0}\sum_{\mu}\bar{\varepsilon}_{\mu}\,dx$$

Using Eq. (10a) we obtain for the area outside S:

$$\underline{S} = -\frac{1}{4\pi}(\underline{u}\times\underline{H})\times\underline{H}$$

and in the system K_0:

$$\underline{S} = -\frac{1}{4\pi}(\underline{V}\times\underline{H})\times\underline{H}$$

and consequently: $\left[M\left(\tfrac{1}{2}\underline{V}^2 + \hat{e}\right) + \underline{V}\cdot\underline{\underline{P}}\cdot\underline{n} + q_n + V_n\frac{H^2}{4\pi} - \frac{H_n}{4\pi}(\underline{H}\cdot\underline{V})\right] =$

$$= \int_{x_1}^{x_0}\sum_{\mu}\bar{\varepsilon}_{\mu}\,dx$$

or /34

$$\left[M\left(\tfrac{1}{2}\underline{V}^2 + \hat{e} + \frac{H^2}{8\pi\rho}\right) + q_n + \underline{V}\left(\underline{\underline{P}} + \frac{H^2}{8\pi}\underline{\underline{1}}\right)\cdot\underline{n} - \frac{H_n}{4\pi}(\underline{H}\cdot\underline{V})\right] =$$

$$= \int_{x_1}^{x_0}\sum_{\mu}\bar{\varepsilon}_{\mu}\,dx$$

where $\underline{\underline{1}}$ is the standard tensor.

Now after appropriate modification, the same arguments apply to $\int_{x_1}^{x_0}\sum_{\mu}\bar{\varepsilon}_{\mu}\,dx$ that were used for the impulse conservation equation. Hence,

$$\int_{x_1}^{x_0}\sum_{\mu}\bar{\varepsilon}_{\mu}\,dx = 0$$

and

$$\left[M\left(\tfrac{1}{2}\underline{V}^2 + \hat{e} + \frac{H^2}{8\pi\rho}\right) + \underline{V}\cdot\left(\underline{\underline{P}} + \frac{H^2}{8\pi}\underline{\underline{1}}\right)\cdot\underline{n} + q_n - \frac{H_n}{4\pi}(\underline{H}\cdot\underline{V})\right] = 0 \qquad (13)$$

Integration of the equation div $\underline{H}$ = 0 over x, and taking the mean over y, z, and t will yield:

$$[H_n] = 0 \qquad (14)$$

Now we apply the integrating and mean-taking procedure to the equation

$$\text{rot } \underline{E} = -\frac{\partial \underline{H}}{\partial t}$$

and obtain: 35

$$[\underline{E}_{tr}] = 0$$

where $\underline{E}_{tr}$ is that part of $\underline{E}$ which is located in the plane y, z. The equation $[\underline{E}_{tr}] = 0$ is equivalent to the relationship $[\underline{n} \times \underline{E}] = 0$. Subsequently, Eq. (10a) will yield $[\underline{n} \times (\underline{V} \times \underline{H}) = 0$.

$$[\underline{V} H_n - \underline{H} V_n] = 0 \tag{15}$$

The x-component of this vector equation is satisfied identically.

Moreover, the following statement is useful for the subsequent algebra to determine the step functions. We defined the reference system B_0 in such a way that the area S has a mean velocity component of zero with respect to B_0 in the x direction (cf. Figure 2). We still lack a criterion to define the state of motion of B_0 in the y and z directions. But we are now able to state such a criterion. It is seen from Eq. (15) that in the case of $H_n \neq 0$, that is, $\theta_0 \neq 90°$, a reference system can be achieved, by a translation in the y and z directions, where it applies on either side of S that $\underline{E}_{tr} = 0$, or that

$$\underline{V} H_n = \underline{H} V_n$$

We shall give this system the final denotation B_0.

2.2.3. Treatment of the Pressure Tensor

So far we failed to make a statement on the tensor $\underline{\underline{P}} = \sum_{\mu=\mu} \underline{\underline{P}}$. However, it follows from $C_\mu = 0$ outside of area S as well as from $\frac{\partial}{\partial t} = 0$, $\frac{\partial}{\partial x} = 0$, $\frac{\partial}{\partial y} = 0$ and $\partial/\partial_z = 0$ that

$$(\underline{E} + \underline{v} \times \underline{H}) \cdot \frac{\partial f_\mu}{\partial \underline{V}} = 0 \text{ for all } \mu. \tag{36}$$

Moreover, with Eq. (10a), we obtain

$$((\underline{v} - \underline{u}_D) \times \underline{H}) \cdot \frac{\partial f_\mu}{\partial \underline{V}} = 0$$

This will yield the general form of f_μ according to our model

$$f_\mu = f_\mu \left(v_{\parallel}, (\underline{v} - \underline{u}_D)^2 \right)$$

with

$$v_{\parallel} = \frac{\underline{v} \cdot \underline{H}}{|\underline{H}|} \tag{16}$$

It applies specifically in the reference system B_0 that $f_{\mu} = f\,(\vartheta_{\parallel}\,,\ \underline{v}^2)$, because of $\underline{u}_D = 0$. Consequently, the distribution functions of all the particles have axial symmetry with respect to the magnetic field [Chew, Goldberger, Low, 1956]. According to the definition Eqs. (4) and (8) this means that the pressure tensor has a diagonal shape in a cartesian coordinate system K_0 as shown in Figure 3 which has the coordinates $\bar{x}$, $\bar{y}$, and $\bar{z}$. Since $\bar{y}$ is located in the direction of the magnetic field, the following applies in $\bar{K}_0$:

$$\underline{\underline{P}} = \begin{pmatrix} P_{\perp} & 0 & 0 \\ 0 & P_{\parallel} & 0 \\ 0 & 0 & P_{\perp} \end{pmatrix} \qquad \bar{x},\ \bar{y},\ \bar{z}$$

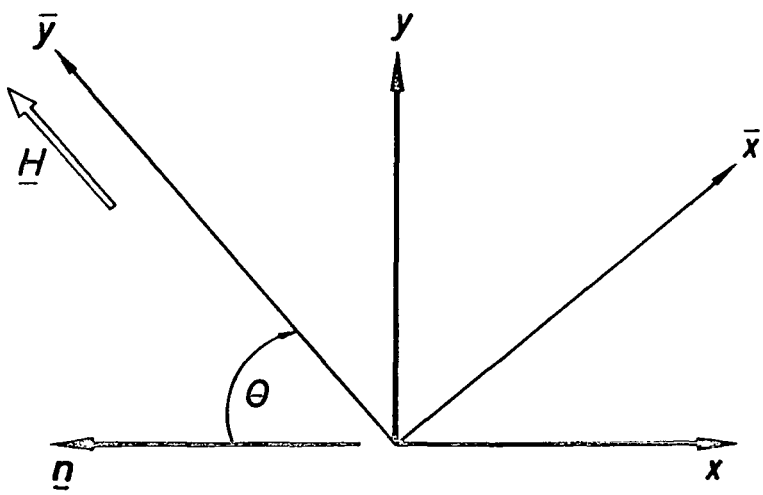

Figure 3. Sketch to define the primary axis coordinate system $\bar{K}_0$ of the pressure tensor $\underline{\underline{P}}$ with respect to the shock wave coordinate system K_0.

Now we calculate the tensor components in the system x, y, z. For this purpose we require the unit vectors in the x, y and z directions in the $\bar{x}$, $\bar{y}$, $\bar{z}$ system:

$$\hat{\underline{x}} = (\sin\Theta, -\cos\Theta, 0)_{\bar{x},\bar{y},\bar{z}}$$

$$\hat{\underline{y}} = (\cos\Theta, \sin\Theta, 0)_{\bar{x},\bar{y},\bar{z}}$$

$$\hat{\underline{z}} = (0, 0, 1)_{\bar{x},\bar{y},\bar{z}}$$

In that case we obtain: /38

$$\underline{\underline{P}} = \begin{pmatrix} P_{xx} & P_{xy} & P_{xz} \\ P_{yx} & P_{yy} & P_{yz} \\ P_{zx} & P_{zy} & P_{zz} \end{pmatrix}_{\bar{x},\bar{y},\bar{z}}$$

with

$$\begin{aligned} P_{xx} &= \hat{\underline{x}} \cdot \underline{\underline{P}} \cdot \hat{\underline{x}} = P_{\perp} \sin^2\Theta + P_{\parallel} \cos^2\Theta \\ P_{yx} = P_{xy} &= \hat{\underline{x}} \cdot \underline{\underline{P}} \cdot \hat{\underline{y}} = 1/2\,(P_{\perp} - P_{\parallel})\sin 2\Theta \\ P_{zx} = P_{xz} &= 0 \\ P_{yy} &= \hat{\underline{y}} \cdot \underline{\underline{P}} \cdot \hat{\underline{y}} = P_{\perp} \cos^2\Theta + P_{\parallel} \sin^2\Theta \\ P_{zy} = P_{yz} &= 0 \\ P_{zz} &= \hat{\underline{z}} \cdot \underline{\underline{P}} \cdot \hat{\underline{z}} = P_{\perp} \end{aligned}$$

(17a)

$$\underline{\underline{P}} = \begin{pmatrix} P_{\perp}\sin^2\Theta + P_{\parallel}\cos^2\Theta & 1/2(P_{\perp} - P_{\parallel})\sin 2\Theta & 0 \\ 1/2(P_{\perp} - P_{\parallel})\sin 2\Theta & P_{\perp}\cos^2\Theta + P_{\parallel}\sin^2\Theta & 0 \\ 0 & 0 & P_{\perp} \end{pmatrix}_{x,y,z}$$

Moreover, we obtain with Eqs. (4) and (8):

$$\hat{e}\,\varrho = P_{\perp} + 1/2\,P_{\parallel} \tag{17b}$$

Finally, it follows from Eq. (16) that the thermal flux vector $\underline{q}$ must be located parallel or antiparallel to $\underline{H}$:

$$\underline{q} \times \underline{H} = 0 \tag{17c}$$

Apart from θ, the pressure tensor is characterized by $P_{\parallel}$ and $P_{\perp}$. /39

Having derived the Eqs. (11), (12), (13), (14), (15), and (17), we must now ask ourselves whether we have an adequate number of equations to achieve the objective of this investigation. This objective is a collection of formulas which can be used to compute the characteristic magnitudes for side 1 of S when these magnitudes are known for side zero. Each side is characterized by ρ, $P_{\parallel}$, $P_{\perp}$; $\underline{V}$, $\underline{H}$ and $\underline{q}$. Because of Eq. (17c), $\underline{q}$ is defined by a scalar magnitude. Consequently, we have 1 + 1 + 1 + 3 + 3 + 1 = 10 unknown quantities. However, the Eqs. (11), (12), (13), (14), (15), and (17) yield only 1 + 3 + 1 + 1 + 2 = 8 defining equations. Consequently, we have two more unknown quantities than we have equations. It is seen immediately that this is due, on the one hand, to the stipulated anisotropy of the plasma and to the possible presence of a thermal flux vector $\underline{q}$ in an homogeneous, steady-state Vlasov plasma. We shall attempt to find two meaningful additional relationships in the next section.

Finally, it shall be noted at the end of this section that we can of course replace the quantity of the ten magnitudes ρ, $P_{\parallel}$, $P_{\perp}$, $\underline{V}$, $\underline{H}$ and $\underline{q}$ on side 0 which are considered known, by some other quantity of ten independent magnitudes. In many cases this will be the more practical procedure.

2.3. Theoretical Models for Noncollision Shock Waves, and Observation Results with Respect to Shock Wave Structure /40

The following section shall first present a brief description of the most important models for the structure of noncollision shock waves. Subsequently, the observation results with respect to shock wave structures, acquired from space probes and satellites, shall be compiled. These data will yield an indication as to the two required additional stipulations.

2.3.1. Review of Some Models of Shock Waves in a Collisionless Plasma

One important magnitude that affects the characteristics of a shock wave is the ratio of gas pressure to magnetic pressure ahead of the shock front. Since the pressure tensor is not a spherical tensor, we shall initially use the arithmetic mean of $P_{\perp 0}$ and $P_{\parallel 0}$ as a measure for the plasma pressure, which is $1/2(P_{\perp 0} + P_{\parallel 0})$. The ratio to magnetic pressure will then be $(P_{\parallel 0} + P_{\perp 0})/\frac{H_0^2}{4\pi}$. However, for the purpose of the following, we shall use the magnitude

$$\hat{s}_o = \frac{5}{6} \frac{P_{\perp o} + P_{\parallel o}}{H_o^2/4\pi} \qquad (18)$$

which already occurred in Table 2 and in Figure 1 and which in the case of $P_{\parallel O} = P_{\perp O}$ turns into the expression s_O of Bazer and Ericson [1958] which then represents the square of the ratio of sonic velocity to Alfvén velocity, V_A.

The models of noncollision shock waves can be classified into two groups according to the value of $\hat{s}_O$; models where $\hat{s}_O \gg 1$ and models where $\hat{s}_O \ll 1$. In this case we usually stipulate that the particle distributions f_μ are isotropic Maxwellian distributions. As a rule they are completely disregarded in the case where $\hat{s}_O \ll 1$. However, the models are easily expanded toward anisotropic distributions if we exclude only those f_μ which cause instabilities with excessively rapid growth periods. / 41

The group where $\hat{s}_O \gg 1$ includes theories proposed by Parker [1959], Moiseev and Sagdeev [1963], Tidman [1967 a, b], Colgate and Hartman [1967], and Kennel and Sagdeev [1967]. Parker [1959] considered two plasma streams without magnetic field that are subject to mutual interaction as a result of dual stream instability. Where the velocity difference was greater than the thermal electron velocity he obtained a thickness of the shock wave transition of about $\approx (m_i/m_e)^{1/2} \cdot L_D$ where L_D represents the Debye length. The thickness of the transition decreases with decreasing velocity differences, to about $\approx L_D$.

The theory of Moiseev and Sagdeev [1963] treats shock waves where $\theta_O = 0^o$ and where Alfvén turbulence is caused as a result of anisotropy within the shock wave.

Tidman [1967 a, b] initially treated a shock wave without magnetic field. The velocity of the shock wave $V_{n,O}$, is stipulated to be considerably smaller than $V_{the,O} = (\varkappa T_{e,O}/m_e)^{1/2}$. A Mott-Smith equation is written for the ion distribution function where the distribution function f_{ion} is assumed to be a weighted mean of the distribution functions in front of and behind the shock front within the area S. On the front side it applies that T_{el}/T_{ion}. The quasilinear theory with ion acoustical waves is used in the forward part of the shock wave. A rough estimate made on the basis of the spatial growth rate will

yield a shock wave thickness of some $V_{n,0}/\omega_{pi,0}$ where $\omega_{pi,0}$ is the ion plasma circular frequency on the front side. The magnetic field is taken into account subsequently, and a thickness of $L_B \approx 2V_{the,1}/\omega_{ce_\perp,0}$ is obtained for the magnetic field transition, where $\omega_{ce_\perp,0}$ is the electron gyro circular frequency that corresponds to the transverse component of the magnetic field. Only one prerequisite is stated for disregarding the magnetic field when studying the plasma transition. This model can be used without major modifications but in any event only for $\hat{s}_0 \gg 1$. The same shock wave model is treated in more detail with respect to magnetic field structure in two other papers [Tidman, 1967; Tidman and Northrop, 1968]. Waves in front of and behind the shock front are discussed in particular. /42

Colgate and Hartman [1967], using a computer model, considered the interaction between two plasma streams resulting from reflection of a plasma stream against a wall. It is stipulated that the plasma streams in question are almost cold where $T_{el}/T_{ion} = 2.7$, and they are represented by positive and negative "plates." In other words, a one-dimensional calculation procedure is used. This will yield a shock wave thickness of about $V_{n,0} \cdot 88(m_i/m_e)^{1/2}/\omega_{pi,0}$ for the transition of the ion distribution function. The thermalization of the electrons takes place at a faster rate.

Two other theoretical models for noncollision shock waves where $\theta_0 = 0°$ and 90° and where $\hat{s}_0 \gg 1$ were proposed by Kennel and Sagdeev [1967, a, b]. Here, in the case where $\theta_0 = 0$, the "fire-hose" instability will cause Alfvén turbulence which is carried downstream for an extended distance because of weak damping. The fading distance of Alfvén turbulence is much greater than the thickness of the transition area for the velocities and pressure tensors of the ions and electrons as well as the magnetic field. Magnetosonic waves are considered in the case where $\theta_0 = 90°$.

Let us now consider the case where $\hat{s}_0 \ll 1$. This includes theories by Parker [1958, 1961], Davis et al. [1958], Auer et al. [1961, 1962], Fishman et al. [1960], as well as Litvak [1960] and Camac et al. [1962], Rossow [1965, 1967], some papers by members of the Courant Institute of New York [Gardner et al. 1958; Morawetz, 1961 and 1962; Morton, 1964], and Sagdeev [1966].

Parker [1958, 1961] considered shock waves where $\theta_0 = 0$, associated with the /43
generation of Alfvén waves by two plasma streams with $\underline{V}_0$ and $\underline{V}_1$ which penetrate each other for a certain distance.

In the case of Davis et al. [1958], the shock wave under consideration with $\theta_0 = 90°$ propagates into a cold plasma. The transition area between the two sides 0 and 1 includes a laminary, nonlinear wave train having a wavelength in the order of $2\pi V_A (\omega_{ci}\ \omega_{ce})^{-\frac{1}{2}}$. This wave train is bounded by collisions so that the width of the transition area corresponds approximately to the mean free path length.

Auer et al. [1961, 1962] used a one-dimensional computer model to investigate a shock wave with $\theta_0 = 90°$ which was generated by energizing an electrical field oriented vertically with respect to the magnetic field. In this case, the plasma in front of the shock wave is cold and is represented by positive and negative "plates." In the case of Alfven Mach numbers $V_{n,0}/V_{A,0} = M_A$ which are sufficiently smaller than two, this will yield a transition area consisting of a laminar wave train similar to that of Davis et al. [1958]. In the case of sufficiently great M_A-values a disordered transition area is obtained whose width is $\approx V_{A,0}/\omega_{ci,0} = c/\omega_{pe,0} \cdot (m_i/m_e)^{1/2} = c/\omega_{pi,0}$ and whose start has a fine structure of length scale $c/\omega_{pe,0}$ which decreases in strength and length scale over time. $\omega_{pe,0}$ is the electron plasma circular frequency.

These calculations were expanded by Rossow [1965; 1967] to the case where the stipulation $n_i \approx n_e$ is dropped and where oblique shock waves are used. In this case, n_i is the numerical ion density and n_e the numerical electron density.

Sagdeev [1966] considered shock waves with $\hat{s}_0 \ll 1$ and $\theta_0 = 90°$. The currents that cause the change of the magnetic field lead to large velocity differences, especially in the case of small densities, that will trigger electron oscillations via dual current instability.

The papers from the Courant Institute which were mentioned before are con- /44
cerned with laminar structures similar to those of Davis et al., that is, wave trains with ordered particle trajectories. These models resulted in objections with respect to their stability. The magnetic field variations are caused by currents of the type that, for instance, in the case of Sagdeev [1966], can trigger instabilities of the dual current instability type.

Probably the most satisfactory and progressive theory of collisionless shock waves with $\hat{s}_0 \ll 1$ is the theory advanced by Fishman et al. [1966], Litvak [1960], and Camac et al. [1962] for shock waves with $\theta_0 = 90°$. In this theory a part of the ordered energy in front of the shock wave is transformed into wave energy. These are waves having the "whistler" type of wave form in the wave length range from $c/\omega_{pe} = r_e$ through $c/\omega_{pi} = r_i$. These waves contribute to pressure, energy density, and energy flux. Similar to phonons in a solid, they are described as plasmons by a kinetic wave equation. These plasmons are generated when a plasma performs work opposing the wave pressure. In the birth interval of the plasmons, the magnitudes of density $\bar{\rho}$, velocity $\underline{\bar{u}}$, magnetic field $\underline{\bar{H}}$, and so on will vary in order to assume their new values. The width of this transition area L_u was estimated by the authors at $8/\beta_w k$, where k is a typical wave vector of the above wave distribution, meaning that k amounts to some $1/r_i$. β_w is the ratio of wave pressure to magnetic field pressure. In the beginning of the shock wave transition, the plasmon distribution in the $\underline{k}$ space is characterized by two sharply defined maxima which are located symmetrically with respect to the k_y - 0 plane. The location of the maxima in the $\underline{k}$ space is determined by the fact that the frequency in the equilibrium plasma system assumes a minimum at these points, under the secondary condition that the plasmons move only in the y direction within the shock wave coordinate system. Upon propagation in the negative x direction, the wave distribution will become continuously broader and more symmetrical. Wave energy is no longer produced in the interval behind the transition area, because of the absence of velocity gradients. Plasmon collisions under simultaneous symmetrization of the wave distribution will produce waves of progressively increasing frequency which are finally lost as a result of damping. The slow MHD waves which are also produced by collisions can experience only higher-order collisions among each other. This will result in a lesser degree of damping so that they finally predominate. At a greater distance even they will be lost due to damping. Finally, under x = 0 (cf. Figure 2) all the wave energy has been transformed into thermal energy. /45

These models can be described qualitatively approximately as follows, using Figures 2, 4, and 5, if we disregard the laminar models which are subject to strong objections because of the stability problem. The orderly energy of the plasma on the front side of the shock wave is partly transformed into wave

energy in an area whose width is $L_u^{\cdot\cdot}$. This area corresponds to the x-interval ($L_s - L_v - L_u^{\cdot\cdot}$, $L_s - L_v$). This interval is preceded by the interval ($L_s - L_v$, L_s) which is entered by the lesser part of the wave energy by means of propagation against the direction of the flow; we call this the advance area. However, the greater part of the wave energy enters the interval (0, $L_s - L_v - L_u^{\cdot\cdot}$) via propagation and convection. Here, the wave spectrum is modified during propagation in the negative x-direction as a result of wave-wave interaction and particle-wave interaction so that, naturally, the distribution functions of the particles will change as well. Subsequently, the wave energy continues to decrease at the expense of particle energy until it becomes so small at point x = 0 that it can be disregarded. During this process, relatively great gradients of ($L_s - L_v - L_u^{\cdot\cdot}$, $L_s - L_v$) etc. will be encountered in the interval $\bar{\rho}$, $\bar{u}$, and the lesser gradients in the interval (0, $L_s - L_v - L_u^{\cdot\cdot}$). The strong wave spectrum develops in the interval ($L_s - L_v - L_u^{\cdot\cdot}$, $L_s - L_v$) as a result of the inhomogeneity of the medium and/or of the peculiarities of the particle distributions in the velocity space. /46

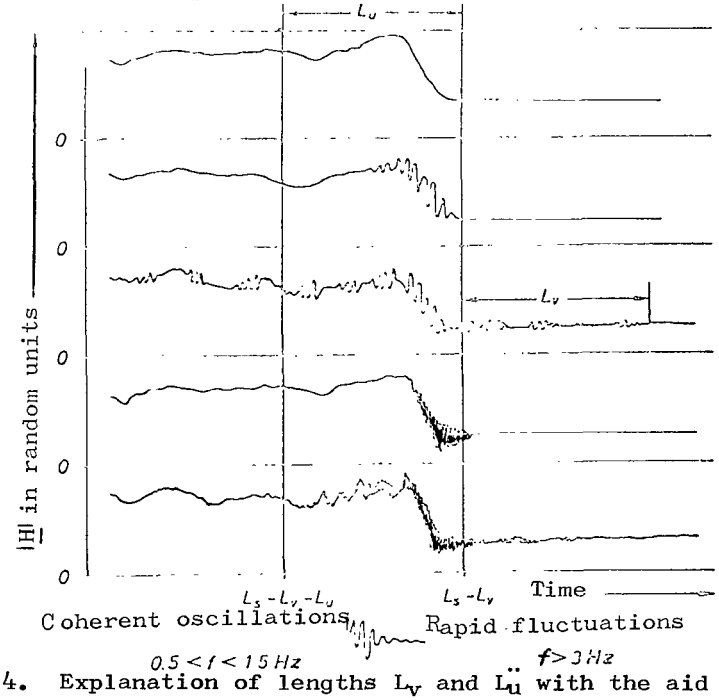

Figure 4. Explanation of lengths L_v and $L_u^{\cdot\cdot}$ with the aid of five typical magnetic field profiles recorded upon penetration of the earth' shock wave, according to Heppner et al. [1967]. Plotted are intervals ($L_s - L_v - L_u^{\cdot\cdot}$, $L_s - L_v$) and one example for an interval ($L_s - L_v$, L_s), all of which are contained in the interval (0, L_s) which, however is too large to be represented.

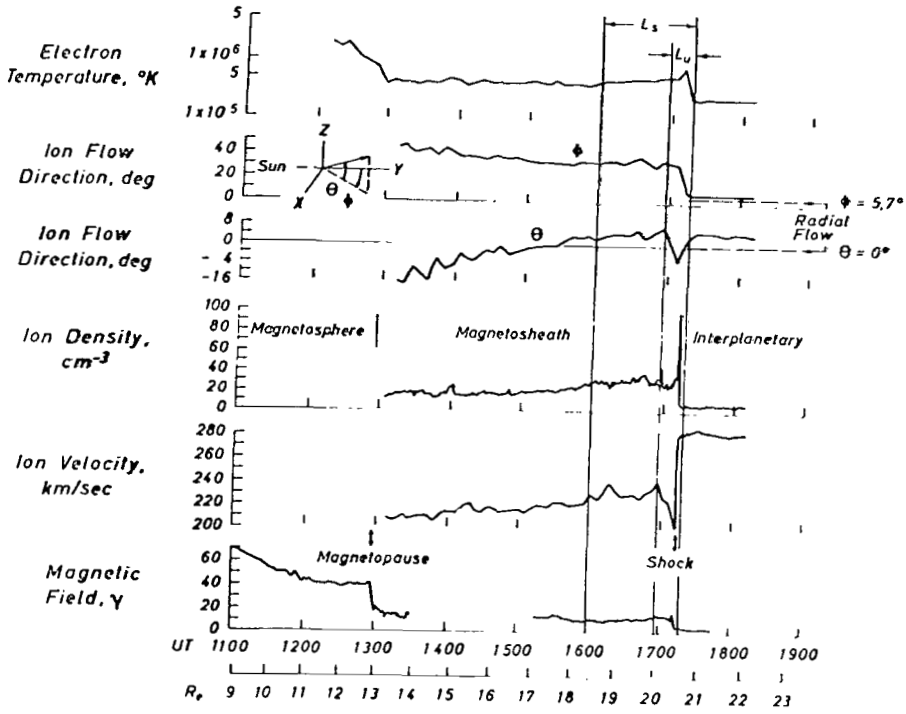

Figure 5. Plasma and magnetic field observations by Pioneer 6, recorded upon penetration of the transition region and the earth's shock wave, according to Wolfe and McKibbin [1968] and Ness [1966] with an explanation of the magnitudes L_u and L_s which define the intervals ($L_s - L_v - L_u$, $L_s - L_v$) (where $L_v = 0$) and (0, L_s). UT denotes universal time. The distance from earth is stated in earth radii, R_e.

Now we shall establish some nomenclature once and for all: the transition interval ($L_s - L_v - L_u$, $L_s - L_v$) shall simply be called the shock wave. The interval (0, $L_s - L_v - L_u$) shall be called wave region. The total interval (0, L_s) shall be called the shock wave region, S. /48

What is the picture of the shock wave structure that is conveyed by the observation data acquired from space probes and satellites?

2.3.2. Observed Data on Shock Wave Structure Acquired from Space Probes and Satellites

Some observation data on the structure of the shock wave that is generated in the flow about the earth's magnetosphere are already available, while very little is known on the structure of shock waves propagating freely in solar wind. This is due primarily to the high time resolution required for such investigations which so far could be achieved only in proximity of earth when investigating the earth's shock wave. The most informative observations of the structure of the earth's shock wave to date were acquired with the aid of the satellites OGO - A [Holzer et al., 1966; Smith et al., 1967; Heppner et al., 1967], Vela 2A and 2B, and specially Vela 3A and 3B [Argo et al., 1967; Greenstadt et al., 1968] in addition to the space probes Mariner IV [Siscoe et al., 1967] and Pioneer 6 [Ness et al., 1966; Wolfe and McKibbin, 1968]. These are measurements of particle distribution functions and especially magnetic field measurements. When we compare these measurements with each other and with the theory we must keep in mind that the density, velocity, and pressure tensor components of the ions and electrons in solar wind as well as the magnetic field are subject to fluctuations. Another difficulty is due to the fact that the measurements at any point of time are taken at only one point in space. Consequently, spatial and time fluctuations cannot be separated from the outset. Moreover, the different positions must be taken into consideration when comparing the measurements. Even in these measurements the time resolution of the plasma detectors /49 is not adequate.

The magnetic field structure as acquired from the measurements of OGO - A was investigated in detail by Heppner et al. [1967]. Figure 20 of that paper lists some typical observations made aboard this satellite of the magnitude of the magnetic field as a function of time, presented for classification of the majority of the observed shock waves. Figure 4 was plotted on the basis of

this information. The steep rise on the front side of the shock front takes place within about 50 to 100 km, which corresponds approximately to the ionic Larmor radius at Alfvén velocity, and this in front of the shock wave (typically at 70 km where n = 10 cm^{-3}). The smoothed magnetic field profile consists of a steep rise of the thickness mentioned above, and a relatively broad maximum. Subsequently a new value is reached asymptotically. The first minimum indicated behind the maximum in Figure 4 is seen more pronounced in several examples and should be given more emphasis as part of the structure. The fact that the magnetic-field profile remains constant in the shock wave over a period of several minutes, even down to details, has been emphasized by Greenstadt et al. [1968]. A similar, smoothed magnetic field profile was also measured by Pioneer 6. The magnetic field measurements near the earth that are described there [Ness et al., 1966] are remarkable insofar as they were acquired under very low Kp-values, 0+ and 0o. Consequently, we can assume that only a small part of the variations are due to irregularities in solar wind. The smoothed magnetic field profile measured by Pioneer 6 started out with 13 γ in the outer transition region, dropped to about 9 γ, rose to 18 γ, and finally dropped to the interplanetary value of 3 γ. This magnetic field profile can be seen in the bottom curve of Figure 5. If we consider the region which is characterized by large values of the variance σ of a magnetic field component over 30 s to be the shock wave region, the stated value of $L_s \approx 2\ R_e$ will result since the variances become small at a distance of about 2 R_e from the steep rise. However, we also note that the condition / 50 $L_s \ll L$ which was stipulated at the beginning of Para. 2.2.1. is not satisfied. Consequently, L_s can have a different value in the truly "one-dimensional" case. Advance waves cannot be identified in this example. Therefore, $L_v = 0$. The nonsteady processes mentioned above are superimposed on the smoothed magnetic field profile. They are strongest in proximity of $x \approx L_s - L_v \approx L_s$. Heppner et al. [1967] frequently observed wave trains extending over some periods with frequencies between 0.5 and 1.5 Hz. Amplitudes of 4 γ in one magnetic field component were observed behind the start of the steep rise. These were interpreted as being waves in the whistler mode in the wave length range theoretically required by Fishman et al. [1960], Litvak [1960] and Camac et al., [1962]. These waves are also encountered with a small amplitude as advance waves in the plasma on the solar wind side of the steep rise, that

is where $L_s - L_v < x < L_s$ in accordance with Figure 4. Moreover, waves of higher frequencies $f > 3$ have been observed. Also, according to Siscoe et al. [1967], based on the measurements of Mariner IV, the amplitudes of the nonsteady processes increase in proximity of $x = L_s - L_v$. These authors discussed periods in excess of several seconds and obtained relative maxima in the power spectra during periods from 30 s to 60 s which were interpreted as being torsional oscillations oriented perpendicularly to the normal vector $\underline{n}$.

In addition to the experiment by Heppner et al. [1967] which was described above, the OGO - A satellite also had aboard an experiment to determine higher frequency magnetic field variations in all three magnetic field components [Holzer et al., 1966; Smith et al., 1967]. The useful part of the measured magnetic field spectrum included the frequency range between 3 Hz and 300 Hz. Squared spectra were acquired at time intervals of five minutes [Smith et al., 1967]. These reflected changes by several orders of magnitudes from one measuring interval to the next. A mean taken over several spectra revealed a squared spectrum of $B(f) \approx 1\ \gamma^2\ Hz^2/f^3$ ranging between 3 Hz and 300 Hz. Extrapolation for 1 Hz provided a variance component for all frequencies above 1 Hz which is $\sigma^2 = 2 \int \int B(f)\, df = 1\ \gamma^2$. The contribution of high-frequency variations to magnetic field energy is very small, if we consider that the background field is greater than 15 γ. One five-minute interval which began in the outer transition region and ended upon entry into the interplanetary plasma, yielded $B(f) \approx 5\ \gamma^2 Hz^2/f^3$. In general, it was found again that the nonsteady magnetic fields increased in the direction toward the shock wave. Frequently the varying magnetic fields are distributed simultaneously over all frequency ranges. The signals in the different components are similar. More recent measured data [Olson et al., 1968; McLeod et al., 1968] indicated continuous power spectra in the shock wave ranging all the way up to 10 Hz. Noise strays were measured in the frequency range from 10 to 300 Hz, with magnetic field amplitudes from 0.01 γ to 0.1 γ. Monochromatic signals were measured frequently in the "magneto-sheath" between shock wave and magnetopause in the frequency range from 14 Hz to 140 Hz; sometimes these signals reached amplitudes up to 1 γ. The spectral density is much smaller on the solar wind side of the shock wave, However, advance waves are encountered again and again at a distance of several earth radii from the shock wave. Since these advance waves do not contribute greatly to the

/51

energy density, the energy flux, and the pressure, they can be neglected in the shock relationships. However, they can be significant to the shock wave structure.

We can recognize in the data on magnetic field observations the qualitative picture which is common to these theories. A steep rise of the magnetic field, possibly preceded by advance waves, is followed by a broad region of nonsteady magnetic fields whose behavior is subject to intensive change with respect to time and space.

In the case of the plasma measurements the experiments in the satellites of the Vela series [Argo et al., 1967; Greenstadt et al., 1968] and in Pioneer 6 [Wolfe et al., 1968] must be emphasized. The measurements aboard Pioneer 6 conveyed the following picture: at some distance from the shock wave in the region (0, L_s - L_v - L_u) the plasma has a velocity $|\underline{V}|$ = 225 - 240 km/s, an ion concentration $n \approx 25 - 35$ cm^{-3}, an electron temperature $T_{el} = 4 \times 10^5$°K, and a proton temperature of $T_{ion} \approx 5.0 - 7.5 \times 10^5$°K. More exactly speaking, the ion distribution can be expressed by a Maxwellian distribution of the above temperature and an additional high-energy tail oriented in a certain direction [Wolfe et al., 1968]. The uncertainty in determining T_{ion} results from the difficulty involved in the separation of this high-energy tail during evaluation. According to an evaluation of the measured spectra made by the author, T_{ion} is located closer to 7.5×10^5°K. The high-energy tail is relatively well developed in the rear of the shock wave. Again the question arises as to the nature of the effect of the inhomogeneity of the flow behind the shock wave on the behavior of the distribution functions. During the approach to the magnetic field, maximum of 18 γ, n and T_{el} increased, while $|\underline{V}|$ decreased. At the maximum, we find that T_{ion} is approximately unchanged, while $T_{el} \approx 7 \times 10^5$°K, $|\underline{V}| < 200$ km/s, and $n \approx 108$ cm^{-3}. Finally, in the solar wind the data were $n \approx 11$ cm^{-3}, $|\underline{V}| \approx 280$ km/s, $T_{el} \approx 2 \times 10^5$°K, $T_{i,\parallel} \approx 1 \times 10^4$°K and $T_{i,\perp} \approx 4 \times 10^4$°K. The index i refers to ions. The two last-named values must be considered to be quite uncertain since they were located at the limit of the resolution of the plasma analyzer.

/52

We shall now consider some additional plasma measurements. A remarkable feature in conjunction with our search for an additonal stipulation for the shock wave theory is the statement in [Wolfe et al., 1966] that the distribution function of the ions in the "magnetosheath" is almost isotropic. According to Asbridge et al. [1966], the electrons in the transition region frequently have almost isotropic distributions.

The paper by Greenstadt et. al., [1968] reported on the measurements made /53
by the plasma analyzers aboard Vela 3A in comparison to magnetic field measurements. Since only the magnetic field component perpendicular to the spin axis is stated, and since the plasma data are not provided in very favorable form, it is not possible to draw many conclusions. It is merely seen that the ion streams are subject to greater fluctuations than they are in solar wind. Argo et al., [1967] stated the plasma parameters on both sides for several passes through the shock wave. However, except for one instance the ion temperature stated was acquired by taking a mean, and this of course does not permit any statement as to the exact distribution functions or the pressure tensor. In the one case which was investigated in greater detail the ion temperature acquired from measurements just prior to entry into the solar wind plasma was 1×10^6 °K based on directional distribution, and 5×10^5 °K based on energy distribution. The measured points in the spectra indicated a strong dispersion which was due to time variations. Moreover, the flux maximum of the directional distribution is not substantiated by measurements but was acquired through interpolation by means of an anisotropic Maxwellian distribution. Therefore, these measurements are not very dependable. Theoretically speaking, an anisotropic ion distribution in the transition region ($L_s - L_v - L_u$, $L_s - L_v$) would not be surprising. Even gas dynamic shock waves show anisotropy in the corresponding transition area.

Another interesting observation is that positive ions are accelerated in the earth's shock wave and are then scattered in the upstream direction [Asbridge et al.,1968]. The numerical density of these ions (again primarily consisting of protons) in most instances amounted to $\lesssim$ 1 % of the numerical density in the solar wind, while the mean particle energy was typically four times as great as it was for the solar wind ions. However, numerical densities /54
amounting to 10 % of the data for the inflowing solar wind have been measured, too.

We have two possibilities for taking this ion contribution into consideration. For one, it is possible that these ions move for an adequately great distance L_A along the interplanetary magnetic field in the direction of the sun, where the helix angle distribution and energy distribution are more or less retained. In that case we could allow for these ions by using them for the calculation of the different velocity moments as well as for the application of the H-theorem which we shall discuss in the next chapter. Here we consider the back-scattered ions to be part of the plasma on the front side.

For the second possibility, we can start out from the premise that the back-scattered ions have a destabilizing effect. The resulting fluctuation increase will cause a trend toward greater isotropy even within the stability limits where, moreover, the secondary maximum in the distribution functions is reduced which corresponds to the back-scattered ions. If this process is sufficiently effective, L_A will amount to only a few earth radii R_e. In that case the shock wave region S will already begin a few earth radii in the upstream direction. The advance wave region will contain advance waves and the processes just described. Now, we must use measurements acquired at a sufficient distance from the shock wave itself in order to determine the plasma state on the front side of the shock wave. It is our expectation that the anisotropy of the ion distribution functions is somewhat greater there than the anisotropy of that part of the distribution functions which are located about the primary maximum in the vicinity of the shock wave. In that case, we might be able to explain part of the discrepancy between the anisotropy measurements of Wolfe et al. [1966] aboard Pioneer 6 and of Hundhausen et al. [1966] aboard the Vela satellites in relatively close proximity to earth. In any event, the back-scattered ions will not cause any difficulties with respect to derivation of the step functions.

In summary, we can state under the reservations named above that the ions have an almost isotropic distribution function behind the shock wave region [Wolfe et al., 1966]. According to the information furnished by J. Wolfe, the anisotropy measurements of the electrons must be considered highly uncertain because of the encountered interference potentials caused by photoelectrons. On the other hand, the mean electron temperature in the rear of

/55

the shock wave of earth, that is, where $x < 0$, is lower than the mean ion temperature so that the uncertainty with respect to exact information on the anisotropy assumes a lesser significance [Olbert et al. 1967]. Based on what we stated above, it is a natural idea to make the additional stipulation that the particle distributions behind the shock wave region are isotropic. In that case, it follows that $P_{//,1} = P_{\perp,1}$ and that $q_{n,1} = 0$. Moreover, if we limit the given distributions on the front side to those where $q_{n,0} = 0$, it also follows that $[q_n] = 0$.

In doing so, we are aware of the fact that the measurements provide statements only for specific values of the anisotropies and pressure contributions of the individual particles, of the magnitude $\hat{s}_0$ in the vicinity of earth ($0.1 \lesssim \hat{s}_0 \lesssim$ in the tens), of the angle θ_0, and so on.

Strict justification for these stipulations, and a statement of their validity range, can be provided only by a general theory on the structure of shock waves in an anisotropic plasma. However, the following section contains some physical considerations of a more generalized nature which appear to make these stipulations meaningful under certain assumptions with respect to shock wave strength.

2.4. Physical Justification of the Additional Stipulations, and Introduction of the H-Theorem

/56

We have seen in the preceding section that all important models of shock wave structure state that turbulence develops in a collision-free plasma in the vicinity of the shock wave as a result of instabilities and the effect of inhomogeneity. After manifold processes this turbulence is finally attenuated until the end of the wave region is reached. The waves used to describe this turbulence have been substantiated at least qualitatively through observations. While the constant magnetic field is the dominant field in front of the shock wave region $(0, L_s)$ and behind it, and while the wave fields $\underline{E}$, $(\underline{x}, t)$ and $\underline{H}$ $(\underline{x}, t)$ as well as the fluctuations $\delta\underline{E}$ and $\delta\underline{H}$ can be disregarded over the length and time scales under consideration here, all of these magnitudes play a significant role within the shock wave region S. In order to investigate this problem further, we shall consider the H-theorem for the shock wave transition. We define

$$\hat{H}_\mu = \frac{1}{n_\mu} \int f_\mu \log f_\mu \, d\underline{v} \tag{19}$$

$$H = \sum_\mu \frac{1}{n} \int f_\mu \log f_\mu \, d\underline{v} = \sum_\mu \frac{n_\mu}{n} \hat{H}_\mu$$

where $n = \sum_{\substack{\mu \\ \text{all ion types}}} n_\mu$ = numerical ion density

Now we multiply Eq. (3a) by $(1 + \log f_\mu)$, summate over all particle types, and integrate over the velocity space. We obtain:

/ 57

$$\int d\underline{v} \sum_\mu \frac{\partial f_\mu}{\partial t} (1 + \log f_\mu) = \frac{\partial}{\partial t} \int \sum_\mu f_\mu \log f_\mu \, d\underline{v}$$

$$\int d\underline{v} \sum_\mu \underline{v} \cdot \frac{\partial f_\mu}{\partial \underline{x}} (1 + \log f_\mu) = \frac{\partial}{\partial \underline{x}} \left(\int \sum_\mu f_\mu \underline{v} \log f_\mu \, d\underline{v} \right)$$

$$\int d\underline{v} \sum_\mu \frac{e_\mu}{m_\mu} (\underline{E} + \underline{v} \times \underline{H}) \frac{\partial f_\mu}{\partial \underline{v}} (1 + \log f_\mu) = 0$$

and consequently

$$\frac{\partial}{\partial t} \sum_\mu \int f_\mu \log f_\mu \, d\underline{v} + \frac{\partial}{\partial \underline{x}} \sum_\mu \int f_\mu \underline{v} \log f_\mu \, d\underline{v} =$$

$$= \sum_\mu \int C_\mu (1 + \log f_\mu) \, d\underline{v} = \sum_\mu G_\mu = G$$

Taking the mean over y, z, and t, as well as integration over x will then yield:

$$\left[\sum_\mu \int f_\mu v_x \log f_\mu \, d\underline{v} \right] = \int_{x_o}^{x_1} \overline{G} \, dx \tag{20a}$$

According to our statements at the end of Para. 2.2.1., the left side of Eq. (20a), using the ensemble $\mathcal{E}_1$, will yield the same value as for $\mathcal{E}$. Consequently,

$$\left[\sum_{\mu}\int f_{\mu}\, v_x \log f_{\mu}\, d\underline{v}\right] = \int_{x_0}^{x_1} \overline{G}_{\mathcal{E}_1}\, dx = \int_{x_0}^{x_1} G_{\mathcal{E}}\, dx \qquad (20b)$$

58

Moreover, the Eqs. (11), (12), (13), (14), (15), and (17) will remain unchanged, and so will the values of the magnitudes in them. The difference between the ensembles $\mathcal{E}$ and $\mathcal{E}_1$ is felt only within the shock wave region.

This means that the right-hand side of Eqs. (20a) and (20b) is determined only by the fluctuations defined in $\mathcal{E}_1$ which incorporate primarily the effect of the discrete nature of the plasma matter. We can also express this in a different way. According to Dupree [1963, p. 1717, right-hand column], it is possible to split off a component from the functions occurring in the Mayer cluster development of the ensemble means of the fluctuation products, which component expresses the discrete nature of the plasma matter. If we drop this component, we will obtain the description of a "fluid type" medium which is described completely by the Vlasov equation.

Therefore, we shall briefly investigate the consequences resulting from the stipulation that $f_{\mu,\mathcal{E}_1}$ will satisfy the Vlasov equation for all particle types μ. In that case, it will apply that $C_{\mu,\mathcal{E}_1} = 0$ and $G_{\mu,\mathcal{E}_1} = 0$, and hence also that

$$\left(\int_{x_0}^{x_1} \overline{G}_{\mu}\, dx\right)_{\mathcal{E}_1} = 0 = \left(\int_{x_0}^{x_1} G_{\mu}\, dx\right)_{\mathcal{E}}$$

and even more so that

$$\sum_{\mu}\left(\int_{x_0}^{x_1} \overline{G}_{\mu}\, dx\right)_{\mathcal{E}_1} = \sum_{\mu}\left(\int_{x_0}^{x_1} G_{\mu}\, dx\right)_{\mathcal{E}} = 0$$

Before we can derive some statements from the observations, we must still discuss the interrelationship existing between the measured magnitudes and the ensemble means. According to the magnetic field measurements with relatively great time resolution which were cited in Section 2.3, there are highly instationary processes of small time scales present within the shock wave region $(0, L_s)$ which make it appear that the time resolution of the plasma experiments is insufficient by far in order to acquire $f_{\mu,\varepsilon_1} = \langle N_\mu \rangle_{\varepsilon_1}$. Therefore, we can only hope that we will be able to determine the distribution functions $f_{\mu,\varepsilon} = \langle N_\mu \rangle_\varepsilon$ which do not include the instationary processes by definition. Since, according to the principle of plasma analyzers, only random samples of distributions are measured in different regions of the velocity space during one measuring cycle, it will then be necessary to take means over several measuring cycles. During this period, $f_{\mu,\varepsilon}$ must not be subject to major change, for instance, due to the satellite's motion. Except in the shock wave of thickness L_u itself, in most instances this condition is satisfied, for instance throughout the transition region between magnetopause and the earth's shock wave. Since the plasma measurements in the transition region always took place in areas subject to magnetic field fluctuations that cannot be neglected per se, we shall attempt to derive an equation corresponding to Eq. (20a) where the upper integration limit x_s is still located in the wave region. Using the definition $A(x = x_s) - A(x = x_0) = \left[A \right]_{x_0}^{x_s}$, it applies that

$$\left[\int \overline{f_{\mu,\varepsilon}\, v_x \log f_{\mu,\varepsilon}}\, d\underline{v} \right]_{x_0}^{x_s} = \int_{x_0}^{x_s} \overline{G}_\varepsilon \, dx$$

Where $x = x_0$ it applies, of course, that $f_\mu = f_{\mu,\varepsilon_1} = f_{\mu,\varepsilon}$ and that $\frac{\partial}{\partial x} = \frac{\partial}{\partial y} = \frac{\partial}{\partial z} = 0$ as well as $\partial/\partial t = 0$. We can also write

$$\left[\sum_\mu \int f_{\mu,\varepsilon}\, v_x \log f_{\mu,\varepsilon}\, d\underline{v} \right]_{x_0}^{x_s} \tag{20c}$$

$$= \int_{x_0}^{x_s} \overline{G}_\varepsilon \, dx + \left\{ \sum_\mu \int f_{\mu,\varepsilon}\, v_x \log f_{\mu,\varepsilon}\, d\underline{v} - \sum_\mu \int \overline{f_{\mu,\varepsilon}\, v_x \log f_{\mu,\varepsilon}}\, d\underline{v} \right\}_{x=x_s}$$

The left-hand side of Eq. (20c) is determined by the measurements. If we can neglect the curly bracket we will obtain the integral $\int_{x_0}^{x_s} \overline{G}_{\varepsilon,} \, dx$ which must be equal to zero when the Vlasov equation applies.

Now we shall assume that the distribution functions are subject to point symmetry with respect to the mass velocity $\underline{v}_\varepsilon = \frac{1}{\rho_\varepsilon} \sum_\mu \int \underline{v} \, f_{\mu,\varepsilon} \, d\underline{v} \, m_\mu$ where $\rho_\varepsilon = \sum_\mu \int f_{\mu,\varepsilon} \, d\underline{v} \, m_\mu$. The observations indicate that this approximation will be adequate for our purposes. In that case we will obtain the following if we neglect the curly bracket:

$$\left[V_{x,\varepsilon} \sum_\mu \int f_{\mu,\varepsilon} \, \log f_{\mu,\varepsilon} \, d\underline{v} \right]_{x_0}^{x_s} \tag{21}$$

$$= - \left[V_{n,\varepsilon} \sum_\mu \int f_{\mu,\varepsilon} \, \log f_{\mu,\varepsilon} \, d\underline{v} \right]_{x_0}^{x_s}$$

$$= - V_{n,\varepsilon} \cdot n_\varepsilon \left[H_\varepsilon \right]_{x_0}^{x_s} = \int_{x_0}^{x_s} \overline{G}_{\varepsilon,} \, dx$$

or

$$- \left[H_\varepsilon \right]_{x_0}^{x_s} = - \sum_\mu \frac{n_{\mu,\varepsilon}}{n_\varepsilon} \left[\hat{H}_{\mu,\varepsilon} \right]_{x_0}^{x_s} = \frac{1}{V_{n,\varepsilon} \cdot n_\varepsilon} \int_{x_0}^{x_s} \overline{G}_{\varepsilon,} \, dx$$

/ 61

where we have used the particle number conservation equation $\left[V_{n,\varepsilon} \cdot n_\varepsilon \right]_{x_0}^{x_s} = 0$ Moreover, we first approximate $f_{\mu,\varepsilon}$ by means of an anisotropic Maxwellian distrubution and calculate $H_{\mu,\varepsilon}$ and H_ε. The notations $\parallel$ and $\perp$ designate the magnitudes located parallel and perpendicular to the magnetic field in the usual manner.

$$f_{\mu,\varepsilon} = n_{\mu,\varepsilon} \left(\frac{m_\mu}{2\pi \times T_{\parallel,\mu,\varepsilon}} \right)^{1/2} \cdot \left(\frac{m_\mu}{2\pi \times T_{\perp,\mu,\varepsilon}} \right) \cdot$$

$$\cdot \exp \left(- \frac{m_\mu (v_\parallel - V_{\parallel,\varepsilon})^2}{2 \times T_{\parallel,\mu,\varepsilon}} - \frac{m_\mu (v_\perp - V_{\perp,\varepsilon})^2}{2 \times T_{\perp,\mu,\varepsilon}} \right)$$

where $\varkappa$ is the Boltzmann constant.

Moreover, we obtain

$$\hat{H}_{\mu,\epsilon} = \frac{1}{n_{\mu,\epsilon}} \int f_{\mu,\epsilon} \log f_{\mu,\epsilon} \, d\underline{v} = \text{const.} + \log \frac{n_{\mu,\epsilon}}{T_{\parallel,\mu,\epsilon}^{1/2} \, T_{\perp,\mu,\epsilon}}$$

The constant includes only natural constants.

Now we obtain

$$-\left[\hat{H}_{\mu,\epsilon}\right]_{x_0}^{x_1} = \left[\log \frac{T_{\parallel,\mu,\epsilon}^{1/2} \, T_{\perp,\mu,\epsilon}}{n_{\mu,\epsilon}}\right]_{x_0}^{x_s} \tag{22a}$$

/62

and

$$-\left[H_\epsilon\right]_{x_0}^{x_1} = \sum_\mu \frac{n_{\mu,\epsilon}}{n_\epsilon} \left[\log \frac{T_{\parallel,\mu,\epsilon}^{1/2} \, T_{\perp,\mu,\epsilon}}{n_{\mu,\epsilon}}\right]_{x_0}^{x_1} = \frac{1}{V_{n,\epsilon} \cdot n_\epsilon} \int_{x_0}^{x_1} \bar{G}_\epsilon \, dx \tag{22b}$$

Now we also make use of the observation that the next frequent ion type in solar wind after the protons, which is He^{++}, has always been measured at four times the temperature. Under the assumption that the temperatures of all ion types change at the same ratio during the shock wave transition, and that this applies to $T_{//}$ and well as to $T_\perp$, we obtain the result that $\left[\hat{H}_\mu\right]_{x_0}^{x_s}$ is equal for all ion types and that, consequently,

$$-\left[H_\epsilon\right]_{x_0}^{x_1} = \left[\log \frac{T_{\parallel,i,\epsilon}^{1/2} \, T_{\perp,i,\epsilon}}{n_{i,\epsilon}}\right]_{x_0}^{x_s} + \left[\log \frac{T_{\parallel,e,\epsilon}^{1/2} \, T_{\perp,e,\epsilon}}{n_{e,\epsilon}}\right]_{x_0}^{x_s}$$

The plasma measurements by Wolfe et al. [1968] aboard Pioneer 6 yield the following for the earth's shock wave:

$$\left[\log \frac{T_{\parallel,e,\ell}^{1/2}\, T_{\perp,e,\ell}}{n_{e,\ell}} \right]_{x_o}^{x_s} = +0.05 \pm 0.16$$

$$\left[\log \frac{T_{\parallel,i,\ell}^{1/2}\, T_{\perp,i,\ell}}{n_{i,\ell}} \right]_{x_o}^{x_s} = +3.5 \pm 0.5 \qquad /63$$

and, consequently,

$$-\left[H_\ell\right]_{x_o}^{x_s} = 3.5 \pm 0.7$$

This makes allowance for the experimental uncertainties. Moreover, the uncertainties include an estimate of the possible effect of the back-scattered ions described by Asbridge et al. [1968]. The point of least magnetic variations was used as the reference point in the rear of the shock wave. Allowing for the flow inhomogeneity behind the shock wave will cause little change in these results, nor will the approximate incorporation of the effect of the turbulence which is expressed by the remaining H- variations. For, if we assume that the magnetic field fluctuations in the vicinity of the reference point represent a wave field of MHD waves, the associated velocity fluctuations can be estimated and compared to the thermal velocities. It is found that these variations can be neglected. However, the possibility remains that turbulent wave fields could play a role which do not have magnetic field variations like, for instance, ion acoustical waves. But a large error caused by these waves in the temperature determination in the vicinity of our reference point is improbable because it applies in the "magnetosheath" in this example that $T_{i,\ell}/T_{e,\ell} \approx 1.5$ which implies a strong attenuation of ion acoustical waves [cf., for instance, Fried and Gould, 1961].

An interplanetary shock wave was observed on October 7, 1962, with the aid of the Mariner 2 space probe [cf. Sonett et al., 1964]. For this wave we obtain $\left[\log\left(T_{\parallel,i,\ell}^{1/2}\, T_{\perp,i,\ell}/n_{i,\ell}\right)\right]_{x_o}^{x_s} \approx 0.23$ Since isotropy was assumed for this evaluation, and since the magnetic variations are known only with poor time resolution, the

uncertainty in this case is greater than 0.26, so that $\left[\quad\right]_{x_0}^{x_s} > 0$,* too, would be compatible with the data.

Moreover, interplanetary shock waves have been observed with the aid of the Vela satellites [Gosling et al., 1968]. A shock wave was observed on January 20, 1966, which yielded a value of $\left[\log\left(T_{\parallel,i,\varepsilon}^{1/2}\, T_{\perp,i,\varepsilon}/n_{i,\varepsilon}\right)\right]_{x_0}^{x_s} \approx +0.53$. On October 5, 1965, a shock wave was observed where $\left[\log\left(T_{\parallel,i,\varepsilon}^{1/2}\, T_{\perp,i,\varepsilon}/n_{i,\varepsilon}\right)\right]_{x_0}^{x_s} \approx 0.50$. Again, however, it was stipulated that isotropy applied. The paper by Argo et al. [1967], which was mentioned above includes observations for 13 passes through the earth's shock wave. Table 3 lists the values of $\left[\log\left(T_{\parallel,i,\varepsilon}^{1/2}\, T_{\perp,i,\varepsilon}/n_{i,\varepsilon}\right)\right]_{x_0}^{x_s}$ for the values listed in Table 1 of the paper by Argo et al.

TABLE 3

$\frac{n_{1,\varepsilon}}{n_{0,\varepsilon}}$	$\frac{T_{1,\varepsilon}}{T_{0,\varepsilon}}$	$\left[\log\left(T_\varepsilon^{3/2}/n_\varepsilon\right)\right]_{x_0}^{x_s}$
2.8	17	+ 3.2
14.0 (?)	16	+ 1.5
2.3	25	+ 4.0
6.8	50	+ 4.0
4.2	10	+ 2.0
3.8	23	+ 3.4
2.3	36	+ 4.5
2.1	17	+ 3.5
3.1	27	+ 4.5
1.25	12	+ 3.5
2.2	36	+ 4.6
2.8	30	+ 4.1
6.8	10	+ 1.5

* Space in brackets blank in original.

Again, the uncertainties in these measurements are greater than the uncertainties in the Pioneer measurements. The temperature ratio $T_{1,\mathcal{E}}/T_{0,\mathcal{E}}$ was formed from mean values. Magnetic field measurements which might indicate the presence of any highly instationary processes are not available for the period when the plasma measurements were taken. However, the authors state that the measured values are normally reproducible from one measuring cycle /65 to the next and on both sides of the shock wave. These measurements confirm the results of Pioneer 6 in spite of considerable uncertainties.

Moreover, the few measurements of the electron distribution functions confirm the results acquired from Pioneer 6. Although we are aware of the uncertainties involved in the plasma measurements, we can draw some important conclusions. The large values of $\left[\log\left(T_{\parallel,\mathcal{E}}^{1/2}\, T_{\perp,\mathcal{E}}/n_{i,\mathcal{E}}\right)\right]_{x_0}^{x_s} = -\left[\hat{H}_{i,\mathcal{E}}\right]_{x_0}^{x_s}$ and also $-\left[H_{\mathcal{E}}\right]_{x_0}^{x_s}$ are incompatible with the statement that the Vlasov equation for $f_{\mu,\mathcal{E}_1}$ is adequate to describe the physical processes taking place within the shock wave region $(0, L_s)$. The nonvalidity of the Vlasov equation within the shock wave region shows that the fluctuating fields which are defined in the ensemble $\mathcal{E}_1$ play an important role in defining the shock wave structure. The effect of the fluctuation fields is best described by a correlation term of the type that occurs in the Balescu-Lenard equation and was already mentioned above. This correlation term has its origin in the discrete nature of plasma matter. In its most simple form the Balescu-Lenard equation

$$\frac{\partial f_e}{\partial t} = C_{e,\,BL}$$

treats an homogeneous, stable plasma of electrons and of an immobile ion background without magnetic field, allowing merely for electrostatic fluctuations. In that case it can be shown, as for instance by [Montgomery and Tidman, 1964], that

$$\frac{d\hat{H}_e}{dt} = G_e \leq 0$$

The generalization of the term $C_{e,\,BL}$ to allow for several particle types /66 $\mu = 1, 2, \ldots$ is found in Dupree's paper [1961] and in the book by Montgomery and Tidman [1964]. Thus we obtain by analogy:

$$\frac{dH}{dt} = \frac{d}{dt} \sum_{\mu} \frac{n_\mu}{n} \hat{H}_\mu = \sum_{\mu} G_\mu = G \leq 0$$

The relationship is usually called the H-theorem and represents a generalization of the entropy relationship $dS/dt \geq 0$. Among other conditions, the H-theorem is satisfied by Boltzmann's collision term which, however, is not of interest in this connection.

If we apply the generalization of the correlation term $C_{e,\,BL}$ to several particle types $C_{\mu,\,BL}$ in order to determine G_{ε_1} in Eqs. (20), we obtain with $x_1 < x_0$

$$\rho V_n [H] = - V_n \rho \sum_{\mu} \frac{n_\mu}{n} [\log (T_{\parallel,\mu}^{1/2} T_{\perp,\mu} / n_\mu)] \leq 0 \qquad (23)$$

as we can also see from the measurements cited above. Of course, the assumptions made to derive the Balescu-Lenard correlation term are much too stringent for our shock wave problem. We are concerned with an inhomogeneous plasma in the magnetic field which may even be instable at some points. Moreover, the limitation to electrostatic fluctuations is certain to be too restrictive. Among other researchers, Eviatar [1967] has expanded the theory to include the case of an homogeneous plasma in a magnetic field with general fluctuations. Incorporation of inhomogeneity is still outstanding. However, it is physically meaningful to assume that the inequality (23) will retain /67
its validity even then. In that case, the inequality (23) will replace the entropy condition of shock wave theory in the isotropic, collision-dominated plasma.

Another interesting characteristic of the Balescu-Lenard equation is that a Maxwellian distribution is obtained for $t \to \infty$ under any desired initial distribution function. In order to characterize these processes we can introduce the deflection period $\tau_D(\underline{v})$ which expresses the time required for the 90° deflection of a test particle of initial velocity $\underline{v}$. Tidman and Eviatar [1965] and Eviatar [1966, 1967] have shown that this period $\tau_D(\underline{v})$ can be smaller by several orders of magnitude in the case of certain particle distributions than it would be in accordance with the relationships that apply

to Coulombian collisions of pairs. One possibility of achieving this is the destabilization of the plasma. In that case, the waves excited by the test particles will be subject to less attenuation, and accordingly, the feedback effect of the wave field will be greater. If the boundary of indifferent equilibrium is exceeded and instability is reached, equations of the Balescu-Lenard type will become invalid. The processes described by these equations will continue to have an effect, but now it is necessary to allow for non-linear effects. In addition to reversible damping by the Landau mechanism and cyclotron damping, the fluctuation fields associated with the discrete nature of the plasma will cause an irreversible contribution to damping. Moreover, they contribute toward greater plasma isotropy. This emphasis on the effects of the discrete nature of the plasma, however, does not mean that the mechanisms described in Para. 2.3.1., above, will be of lesser significance. The final form of the particle distributions is affected just as decisively by the processes described by the Vlasov equation as the structure of the shock wave region. The magnetic field variations measured behind the shock wave of earth are the manifestation of processes which can be described in good approximation by the Vlasov equation. Now, what is the effect of these instationary processes on the final distribution function f_μ of particle type μ? /68

It was mentioned before that an accurate answer to this question presupposes the availability of a theory on shock waves in a collision-free, anisotropic plasma. Any such theory would normally require the availability of a theory on strong plasma turbulence which is practically nonexistent. However, when we progress in the negative x-direction (cf. Figure 2) in the wave region behind the shock wave, the turbulence energy will decrease because of the absence of turbulence-generating processes. In that case, there may exist an area where the fairly well developed theory on weak turbulence can be used [Litvak, 1960; Kovrijnykh, 1964; Kadomtsev, 1965]. This theory can be adequate everywhere in the case of weak shock waves, as shown by the shock wave model of Litvak [1960], Fishman et al. [1960], and Camac et al. [1962]. The theory of weak plasma turbulence regards wave packets (plasmons) under the aspect of the particle-wave and wave-wave interactions and under the

aspect of propagation effects. Necessary criteria for the weakness of the turbulence include weak imaginary components $|k_i| \ll k_r$ of the wave number $k = k_r + ik_i$, and free wavelengths l for the wave collisions that are greater than several typical wavelengths $2\pi/k$. Moreover, the effect of the discrete nature of the plasma can be taken into consideration. As we progress in the negative x-direction, the free path length for wave collisions, l, will continue to increase with the result that, finally, the wave collisions can be disregarded. In that case, we enter an area where the quasilinear theory becomes applicable. The waves no longer have any direct interaction. They merely cause velocity space diffusion and consequently, changes in the distribution functions that have a feedback effect on the waves via the dispersion relations.

The shock wave theories of Para. 2.3.1. provide no statement on the final distribution functions, or only vague statements. Therefore, we shall consider as an example the advanced development of the shock wave model by Litvak [1960], Fishman et al. [1960], and Camac et al. [1962] (cf. Para. 2.3.1.). Using the "number" of plasmons, $n_{\underline{k}}$, per unit of volume in the configuration space and in the wave vector space, $\underline{k}$, and stipulating weak turbulence, the wave transport equation [Camac et al., 1962] will be applicable /69

$$\frac{\partial n_{\underline{k}}}{\partial t} + (u_x + v_g)\frac{\partial n_{\underline{k}}}{\partial x} + k_x \frac{du_x}{dx}\frac{\partial n_{\underline{k}}}{\partial k_x} = 2\gamma_{\underline{k}} \cdot n_{\underline{k}} + \left(\frac{\partial n_{\underline{k}}}{\partial t}\right)_{\text{wave collisions}} \tag{24}$$

where $v_g = \partial\omega/\partial k_x$ is the group velocity component in the x-direction, compared to the plasma at rest. $\omega_{\underline{k}}$ is the circular frequency, measured in the steady-state system of plasma $B_{\underline{R}}$. The equation has been expanded by the damping term. It is stipulated that, at the start of the wave region, the wave collisions shall be predominant and shall determine the form of the function $n_{\underline{k}}$. According to the paper by Litvak [1960] in which damping is neglected, the generally applicable steady-state solution for the wave collision term $\left(\frac{\partial n_{\underline{k}}}{\partial t}\right)_{\text{wave coll.}} = 0$ reads

$$n_{\underline{k}} = \frac{A}{\omega_{\underline{k}} - \hat{\underline{u}} \cdot \underline{k}}$$

where A and $\hat{\underline{u}}$ are constants. Now we could obtain a more accurate solution for $n_{\underline{k}}$ after linearization of the collision term by means of a perturbation calculation about the equilibrium function, similar to the Chapman-Enskog method for gases, where a development about the local Maxwellian distribution is made. In the case of strong wave collisions, we can consider the above formula to be a good approximation. Since the plasmons originating from /70
whistler wave packets which are under consideration here, are strongly attenuated below a wavelength of $r_e = c/\omega_{pe}$, the theory will no longer apply in that region. On the other hand, however, this is an interesting area because plasmons can be moved toward high $\underline{k}$ values as a result of wave collisions, and can be strongly attenuated there. Now, if we consider $n_{\underline{k}} = A/\omega_{\underline{k}} - \hat{\underline{u}} \cdot \underline{k}$, we will find for $\underline{k} \cdot \hat{\underline{u}} > 0$ that $n_{\underline{k}} > n_{-\underline{k}}$. Consequently, waves with $\underline{k} \cdot \hat{\underline{u}} > 0$ are more frequent. We can conclude from this statement that more waves are moved by collisions into the area of strong attenuation where $\underline{k} \cdot \hat{\underline{u}} > 0$ and $k > 2\pi/r_e$. Since the impulse of the plasmons per unit of volume $d\underline{x}$ and $d\underline{k}$ is given by $n_{\underline{k}} \cdot \underline{k}$, the wave field where $k < 2\pi/r_e$ will lose impulse in the direction $\hat{\underline{u}}$. However, in order for the distribution $n_{\underline{k}}$ within $k = 2\pi/r_e$ to correspond approximately to the form $n_{\underline{k}} = A/\omega_{\underline{k}} - \hat{\underline{u}} \cdot \underline{k}$, it must apply that $\hat{\underline{u}} \to 0$. Consequently, $n_{\underline{k}} \sim 1/\omega_{\underline{k}}$ should apply at some distance from the shock wave. In the case of the $\underline{k}$ space, this is a distribution which is symmetrical with respect to the zero point. Moreover, according to the description of this shock wave model provided in [Camac et al., 1962], part of the energy of the fast, clockwise-polarized plasmons is lost through transformation into slow, counterclockwise-polarized plasmons.

When the turbulence becomes weaker, the attenuation effects and propagation effects begin to predominate, and highly damped plasmons are suppressed. Finally, the following equation applies:

$$(u_x + v_g) \frac{\partial n_{\underline{k}}}{\partial x} = + 2 \gamma_{\underline{k}} \cdot n_{\underline{k}}$$

where have used $du_x/dx \approx 0$. Moreover, if we take into consideration that waves

whose propagation is oriented at an angle to the magnetic field are subject to greater attenuation than waves propagating parallel to the magnetic field, /71
and that $\theta_0 = \theta_1 = 90°$ applies to the shock wave model under consideration, we will find for the dominant plasmons that $\left|\frac{\partial \omega_{\underline{k}}}{\partial k_x}\right| \ll |u_x|$ and hence that

$$u_x \frac{\partial n_{\underline{k}}}{\partial x} = + 2 \gamma_{\underline{k}} \; n_{\underline{k}}$$

It applies especially in the steady-state plasma system B_R after transformation of $B_0 \rightarrow B_R$ that

$$\frac{\partial n_{\underline{k}}}{\partial t} = + 2 \gamma_{\underline{k}} \cdot n_{\underline{k}}$$

This means that, in the steady-state plasma system B_R, the quasilinear theory of an homogeneous medium can be used that is subject only to time variation; such a theory is fairly well developed. Where the path transformation of the term with $\partial n_{\underline{k}}/\partial x$ is impossible, the quasilinear theory of inhomogeneous media would have to be used which is still poorly developed [cf., for instance, Tidman, 1967 a].

What is the direction of change of the distribution function in the quasilinear region? Kennel and Engelmann [1966] studied the quasilinear theory of growing waves ($\gamma_{\underline{k}} > 0$) with the result that it must apply in the asymptotic case for $t \rightarrow \infty$ and for all waves that $\gamma_{\underline{k}} = 0$. The incorporation of negative values of $\gamma_{\underline{k}}$ which are of special interest to us, will yield $\gamma_{\underline{k}} \leq 0$ in the asymptotic case. The authors themselves state that the asymptotic case is relatively uninteresting since the periods during which natural processes take place are limited. Yet, the result obtained by Kennel and Engelmann is important because it indicates the direction in which the distribution functions change. In our case, we are interested only in processes that are completed /72
within periods $L_s/|\underline{V}_1| \ll L/|\underline{V}_1|$.

Secondary maxima in the presence of small helical angles in a tail of distribution f_e are rapidly reduced as a result of electrostatic electron oscillations. Moreover, in our case where $\hat{s}_0 \ll 1$, the resonance interactions of the waves considered above are of interest which were described, for instance,

by Kennel and Petschek [1966]; these will prevent any strong anisotropy. Unfortunately, the energies of the interactions under consideration here are located far above the thermal energy of the plasma so that it could still be anisotropic. With these relatively weak isotropization mechanisms, we shall conclude the expanding discussion of the shock wave model of Litvak, Fishman et al., and Camac, which serves as an example for similar considerations.

Another type of instability which is interesting for the case where $\hat{s}_0 > 5/6$, is the so-called "firehose" instability. This is encountered where $P_{\parallel} - P_{\perp} > \underline{H}^2/4\pi$. According to Shapiro and Shevchenko [1964], this instability will stabilize itself, ensuring that $P_{\parallel} - P_{\perp} \leq \underline{H}^2/4\pi$, which would be expected after our statements above.

Reflection instability imposes somewhat more stringent requirements on a stable distribution function. This instability depends not only on the total pressures but also on the ratios of the pressure contributions of the different particle types to $P_{\perp}$ and $P_{\parallel}$. In the most favorable case, instability results only where $P_{\perp} - P_{\parallel} > (P_{\parallel}/P_{\perp}) \cdot \underline{H}^2/8\pi$. Consequently, instability can occur under any value of $\hat{s}_0$. However, instability becomes interesting only for large values of $\hat{s}_0$, if $P_{\perp} - P_{\parallel} > \underline{H}^2/8\pi$ is considered the instability criterion.

However, the two last-named instabilities do not limit the anisotropy to a sufficient degree. For the effect of the remaining anisotropy behind the shock wave on the step functions which we must still derive has approximately the same magnitude as the effect of the inaccurate information on the pressure tensor behind the shock wave, if only the two above-named instabilities are available to limit the anisotropy. /73

We now come to the question as to the circumstances under which the isotropization processes are not adequate. Based on the foregoing, the fluctuations $\delta\underline{E}$ and $\delta\underline{H}$ in the ensemble $\mathcal{E}_1$ play a large role in the isotropization of the plasma. The instationary processes which are incorporated in the ensemble means of $\mathcal{E}_1$ are important to the strength of these fluctuation fields because they yield the highly asymmetrical distribution functions. Moreover, the fluctuation fields $\delta\underline{E}$ and $\delta\underline{H}$ in the ensemble $\mathcal{E}_1$ cause a change in H which is $[H] \leq 0$. If the contributions of the ions and electrons to [H]

disappear, meaning that both have an "adiabatic" behavior, then we cannot expect any isotropization to the degree that would be encountered with a large value of $|[H]|$.

At the end of this chapter, we shall discuss briefly two other additional stipulations which have been proposed for the investigation of the jump relations of shock waves in an anisotropic plasma [Abraham-Shrauner, 1967, a, b; Lynn, 1967]. Both of these authors discuss the case where $\bar{\bar{s}}_0 \ll 1$ in the presence of strong magnetic fields.

Abraham-Shrauner [1967, a, b] started out from the Chew-Goldberger-Low equations. Using the relationships

$$\frac{D}{Dt}\left(\frac{P_{\perp,i}}{\rho\,|\underline{H}|}\right) = 0 \tag{25}$$

and

$$\frac{D}{Dt}\left(\frac{P_{\parallel,i}\,\underline{H}^2}{\rho^3}\right) = 0$$

which are applicable only for a magnetic field of constant direction in the absence of any spatial variations in the magnetic field direction and otherwise only under the stipulation that the heat conduction vector is absent, she derived two energy conservation equations for an energy component which is parallel to $\underline{H}$ and for a component vertical to $\underline{H}$. Again, the derivation of these relationships can be verified only under the stipulation that the magnetic field has a constant direction. However, let us assume that these relationships are correct. In that case we will obtain, using the index i for ion:

/74

$$\frac{\partial W_{\parallel,i}}{\partial t} + \operatorname{div}\,\underline{q}_{\parallel,i} = 0 \tag{26a}$$

$$W_{\parallel,i} = \frac{1}{2}\,\rho_i\,\underline{u}_{\parallel,i}^2 + P_{\parallel,i}$$

$$\underline{q}_{\parallel,i} = \rho_i\,\underline{u}_i\left(\frac{1}{2}\,\underline{u}_{\parallel,i}^2 + \epsilon_{\parallel,i}\right) + \underline{u}_i\cdot\underline{P}_{\parallel,i}$$

$$\epsilon_{\parallel} = \frac{P_{\parallel}}{2\rho}$$

and

$$\frac{\partial W_{\perp,i}}{\partial t} + \operatorname{div} \underline{q}_{\perp,i} = 0$$

$$W_{\perp,i} = \frac{1}{2}\left(\rho_i \underline{u}^2_{\perp,i} + 2\, P_{\perp,i} + \frac{H^2}{4\pi}\right) \qquad (26b)$$

$$\underline{q}_{\perp,i} = \rho_i \underline{u}_i \left(\frac{1}{2}\underline{u}^2_{\perp,i} + \epsilon_{\perp,i}\right) + \underline{u}_i \cdot \underline{\underline{P}}_{\perp,i} + \underline{H} \times (\underline{u}_i \times \underline{H})$$

$$\epsilon_{\perp,i} = \frac{P_{\perp,i}}{\rho_i}$$

Integration over x will yield the two conservation equations (1) and (2) in the paper by Abraham-Shrauner [1967, b]. However, these Eqs. (1) and (2) are not equivalent to the Eqs. (26a) and (26b). We could have summated terms of the form div $\underline{L}$ in Eqs. (26a) and (26b), where it is merely necessary that $\underline{L}$ disappear when $\partial/\partial x = \partial/\partial y = 0$ $\partial/\partial z = 0$, and nothing would have changed in Eqs. (1) and (2). But this also means that the validity of (1) and (2) in Abraham-Shrauner's paper does not include the validity of the Eqs. (25). For instance, let us discuss the case of a shock wave with $\theta_0 = 90°$ on the basis of Abraham-Shrauner's equations. Using Eqs. (1) through (6) of Abraham-Shrauner, we will obtain

/75

$$\frac{P_{\perp 1,i}}{\rho^2_{1,i}} \Big/ \frac{P_{\perp 0,i}}{\rho^2_{0,i}} = \frac{1 + \frac{3}{2}\bar{\eta}_i + \frac{3}{4\pi}\frac{H_0^2}{P_{\perp 0}}\bar{\eta}_i^3}{(1 - \bar{\eta}_i/2)(1 + \bar{\eta}_i)^2}$$

$$\bar{\eta}_i = \frac{\rho_{1,i} - \rho_{0,i}}{\rho_{0,i}}$$

Due to $[H_y/\rho_i] = 0$, this expression would have to yield a continuous result of one in order to be compatible with Eq. (25a), that is $\frac{D}{Dt}\left(P_{\perp,i}/\rho_i |\underline{H}|\right) = 0$. But this expression is equal to one only where $\bar{\eta}_i = 0$. On the other hand, however, Eqs. (25a) and (25b) represent the starting point for Eqs. (26a) and (26b) which are equivalent to the Eqs. (16) and (17) by Abraham-Shrauner [1967]. Consequently, this derivation is contradictory.

This is a different situation as that encountered with a similar "problem" involved in the formulation of the conservation equations for shock waves in gas dynamics. For, in the case of the latter, if we use the generally applicable equation of mass conservation, $\partial\rho/\partial t + \operatorname{div}(\rho \underline{u}) = 0$, the equations of

/76

motion, and the energy conservation equation without dissipation terms (friction and heat conduction), we will obtain, after the customary integration over x, the correct conservation equations of the form [ ] = 0 for the shock wave, and these equations will also yield the correct expressions for the jumps in the different magnitudes. Moreover, except for $[\rho] = 0$ these jumps will yield entropy changes that are incompatible with the absence of the dissipation terms. Again, the reason for this is that none of the dissipation terms will yield a quantity upon integration, so that the same conservation equations are obtained with and without dissipation terms. And this result must be expected because the relationships used there are expressions of generally valid physical principles such as the conservation of mass, conservation of impulse, and conservation of energy, while the two separate energy conservation equations by Abraham-Shrauner require very specific prerequisites: namely Eqs. (25).

Instabilities of the type described by the Chew-Goldberger-Low equations in the form described by Abraham-Shrauner [1967, a] will not be helpful here. The CGL equations can be expanded by allowing for smaller time scales $\tau \leq 2\pi/\omega_{ci}$. In that case, Eqs. (25a) and (25b) will no longer apply even in the case where $\theta_0 = 90°$. Summarizing these considerations we conclude as follows: either the Eqs. (25a) and (25b) are correct with the result that very stringent conditions apply which practically allow only transitions with

$$\left[\log \frac{P_{\parallel}^{1/2} P_{\perp}}{\rho^{5/2}} \right] = \left[\log \left(\frac{P_{\parallel} H^2}{\rho^3} \right)^{1/2} \left(\frac{P_{\perp}}{\rho |H|} \right) \right] = 0$$

Or the Eqs. (25a) and (25b) do not apply within the shock wave region. In 77
that case, the Eqs. (1) and (2) by Abraham-Shrauner [1967, b] are unjustified ad-hoc stipulations. As we mentioned before, the conservation equations by Abraham-Shrauner [1967, b] contain only ionic magnitudes. Now, we subtract from the vector conservation Eq. (12) the corresponding equation by Abraham-Shrauner [1967, b] that contains only ionic magnitudes, and we obtain

$$\left[\frac{m_e}{m_i + m_e} M \underline{V} + \underline{\underline{P}}_e \cdot \underline{n} \right] = 0 \qquad (26c)$$

where e denotes the electronic magnitudes. Moreover, we exploited the circumstance that $n_e = n_i$ and $\underline{V}_i = \underline{V}_e$ must apply outside the shock wave region. If we consider the x-component of Eq. (26c) and compare it with the measurements by Wolfe et al. [1968], we will obtain the following numerical values:

$$\left[\frac{m_e}{m_i + m_e}\,\rho\, V_n^2\right] = \left[m_e\, n\, V_n^2\right] \approx -4 \times 10^{-12}\ \frac{dyn}{cm^2}$$

and

$$\left[P_{xx,e}\right] \approx \left[n\,\varkappa\, T_e\right] \approx 1.35 \times 10^{-9}\ \frac{dyn}{cm^2}$$

Moreover, the observation by Olbert et al. [1967] will yield the same order of magnitude for $[P_{xx,\,e}]$, while the transitions investigated by Argo et al. [1967] confirm the order of magnitude of $[m_e n V_n^2]$. Consequently, Eq. (26c) is not satisfied even in approximation. Since it applies for the measurements by Wolfe et al [1968] that $\hat{s}_0 \approx 3$, the discrepancy can be due to the fact, of course, that $\hat{s}_0 \ll 1$ is not satisfied. In any event, arguing on the basis of Eq. (26c) will merely permit the statement that the theory by Abraham-Shrauner is valid at best within one spherical shell about the sun which is far inside the earth orbit. The inner radius of this spherical shell is determined by the increasing significance of collisions with decreasing distance from the sun. /78

Since Eq. (26c) is also obtained through subtraction of the conservation equation derived from Eq. (1b) of Lynn [1967] from our Eq. [12], the argument stated above will apply in that case, too. Lynn [1967] started out from equations containing ionic magnitudes and especially the ionic pressures. The result was the same as our Eqs. (11), (12), (13), (14), (15), and (17), where our magnitudes are replaced by the corresponding ionic magnitudes. He used the additional assumptions that $[q_n] = 0$, and that

$$\left[\frac{P_{\perp,i}}{\rho_i\, |H|}\right] = 0 \qquad (26d)$$

Neither the observations by Wolfe et al. [1968] and by Ness et al.[1966], nor those of Sonett et al.[1964] will confirm this formula, although this can be due again to the fact that $\hat{s}_0 \ll 1$ is not satisfied.

According to Lynn [1967], Eq. (26d) follows from the conservation of the *first adiabatic invariant*

$$\mu_{ad.} = \frac{\frac{m_i}{2} v_\perp^2}{|\underline{H}|}$$

for each individual particle. The conservation of μ_{ad} requires that the time scales of the field changes in the steady-state system of the particle in question be greater than the gyro period. If we consider the time scales in the models described in Section 2.3. for the structure of collisionless shock waves where $\hat{s}_0 \ll 1$, the time scales will be found to be much smaller than permissible. "Whistler" waves having wavelengths between r_e and r_i are predominant in the shock wave model by Fishman et al. [1960] which applies to shock wave velocities up to $V_{n,\,0} \approx 3\ V_{A,\,0}$ at an Alfvén velocity of $V_{A,0} = |\underline{H}_0| / \sqrt{4\pi\rho_0}$. The associated frequencies in the steady-state system of particles are in most instances greater than f_{ci}, the ion gyro frequency. Moreover, the computer models by Auer et al. [1962] and Rossow [1965; 1967] which, however, are one-dimensional, reflect time scales for large-amplitude fluctuations that are located far below the gyro period of the ions with $2\pi/f_{ci}$. These papers permit the conclusion that assumption 26d is not justified. /79

Finally, a large part of the states in the rear of the shock wave which are obtained with the aid of the jump functions by Lynn [1967], are unstable. For instance, where $\theta_0 = 90°$ and $\hat{s}_0 \ll 1$ it follows from Lynn's equations that in the case of $|\underline{H}_{-1}| / |\underline{H}_0| \gtrsim 4.4$ the plasma behind the shock wave is unstable with respect to fire hose instability when there is isotropy in front of the shock wave. This instability will start even earlier when there is positive anisotropy on the front side. Electron pressure was neglected in this stability consideration. More precise investigation, however, will show that electron anisotropy will even increase the instability. Even in the case where $\theta_0 = 90°$, a large part of the resulting plasma states in the rear of the shock wave will be unstable.

It is seen from this section that the stipulation of plasma isotropy behind the shock wave is meaningful when the shock wave is sufficiently strong, although precise theoretical justification will be difficult. The assumptions made by Abraham-Shrauner and Lynn, however, will encounter difficulties. One /80

important result acquired during the investigation of measured data from satellites and space probes is the statement that, in the case of collision-free shock waves, correlations between particles can be neglected in the regions located in front of the shock wave region and behind it, but not within the shock wave region itself. The Vlasov equation will provide a good description for many aspects.

2.5. The Jump Relations for Contact Discontinuities and Shock Waves in an Anisotropic Plasma /81

Jump relations are defined as formulas which, for given values of ρ, $\underline{\underline{P}}$, $\underline{H}$ on the one side of a transition state the physical magnitudes prevailing on the other side of that transition as functions of a parameter which describes the strength of the transition. Wherever possible we shall adapt the denotations and classification types of the results obtained from Eqs. (11), (12), (13), (14), (15), and (17), and the additional assumptions to the paper by Bazer and Ericson [1958], in order to simplify the comparison. Consequently, we shall define transitions with $V_n = 0$ as contact discontinuities and shall include them in the discussion for completeness. By definition, shock waves are transitions where $V_n \neq 0$. The subdivision of shock waves into waves with and without density change, which was made by Bazer and Ericson [1958], is not advantageous here. We shall show in Para. 2.5.2. that a distinction between collinear shock waves and non-collinear shock waves is advantageous. The latter we shall also designate as rotational discontinuities.

Before we start, we shall also define the transverse part $\underline{Q}_{tr}$ of a vector $\underline{Q}$ with the aid of the vector $\underline{n}$ in Figure 2:

$$\underline{Q}_{tr} = \underline{Q} - \underline{n}\,(\underline{Q} \cdot \underline{n})$$

Moreover, let us reiterate that we shall not make any statement on the stability of the transitions to be obtained below.

2.5.1. Contact Discontinuities

There will not be any mass flow $M = \rho V_n$ through the discontinuity because of $V_n = n$ (here we define discontinuity in the sense of $L_s \ll L$). In general, we assume anisotropic plasma states on both sides of the transition. In

that case, we can make a distinction between two cases: /82

$$H_n \neq 0.$$

It follows from Eq. (14) that H_n is equal on both sides of the transition. Eq. (15) yields $[\underline{V}] = 0$ or $[\underline{V}_{tr}] = 0$. Consequently, the velocity vectors are equal on both sides. The normal component of Eq. (12) yields

$$[P_{\parallel} \cos^2\Theta + P_{\perp} \sin^2\Theta + \underline{H}^2/8\pi] = 0$$

Using Eq. (17a), it follows from the transverse component of Eq. (12) that

$$\left[\underline{H}_{tr}\left(1 + \frac{P_{\perp} - P_{\parallel}}{\underline{H}^2/4\pi}\right)\right] = 0$$

Consequently, in the case of an isotropic plasma we have $[\underline{H}_{tr}] = 0$. In the anisotropic case within the stability boundary toward fire hose instability, it applies that $H_{tr_1} \parallel H_{tr_0}$. Therefore, we can always find a reference system where $\underline{V}_0$, $\underline{V}_1$, $\underline{H}_0$, $\underline{H}_1$ are located in <u>one</u> plane which is oriented perpendicularly to the y, z-plane. Finally, Eq. (13) yields

$$\left[q_n - H_n/4\pi\,(\underline{H}\cdot\underline{V})\left(1 + \frac{P_{\perp} - P_{\parallel}}{\underline{H}^2/4\pi}\right)\right] = 0$$

When $\left[\underline{H}_{tr}\left(1 + \frac{P_{\perp} - P_{\parallel}}{\underline{H}^2/4\pi}\right)\right] = 0$, $[H_n] = 0$ and $[\underline{V}] = 0$, it follows that

$$[q_n] = 0.$$

Additional equations are not obtained. Let us summarize these relationships:

$$[\underline{V}] = 0$$

/83

$$[P_{\parallel} \cos^2\Theta + P_{\perp} \sin^2\Theta + \underline{H}^2/8\pi] = 0 \qquad (27)$$

$$\left[\underline{H}_{tr}\left(1 + \frac{P_{\perp} - P_{\parallel}}{\underline{H}^2/4\pi}\right)\right] = 0$$

$$[q_n] = 0$$

Only the first and second velocity moments, $\underline{V}$, $P_{\parallel}$ and $P_{\perp}$ occur as plasma magnitudes. This means that $[\rho]$ can be selected at random.

Inequality (23) is satisfied automatically for distribution functions which are point-symmetrical to $\underline{V}$ on both sides within the $\underline{v}$-space, since $V_n = 0$. Moreover, it will apply that $q_n = 0$. In the case of other than point-symmetrical functions,

$$\left[\sum_{\mu} \int f_{\mu} v_x \log f_{\mu} \, d\underline{v}\right] \geq 0$$

must be satisfied. The equality sign will apply when the Vlasov equation is also sufficient within the transition region.

$$H_n = 0. \qquad /84$$

Subsequently, because of $\theta_0 = \theta_1 = 90°$, the normal component of Eq. (12) together with (17a) will yield

$$\left[P_{\perp} + \underline{H}^2/8\pi\right] = 0 \qquad (28)$$

The transverse components of Eq. (12) are satisfied automatically. $[\underline{V}] = 0$ is a random magnitude because of Eq. (15). No additional relationship is obtained from Eq. (13) because of Eq. (17c). When the Vlasov equation applies, Eq. (20) will always be satisfied because of Eq. (16).

Consequently, the states on both sides of the contact discontinuity where $H_n = 0$, a so-called tangential discontinuity, are arbitrary except for satisfying the Eq. (28).

2.5.2. The Collinearity Theorem and Generalized Alfven Shock Waves

Now we shall investigate quite generally the nature of the changes in the plane formed by the vectors $\underline{n}$ and $\underline{H}$ during the transition from one side to the other of any random shock wave or contact discontinuity. We shall stipulate that anisotropy is allowed on both sides. Since $[H_n] = 0$ and $[M] = 0$, we can use the transverse part of Eq. (15) to eliminate $\underline{V}_{tr}$ in the transverse part of Eq. (12) by a simple routine:

$$H_n [\underline{V}_{tr}] = [V_n \underline{H}_{tr}] \qquad \text{according to Eq. (15)}$$

$$M [\underline{V}_{tr}] = [-(\underline{\underline{P}} \cdot \underline{n})_{tr} + \frac{H_n}{4\pi} \underline{H}_{tr}] \qquad \text{according to Eq. (12)} \qquad /85$$

Consequently,

$$H_n M [\underline{V}_{tr}] = [M V_n \underline{H}_{tr}] = [\frac{H_n^2}{4\pi} \underline{H}_{tr} - H_n (\underline{\underline{P}} \cdot \underline{n})_{tr}]$$

Using Eq. (17a), we can express $\underline{\underline{P}} \cdot \underline{n}$ in vector terms as follows:

$$\underline{\underline{P}} \cdot \underline{n} = \underline{n} (P_\perp \sin^2 \Theta + P_\parallel \cos^2 \Theta) + \left(\left(\underline{n} \times \frac{\underline{H}}{|\underline{H}|}\right) \times \underline{n}\right)(P_\parallel - P_\perp) \cos \Theta \qquad (29)$$

where

$$\cos \Theta = \underline{H} \cdot \underline{n} / |\underline{H}|$$

Consequently,

$$(\underline{\underline{P}} \cdot \underline{n})_{tr} = \left(\left(\underline{n} \times \frac{\underline{H}}{|\underline{H}|}\right) \times \underline{n}\right)(P_\parallel - P_\perp) \cos \Theta$$

$$= \frac{\underline{H}_{tr}}{|\underline{H}|} (P_\parallel - P_\perp) \cos^2 \Theta$$

and finally, /86

$$[\underline{H}_{tr} (M V_n - \frac{H_n^2}{4\pi} + (P_\parallel - P_\perp) \cos^2 \Theta)] = 0 \qquad (30)$$

When the round bracket on both sides of the shock wave is different from zero, the result will be that $\underline{H}_{tr_1}$ and $\underline{H}_{tr_0}$ are parallel or antiparallel. But when will one of these round brackets disappear? We state $MV_n - H_n^2/4\pi + (P_\parallel - P_\perp) \cos^2 \Theta = 0$ and solve with respect to V_n, using $M = \rho V_n$.

In that case we obtain

$$V_n = \frac{|H|}{\sqrt{4\pi\rho}} \cos\Theta \left(1 - \frac{P_{\parallel} - P_{\perp}}{H^2/4\pi}\right)^{1/2} \equiv \bar{b}_n \qquad (31a)$$

or

$$\bar{b}_n = V_A \cos\Theta \left(1 - \frac{P_{\parallel} - P_{\perp}}{H^2/4\pi}\right)^{1/2}$$

where V_A is the Alfven velocity defined above. $\bar{b}_n$ is the phase velocity of the well known generalization of the Alfvén wave solution applied to an anisotropic plasma for propagation in the $\underline{n}$ direction, that is, in a direction enclosing the angle θ with the magnetic field $\underline{H}$ [cf., for instance, Barnes, 1967]. The instability of this wave for $P_{\parallel} - P_{\perp} > H^2/4\pi$ is the well known fire hose instability. In the case of stability toward this instability, the radicand in $\bar{b}_n$ will be negative. We shall exclude this case from the outset. Different cases will result when we evaluate Eq. (30). We shall summarize the results of this evaluation. First, we shall formulate the collinearity theorem: /87

In the case where $V_{n,0} \neq \bar{b}_{n,0}$ and $V_{n,1} \neq \bar{b}_{n,1}$, the transverse part of the magnetic field on the front side of a shock wave is collinear with the transverse part of the magnetic field in the rear, meaning that the magnetic field vectors $\underline{H}_0$ and $\underline{H}_1$ as well as the normal vector $\underline{n}$ are located in the same plane.

We designate shock waves that are subject to collinearity as collinear shock waves.

Shock waves with $V_{n,0} \neq \bar{b}_{n,0}$ and $V_{n,1} \neq \bar{b}_{n,1}$ are designated Alfvén shock waves for obvious reasons. It is seen from Eq. 30 that these shock waves can be subject to random rotational angles between $\underline{H}_{tr_0}$ and $\underline{H}_{tr_1}$. Therefore, we call them rotational discontinuities when the noncollinear case applies. Now, are the other conservation equations satisfied in the case of Alfvén shock waves? Because of $V_n \neq 0$ and $H_n \neq 0$, we can continue to define the reference system in which the shock wave rests, without loss of generality, by demanding that $\underline{E}_{tr} = 0$. This was already mentioned at the end of Para. 2.2.2. In that case, $\nabla \times H = 0$ will apply on both sides of the shock wave. It is especially easy to see in this reference system B_0 that the remaining equations

do not furnish any additional statement on the angle between $\underline{H}_{tr_0}$ and $\underline{H}_{tr_1}$. Consequently, with fixed θ_1 and $\underline{H}_{tr_1}$ we can rotate the vector $\underline{H}_{tr_1}$ at random against $\underline{H}_{tr_0}$ without violating the conservation equations, provided that they were satisfied at the outset. In particular, we can also rotate $\underline{H}_{tr_1}$ into the plane formed by $\underline{n}$ and $\underline{H}_{tr_0}$ so that the shock wave becomes collinear.

In the case of isotropy, we find the following for the Alfvén shock waves /88 because of Eq. (11):

$$\frac{V_{n,1}}{V_{n,0}} = \frac{\rho_0}{\rho_1} = \frac{H_n}{\sqrt{4\pi\rho_1}} \frac{\sqrt{4\pi\rho_0}}{H_n}$$

and hence that $\rho_0 = \rho_1$ or $[\rho] = 0$. Let us briefly study the special case where $[\rho] = 0$ for Alfvén shock waves in an anisotropic plasma. From $[\rho] = 0$ we obtain $[V_n] = 0$, and hence because of $V_n = \bar{b}_n$, the relationship $\left[(P_\parallel - P_\perp)/\frac{H^2}{4\pi}\right] = 0$. Since, once again, we do not have enough equations, we shall make the additional stipulations that $[q_n] = 0$ and $[\underline{H}_{tr}^2] = 0$. In that case, the normal component of Eq. (12) will yield $[P_\perp] = 0$, and the above relationship will yield $[P_\parallel] = 0$. Consequently, we are dealing with an Alfvén shock wave that has the following characteristics:

$$\begin{aligned}
&[P_\perp] = 0\\
&[P_\parallel] = 0\\
&[\underline{H}^2] = 0\\
&[\rho] = 0\\
&V_{n,0} = V_{n,1} = \bar{b}_{n,0} = \bar{b}_{n,1}\\
&[\underline{V}_{tr}] = V_n/H_n\,[\underline{H}_{tr}]
\end{aligned}$$

In general, the expression $(P_\parallel - P_\perp) / \frac{H^2}{4\pi}$ can change during the transition. In that case we obtain $V_{n,0} \neq V_{n,1}$, and consequently, $[\rho] \neq 0$. Generally speaking, Eq. (12) will yield the following for all Alfvén shock waves:

$$\left[P_\perp + \underline{H}^2/8\pi\right] = 0.$$

Of course, in every instance the inequality (23) or the generally applicable relationship $\left[\sum_{\mu} \int f_{\mu} v_x \log f_{\mu} \, dv\right] \geq 0$ must be satisfied, too.

Now, we shall assume that isotropy prevails behind the shock wave region. /89
In that case, it will follow from Eqs.(11) and (31) that

$$\frac{V_{n,1}}{V_{n,0}} = \frac{\rho_0}{\rho_1} = \frac{H_n}{\sqrt{4\pi\rho_1}} \frac{\sqrt{4\pi\rho_0}}{H_n} \left(1 - \frac{p_\parallel - p_\perp}{H_0^2/4\pi}\right)^{-1/2}$$

Consequently,

$$\left(\frac{\rho_1}{\rho_0}\right)^{1/2} = \left(1 - \frac{p_\parallel - p_\perp}{H_0^2/4\pi}\right)^{1/2}$$

and

$$\frac{\rho_1 - \rho_0}{\rho_0} = - \frac{p_\parallel - p_\perp}{H_0^2/4\pi}$$

Using the nomenclature of Para. 2.5.3., and the definitions

$$\bar{\zeta} = \frac{\rho_1 - \rho_0}{\rho_0} \qquad \Delta s = \frac{5}{3} \frac{p_\parallel - p_\perp}{H_0^2/4\pi}$$

this will correspond to

$$\bar{\zeta} = - \frac{3}{5} \Delta s \tag{31b}$$

Inversely, Eq. (31b) in itself is only a necessary condition for a shock wave ($V_n \neq 0$) with isotropy in its rear to be an Alfvén shock wave. If we add /90
to this the condition $[\underline{V}_{tr}] = [\underline{u}_{tr}] \neq 0$, we will acquire a sufficient and necessary set of conditions to determine that a shock wave having isotropic pressure in its rear is in fact an Alfvén shock wave. This can be shown by means of Eqs. (12) and (15). Based on the statement made at the outset of the discussion of Alfvén shock waves, the jump functions for collinear shock waves can be used to calculate other interesting magnitudes of Alfvén shock waves.

At the end of this section we shall list two important boundary cases that are of interest in conjunction with Eq. (30). In the case where $\underline{H}_{tr,0} = 0$ and $\underline{H}_{tr,1} \neq 0$, it must apply behind the shock wave that $V_{n,1} = \bar{b}_{n,1}$, according to Eq. (30). These shock waves are called switch-on shocks because a transverse magnetic field is switched on upon passage through the shock wave region.

Accordingly, it must apply in the case of $\underline{H}_{tr,0} \neq 0$ and $\underline{H}_{tr,1} = 0$ that $V_{n,0} = \bar{b}_{n,0}$. We designate this type of shock waves as switch-off shocks.

2.5.3. Collinear Shock Waves

We shall now discuss shock waves in which the isotropization processes in the shock wave region $(0, L_s)$ are sufficiently strong to achieve isotropy in the rear of the shock wave. Moreover, we shall consider collinear shock waves exclusively. On the front side, we shall merely stipulate that $q_{n,0} = 0$. Generalization to include the case where $q_{n,0} \neq 0$ is easily accomplished. Subsequently, we assume on the front side of the shock wave the density ρ_0, the angle θ_0, the pressure tensor $\underline{P}_0$, according to Eq. (17a), and the magnetic field $\underline{H}_0$. As a result of the collinearity of the transverse magnetic fields, $\underline{H}_1$ as shown in Figure 2 will be located in the x, y-plane, too. We use $h = H_{y,1} - H_{y,0} / |\underline{H}_0|$, in order to characterize the shock wave transition. This means that, in the case where $h > 0$, we have a magnetic field increase during the shock wave passage, since it applies (by definition) that $H_{y,0} \geq 0$. /91 In the case where $-\sin\theta_0 \leq h \leq 0$, it will also apply that $H_{y,1} \geq 0$, however, $|\underline{H}|$ will not continue to grow. Nor will $\underline{H}$ grow in the area where $-2\sin\theta_0 \leq h \leq -\sin\theta_0$. However, it will apply that $H_{y,1} \leq 0$. $h < -2\sin\theta_0$ again corresponds to a magnetic field increase with $H_{y,1} < 0$.

Using the magnitudes defined above, we can calculate all other physical magnitudes that are of interest for the shock wave; these are ρ_1, $V_{n,0}$, $V_{n,1}$, $P_{//,1} = P_{\perp,1} = P_1$, $[V_y] = [u_y]$, $[V_n] = [u_n]$, $-[H]$, and in a trivial manner, $\underline{H}_1$. We stated that $[V_y] = [u_y]$ etc., in order to express that the differences can be calculated, of course, in any reference system. We use the magnitudes η, $\bar{\eta}$, Y, $\bar{Y}$ to express the results. All the important parameters are summarized again in the following system of defining equations:

$$P_\perp = P_{\perp,0}$$

$$P_\parallel = P_{\parallel,0}$$

$$P_0 = P_\perp \sin^2\Theta_0 + P_\parallel \cos^2\Theta_0$$

$$P_1 = P_{\perp,1} = P_{\parallel,1}$$

$$Y = \frac{P_1}{P_0}$$

$$\bar{Y} = \frac{P_1 - P_0}{P_0}$$

$$\hat{s}_0 = \frac{5}{6}(P_\perp + P_\parallel) \Big/ \frac{H_0^2}{4\pi}$$

$$s_0 = \frac{5}{3} P_0 \Big/ \frac{H_0^2}{4\pi}$$

$$\bar{s}_0 = \frac{1}{3} \frac{P_\parallel(2 + \cos^2\Theta_0) + P_\perp(2 + \sin^2\Theta_0)}{H_0^2/4\pi} = s_0 + \frac{2}{5}\Delta s(1 - 2\cos^2\Theta_0)$$

$$\Delta s = \frac{5}{3} \frac{P_\parallel - P_\perp}{H_0^2/4\pi}$$

$$\ell = (H_{y,1} - H_{y,0}) / |H_0|$$

$$\bar{\ell} = \ell + \frac{3}{5} \sin\Theta_0 \, \Delta s$$

(32)

$$b_n = \frac{H_n}{\sqrt{4\pi\rho}}$$

$$\bar{b}_n = b_n \left(1 - \frac{P_\parallel - P_\perp}{H^2/4\pi}\right)^{1/2}$$

$$\eta = \rho_1 / \rho_0$$

$$\bar{\eta} = (\rho_1 - \rho_0)/\rho_0$$

92

Now we shall compile all the important relationships in the reference system B_0, using the coordinate system K_0, in accordance with Eqs. (11), (12), (13), (14), (15), (17) and (23):

$$\rho_0 V_{n,0} = \rho_1 V_{n,1} \tag{33a}$$

$$M V_{n,0} + P_0 + H_{y,0}^2 / 8\pi = M V_{n,1} + P_1 + H_{y,1}^2 / 8\pi \tag{33b}$$

$$M V_{y,0} + \tfrac{1}{2}(P_\parallel - P_\perp)\sin 2\Theta_0 - \frac{H_n H_{y,0}}{4\pi} = M V_{y,1} - \frac{H_n H_{y,1}}{4\pi} \tag{33c}$$

$$V_{n,0} H_{y,0} - V_{y,0} H_n = V_{n,1} H_{y,1} - V_{y,1} H_n = 0 \tag{33d}$$

$$H_{n,0} = H_{n,1} = H_n \tag{33e}$$

$$M\tfrac{1}{2}(V_{n,0}^2 + V_{y,0}^2) + \tfrac{1}{2}V_{n,0}(P_{11} + 2P_{\perp}) + V_{n,0}\,P_0$$

$$+ V_{y,0}\,\tfrac{1}{2}(P_{11} - P_{\perp})\sin 2\Theta_0 + V_{n,0}\,\frac{H_{y,0}^2}{4\pi} - V_{y,0}\,\frac{H_{y,0}H_n}{4\pi} \tag{93}$$

$$= M\tfrac{1}{2}(V_{n,1}^2 + V_{y,1}^2) + \tfrac{5}{2}V_{n,1}P_1 + V_{n,1}\,\frac{H_{y,1}^2}{4\pi} - V_{y,1}\,\frac{H_{y,1}H_n}{4\pi} \tag{33f}$$

$$-[H] = \sum_{\mu} \frac{n_\mu}{n}\left[\log \frac{P_{11,\mu}^{1/2}\,P_{\perp,\mu}}{n_\mu^{5/2}}\right] \geq 0 \tag{33g}$$

The inequality $V_n \geq 0$ in Figure 2 involves no loss of generality. It is seen from the equation system (33) that θ_0 can be limited to $0 \leq \theta_0 \leq 90°$ without any significant loss of generality.

Now, we can use the given magnitudes to calculate, for instance, $\bar{\eta}$. For this purpose, we start out by eliminating $V_{y,0}$ and $V_{y,1}$ by means of Eq.(33d). Subsequently, we eliminate P_1, and finally, we use Eq. (33a) to eliminate $V_{n,1}/V_{n,0}$. After some calculation, we obtain

$$\bar{\eta}^2\left(2\sin\Theta_0\,\bar{\bar{s}}_0 - \frac{2}{5}\sin\Theta_0\,\Delta s - \frac{2}{3}h\right) \tag{34}$$

$$+\bar{\eta}\left(\frac{5}{3}\sin\Theta_0\,h^2 + 2(1-\bar{\bar{s}}_0)h + \frac{2}{5}\Delta s\sin\Theta_0\cos^2\Theta_0\right)$$

$$-h\left(h^2 + 2\sin\Theta_0\left(1 - \frac{1}{5}\Delta s\right)h - \frac{4}{5}\Delta s\cos^2\Theta_0\right) = 0$$

When we selected the denotations and definitions, we assumed that $\bar{\eta}$ and h should not be defined differently than in the paper by Bazer and Ericson [1958]. $\bar{\bar{s}}_0$, s_0, and $\hat{s}_0$ were selected so that in the case where $\Delta s = 0$, $\bar{\bar{s}}_0 = \hat{s}_0 = s_0$ merge into s_0 as defined by Bazer and Ericson. Moreover, $\bar{\bar{s}}_0$ was so selected that Eq. (34) will deviate as little as possible from its form in the case of $\Delta s = 0$. 94

Solution with respect to $\bar{\eta}$ will yield the following from Eq. (34):

$$\bar{\eta} = \frac{-\frac{5}{6}\sin\Theta_0\,\bar{k}^2 - (1-\bar{s}_0)\bar{k} - \frac{1}{5}\Delta s \sin\Theta_0\cos^2\Theta_0 \pm \sqrt{\bar{k}^2 R}}{2\sin\Theta_0\,\bar{s}_0 - \frac{2}{3}\bar{k} - \frac{2}{5}\sin\Theta_0\,\Delta s} \tag{35}$$

where

$$R\bar{k}^2 = \left(\frac{5}{6}\sin\Theta_0\,\bar{k}^2 + (1-\bar{s}_0)\bar{k} + \frac{1}{5}\Delta s \sin\Theta_0\cos^2\Theta_0\right)^2$$

$$+\left(\left(2\sin\Theta_0\,\bar{s}_0 - \frac{2}{5}\sin\Theta_0\,\Delta s\right)\bar{k} - \frac{2}{3}\bar{k}^2\right)\cdot$$

$$\cdot\left(\bar{k}^2 + \left(2\sin\Theta_0 - \frac{2}{5}\sin\Theta_0\,\Delta s\right)\bar{k} - \frac{4}{5}\Delta s\cos^2\Theta_0\right)$$

Now, we shall calculate the other jump relations. Using Eqs. (33a) through (33d), we obtain

$$\bar{Y} = \frac{5}{3}\frac{1}{s_0}\left\{-\frac{1}{2}\bar{k}^2 + \bar{k}\,\frac{\bar{\eta}/\bar{k} - \sin\Theta_0 + \frac{\bar{k}-\bar{k}}{\bar{k}}\frac{\bar{\eta}}{\bar{k}}\cos^2\Theta}{1 - \frac{\bar{\eta}}{\bar{k}}\sin\Theta_0}\right\} \tag{36}$$

/95

Moreover,

$$\frac{V_{n,1}}{b_{n,1}} = \eta^{-1/2}\,\frac{V_{n,0}}{b_{n,0}} = \left(\frac{\bar{k} - \bar{\eta}\sin\Theta_0}{\bar{k}}\right)^{-1/2} \tag{37}$$

$$\frac{[u_n]}{b_{n,1}} = \frac{[V_n]}{b_{n,1}} = -\bar{\eta}\left(\bar{k} - \frac{\bar{\eta}\sin\Theta_0}{\bar{k}}\right)^{-1/2} \tag{38}$$

$$\frac{[u_y]}{b_{n,1}} = \frac{[V_y]}{b_{n,1}} = \frac{\bar{k}}{\cos\Theta_0}\left(\bar{k} - \frac{\bar{\eta}\sin\Theta_0}{\bar{k}}\right)^{+1/2} \tag{39}$$

We selected b_n instead of $\bar{b}_n$ as reference velocities in Eqs. (37) through (39) in order to have a reference velocity which is independent of anisotropy. This will facilitate discussion of the effect of anisotropy on the velocities and velocity jumps.

3. Discussion of the Jump Relations of Collinear Shock Waves in an Anisotropic Plasma

/96

3.1. Introduction

The following chapter is devoted to the jump functions for collinear shock waves. We shall confine ourselves to plasma states on the front side of the shock wave which are stable against fire hose instability and reflected instability in their most unfavorable case. This means that a permissible region is defined in the Δs, $\bar{\bar{s}}_0$-plane. This region is defined by the conditions $P_{//} - P_{\perp} \leq \underline{H}_0^2/4\pi$ according to the stability criterion for fire hose instability, $P_{\perp} - P_{//} \leq (P_{//}/P_{\perp})\, \underline{H}_0^2/8\pi$ for reflected instability, and $P_{\perp} \geq 0$, $P_{//} \geq 0$. The boundaries are mildly dependent on θ_0, since $\bar{\bar{s}}_0$ depends slightly on θ_0. They are represented by solid lines in Figure 6 which originate from the zero point. The boundary curves for $\Delta s < 0$ correspond to the reflection instability boundary. The solid straight lines at $\Delta s > 0$ which are numbered by different angles, correspond to the relationship $P_{\perp} = 0$. When the point $\Delta s = 5/3$ is reached, the boundary line makes a bend and merges into the straight line that defines the instability boundary of fire hose instability. The additional requirement of quasistability toward other types of plasma instability requires special treatment and shall be neglected here.

Now, we must still define the solutions which we wish to consider permissible. Comparable to the definition used in the paper by Bazer and Ericson [1958], we can start out with the requirement that the plasma state in the rear of the shock wave has a steady-state dependence on the state prevailing in front of the shock wave and on a strength parameter. In the case of the Alfvén shock waves this requirement will lead to difficulties since the rotational angle between $\underline{H}_{tr_0}$ and $\underline{H}_{tr_1}$ is entirely random.

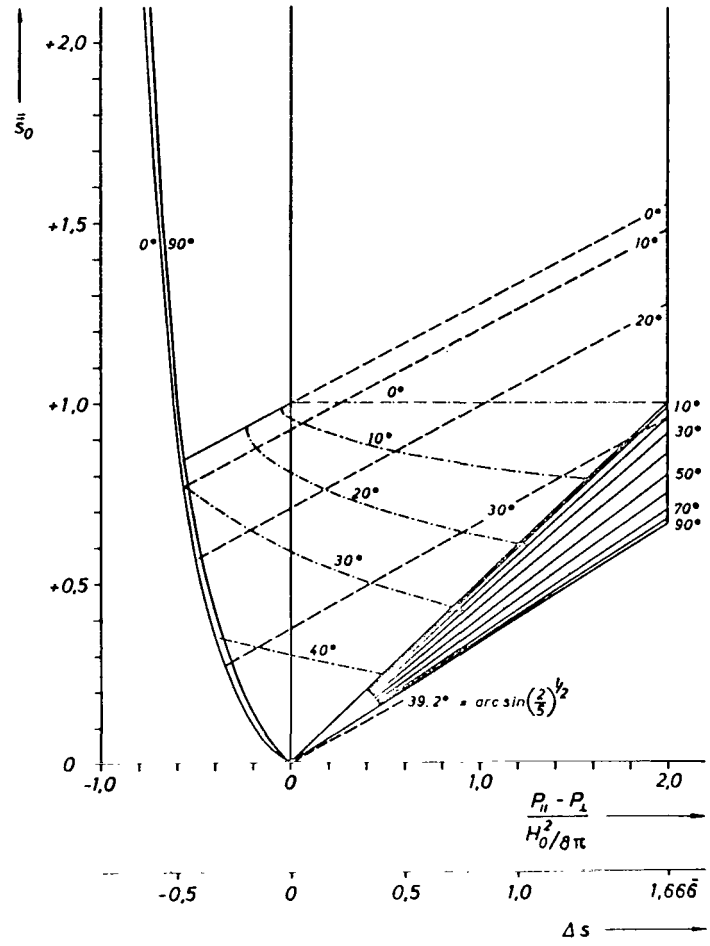

Figure 6. Boundary lines of the different shock wave types according to Section 3.3 within the limits defined by the fire hose instability, reflection instability, and $P_{\perp} \geq 0$. The curve parameter is θ_0.

The entropy condition is the second condition for shock waves that are dominated by collisions so that they have Maxwellian distributions on both sides, with equal temperatures for all particle types. The entropy change can be calculated precisely from the pressure and density prevailing on both sides of the shock wave so that an accurate answer to the permissibility question is possible. In our case, it is not possible to state any relationship which is as strictly defined as the classical entropy condition. After

all, the inequalities (33g) and (23) had been derived from Eq. (20) under very specific conditions that were of interest according to the observations made. In order to characterize the thermal motions we had stipulated (isotropic) Maxwellian distributions in the rear of the shock wave, and anisotropic Maxwellian distributions in front. Now, if we maintain only the isotropy in the rear of the shock wave and the stipulation that $q_{n,\,0} = 0$ in front, the Vlasov equation under known $P_\perp$, $P_{//}$, ρ_0 and P_1 and ρ_1 will permit an infinite number of different distribution functions that are quasistable in themselves and all of which yield different values of $\left[\sum_\mu \int f_\mu v_\cdot \log f_\mu \, dv\right]$ according to Eq.(20). Consequently, $P_\perp$, $P_{//}$, ρ_0, P_1, ρ_1 alone will not be sufficient to decide whether the inequality $\left[\sum_\mu \int f_\mu v_\cdot \log f_\mu \, dv\right] \gtrless 0$ is satisfied. On the other hand, the discussion of the arguments in favor of isotropy has shown that (isotropic) Maxwellian distributions are probable in the rear of the shock wave. However, the question as to the partial pressures of the individual particle types remains open. If we assume anisotropic Maxwellian distributions on the front side we will obtain inequations (23) and (33g). As far as the solar wind relationships are concerned that correspond to the earth's shock wave, it is a natural assumption, based on the observation acquired from Pioneer 6 that was cited in Section 2.4, that the electrons have adiabatic behavior in the sense of $-[\hat{H}]_{El} = 0$. In that case, we will find the following for the electron pressure behind the shock wave region:

$$P_{1,\,El.} = \left(P_{\perp,\,El.}\right)^{2/3} \left(P_{//,\,El.}\right)^{1/3} (1+\bar{\eta})^{5/3} \qquad (40a)$$

/99

We can now calculate the ionic pressure that must be inserted in (33g) on the basis of $P_{1,\,ion} = P_1 - P_{1,\,El.}$

If, by way of another example for the front side, we assume that

$$P_{\perp,El.}/P_{//,El.} = P_{\perp,Ion}/P_{//,Ion} \qquad \text{in addition to}$$

$$P_{\perp,El.}/P_{1,El.} = P_{\perp,Ion}/P_{1,Ion} \qquad \text{and hence also}$$

$$P_{//,El.}/P_{1,El.} = P_{//,Ion}/P_{1,Ion}$$

we will obtain

$$-[H] = -\,\ell\,[\hat{H}]_{Ion} \gtrless 0 \qquad (40b)$$

$-[\hat{H}]_{ion}(h)$ has been plotted in Figure 16 for the example where $\theta_0 = 45°$, $\bar{\bar{s}}_0 = 1.0$ and for different ratios of $P_{\parallel}/P_{\perp}$, and in Figure 23 for $\theta_0 = 20°$ and $\bar{\bar{s}}_0 = 0.5$. Here it applies that

$$-[\hat{H}]_{Ion} = -\tfrac{1}{2}[H] = \log\left(\frac{P_1^{3/2}}{P_\perp P_\parallel^{1/2}}\left(\frac{\rho_0}{\rho_1}\right)^{5/3}\right) \tag{41}$$

Measurements and the theory show that we cannot expect the same ratio of anisotropic pressure components for electrons and ions in solar wind. However, the figures cited above were intended merely to serve as an example for a possible variation of $-[H] = -2[\hat{H}]_{ion}$. Consequently, when we use (33g), the location of the interesting point where it applies that $-[H] = 0$ and which yields a boundary between permissible and nonpermissible solutions, also /100 depends on the distribution of the pressures of the individual particles between the total pressure $P_\perp$, $P_\parallel$, and P_1. Therefore, we must make additional stipulations from one case to another in order to apply the generalized entropy relationship. We can even state that, for a given $P_\perp$, $P_\parallel$, and ρ_0, and with a calculated P_1 and ρ_1, we can always achieve that the inequation (33g) is satisfied by making a suitable selection of additional stipulations on the distribution into different partial pressures. Therefore, we shall drop the generalized entropy condition from our further considerations in this chapter.

3.2. Mathematical Characteristics of the Step Functions of Collinear Shock Waves in an Anisotropic Plasma /101

3.2.1. Generalized Shock Waves Under Arbitrary θ_0

In our discussion of step functions we shall consider primarily the function $\bar{\eta}(h)$ under fixed θ_0, $\bar{\bar{s}}_0$ and Δs. We shall keep in mind that we are limiting θ_0 to $0 \leq \theta_0 \leq 90°$. Since the other step functions are defined relatively simply by $\bar{\eta}$ and h on the basis of Eqs. (36) through (39), we can clarify their characteristics at the same time.

First, because of $\rho_1 \geq 0$ it must apply that $\bar{\eta} \geq -1$, where $\bar{\eta} \to -1$ is usually subject to $V_{n,\,0} \to 0$.

Moreover, because of $P_1 \geq 0$ it must also apply that $\bar{Y} \geq -1$. According to Eq. (36), this condition in the h, $\bar{\eta}$-plane defines a boundary curve which is dependent on θ_0, Δ_s and $\bar{\bar{s}}_0$, respectively s_0. This curve is determined by

$$\bar{\eta} = h \frac{h^2 + 2h \sin\Theta_0 - \frac{6}{5} s_0}{h^2 \sin\Theta_0 + 2h - \frac{6}{5} s_0 \sin\Theta_0 + \frac{6}{5} \cos^2\Theta_0 \sin\Theta_0 \Delta s} \qquad (42a)$$

Any discussion of the curves $\bar{\eta}(h; \Theta_0, \Delta s, \bar{s}_0)$ which would allow for the requirement that $\bar{Y} \geq -1$ would lead to an excessively great number of distinctions between different cases, since this boundary curve is relatively complicated. Therefore, the curves $\bar{\eta}(h; \Theta_0, \Delta s, \bar{s}_0)$ to be discussed in this Section 3.2. shall be treated by analytical means without allowing for the condition that $\bar{Y} \geq -1$.

However, in order to acquire some rapid statements on the profile of $\bar{Y}$, we shall list some of the results acquired from (36). $\bar{Y} = 0$ is satisfied on the curve /102

$$\bar{\eta} = h^2 \frac{h + 2 \sin\Theta_0}{2h + h^2 \sin\Theta_0 + \frac{6}{5} \Delta s \sin\Theta_0 \cos^2\Theta_0} \qquad (42b)$$

Moreover, the relationship $\frac{\partial \bar{Y}}{\partial \bar{\eta}}(\bar{\eta}, h)$ is of interest:

$$\frac{\partial \bar{Y}}{\partial \bar{\eta}} = \frac{5}{3} \frac{1}{s_0} \frac{\cos^2\Theta_0}{\left(1 - \frac{\bar{\eta}}{h} \sin\Theta_0\right)^2} \frac{\bar{h}}{h} \qquad (42c)$$

Hence,

$$\begin{aligned} &\frac{\partial \bar{Y}}{\partial \bar{\eta}} > 0 \text{ for } h > \text{Max } (0, -3/5 \sin\Theta_0 \Delta s) \\ &\quad \text{and } h < \text{Min } (0, -3/5 \sin\Theta_0 \Delta s) \\ &\frac{\partial \bar{Y}}{\partial \bar{\eta}} < 0 \text{ for } \text{Min } (0, -3/5 \sin\Theta_0 \Delta s) < h < \text{Max} \end{aligned} \qquad (42d)$$

Another interesting relationship is $Y(\bar{\eta} = 0, h \neq 0)$

$$\bar{Y}(\bar{\eta} = 0, h \neq 0) = -\frac{5}{3} \frac{1}{s_0} \left(\frac{1}{2} h^2 + h \sin\Theta_0\right) \qquad (42e)$$

This can be used to calculate the value of $\bar{Y}$ at a zero point $h \neq 0$ of $\bar{\eta}(h)$. In addition, we calculate

$$\bar{Y}(h = 0, \bar{\eta} \neq 0) = -\frac{\Delta s}{s_0} \cos^2\Theta_0 \qquad (42f)$$ /103

Finally, we can transform Eq. (36) with the aid of Eq. (34):

$$\bar{Y} = \frac{5\bar{\eta}}{3 - \bar{\eta}} + \frac{5}{3 s_0} \frac{\frac{1}{2} h^2 \bar{\eta} - \frac{3}{5} \Delta s \left(h \sin\Theta_0 + (3\cos^2\Theta_0 - 1)\bar{\eta} + 2\cos^2\Theta_0\right)}{3 - \bar{\eta}} \qquad (42g)$$

This relationship represents a generalization of the Hugoniot relation for a shock wave in gas dynamics which is defined exactly by the first term $5\,\bar{\eta}/(3-\bar{\eta})$. In the case where $\Delta s = 0$, we obtain Eq. (77) of Bazer and Ericson [1958] with $\gamma = 5/3$. From this we can see immediately that in the case of a random compressive shock wave in an isotropic plasma with finite $\bar{\bar{s}}_0$ a given density ratio expressed by $\bar{\eta}$ is always associated with a greater relative pressure jump $\bar{Y}$ than the corresponding shock wave in gas dynamics. In the case of the anisotropic plasma this relationship applies only to part of the shock wave solutions.

These relationships make it considerably easier to establish the profile of $\bar{Y}(h)$.

Another condition that must be taken into consideration for an investigation of $\bar{\eta}(h)$ is given by Eqs. (37) through (39). The radicand of the roots occurring there must not be negative. This requires that

$$(h - \bar{\eta} \sin \theta_0)/\bar{h} \geq 0$$

This requirement excludes certain regions of the h, $\bar{\eta}$-plane that are marked by the absence of shading in Figure 7. In the following discussion of $\bar{\eta}(h)$ we shall allow for the condition that $(h - \bar{\eta} \sin \theta_0) / \bar{h} \geq 0$. Moreover, the curve in the h, $\bar{\eta}$-plane on which it applies that $V_{n,1} = b_{n,1}$, is of interest for the enumeration of the characteristics of different shock wave types. In general, it applies for a curve having a certain value of $V_{n,1}/b_{n,1}$ that:

∠104

$$\bar{\eta} = -\frac{3}{5}\Delta s + \frac{1 - b_{n,1}^2/V_{n,1}^2}{\sin \theta_0}\,\bar{h} \qquad \text{∠105}$$

$$= -\frac{3}{5}\Delta s\left(\frac{b_{n,1}}{V_{n,1}}\right)^2 + \frac{1 - b_{n,1}^2/V_{n,1}^2}{\sin \theta_0}\,h$$

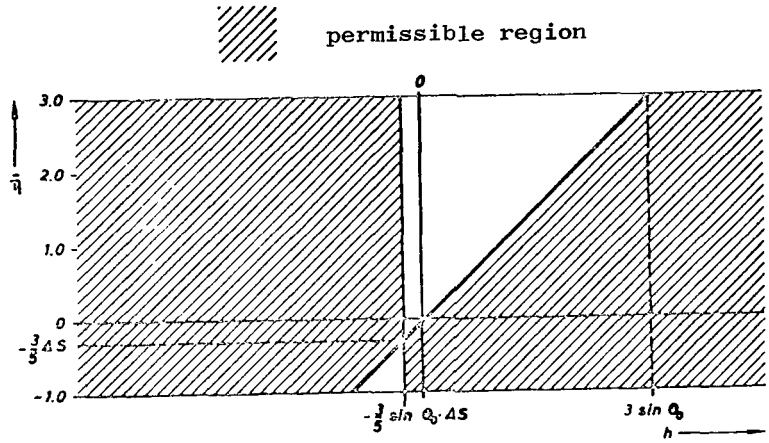

Figure 7. Permissible regions of the h, $\bar{\eta}$-plane, based on the condition that $(h - \bar{\eta}\sin\theta_0)/\bar{h} \geq 0$.

Consequently, we are dealing with straight lines in the h, $\bar{\eta}$-plane. Consequently, it applies for the line with $V_{n,1}/b_{n_\perp 1} = 1$ that $\bar{\eta} = -3/5\,\Delta s$. Hence, $V_{n,1}$ is greater than $b_{n,1}$ when it applies that $\bar{\eta} > -3/5\,\Delta s$ and $\bar{h} > 0$, and when $\bar{\eta} < -3/5\,\Delta s$ and $\bar{h} < 0$ are satisfied. This of course excludes the forbidden regions. $V_{n,1} \leq b_{n,1}$ applies in the other permissible regions. /105

Figures 10 through 23, representing the step functions for $\bar{\bar{s}}_0 = 1.0$, $\theta_0 = 45°$, and for $\bar{\bar{s}}_0 = 0.5$, $\theta_0 = 20°$ and three different ratios $P_{//}/P_\perp$ each, shall serve to illustrate the discussion in this chapter. The conditions that $\bar{\eta} \geq -1$, $\bar{Y} \geq -1$ and that $(h - \bar{\eta}\sin\theta_0)/\bar{h} \geq 0$ are satisfied in these figures.

We shall start out with a discussion of $\bar{\eta}(h;\ \theta_0,\ \Delta s,\ \bar{\bar{s}}_0)$. Eq. (34) shows that a given value of h is associated either with no real value of $\bar{\eta}$ or with two real values. On the other hand, any value of $\bar{\eta}$ is associated either with one or with three real values of h.

In the case of large values of h, Eq. (35) will yield the asymptotic formula

$$\bar{\eta} \approx h\left\{\frac{5}{4}\sin\theta_0 \mp \frac{5}{4}\sqrt{\Delta s^2\theta_0 - \frac{24}{25}}\right\} \qquad (43)$$

Consequently, in the case where $\theta_0 < \theta_{crit}$=arc sin $\sqrt{24/25}$ = 78.5°, the root expression in Eq. (35) will become imaginary if $|h|$ is adequately great. In the case of $\theta_0 \geq \theta_{crit}$, the first term of the curly bracket is entirely predominant, while $\bar{\eta} \to \infty$, applies where $h \to \infty$, and $\bar{\eta} \to -\infty$ where $h \to -\infty$. The second case is not permissible because of $\bar{\eta} \geq -1$. Moreover, the requirement that all other step functions must be real, too, implies that the case where $\bar{\eta} \to +\infty$ is impossible. In order to demonstrate this, we shall again consider the root expression occurring in Eqs. (37) through (39). The radicand reads $(h - \bar{\eta} \sin \theta_0)/\bar{h}$. It must not become negative. The permissible regions in this respect in the $\bar{\eta}$, h-plane are represented in Figure 7 for the case where $-1 \leq \bar{\eta} \leq +3$ only. Of course, the permissible regions with positive $(h - \bar{\eta} \sin \theta_0)/\bar{h}$ extend into the infinite just as the nonshaded forbidden regions do. Now we can see that the asymptotic boundary curve of $\bar{\eta}$ for $h \to \infty$ as defined by Eq. (43) is located within the forbidden region under any value of $\theta_0 \geq \theta_{crit}$. Consequently, h has an upper and lower limit under any angle. /106

Now, we can even show that $\bar{\eta} \leq 3$ must apply. For this purpose, we start out by proving that $\bar{\eta} \to +\infty$ is not possible for finite values of h, either, since h would then be located within the forbidden region. According to Eq. (35), it will apply for numerators other than zero that $\bar{\eta} \to \pm\infty$ when $h \to h_p = 3 \sin \theta_0 \bar{\bar{s}}_0 - 3/5 \sin \theta_0 \Delta s$ or when $\bar{h} \to \bar{h}_p = 3 \sin \theta_0 \cdot \bar{\bar{s}}_0$. Because of $\bar{h}_p > 0$ where $\theta_0 \neq 0$ and $\bar{\bar{s}}_0 \neq 0$, the pole will always be located within the forbidden region. The cases where $\theta_0 \to 0$ and $\bar{\bar{s}}_0 \to 0$ are limiting cases which we shall consider later.

Now, where does the branch of curve $\bar{\eta}(h)$ lead which is inbound from the infinite? In the case where $\theta_0 \geq \theta_{crit}$, it could run along one of the curves defined by Eq. (43), disappearing again in the infinite without departing from the forbidden region. However, our special interest is devoted to the points where the boundary lines of the forbidden region are intersected or only touched by curves. First, we substitute $\bar{\eta} = h/\sin \theta_0$ in Eq. (34) and stipulate that $\theta_0 \neq 90°$. /107

Three solutions are obtained:

$$\sin\Theta_0\,\bar{\eta}-\bar{h}=0 \quad \text{for} \begin{cases} \bar{h}_{Y_1}=3\sin\Theta_0\,, & \bar{\eta}=3 \\ \bar{h}_{Y_2}=-\frac{3}{5}\Delta s\sin\Theta_0\,, & \bar{\eta}=-\frac{3}{5}\Delta s \\ \bar{h}_{Y_3}=0\,, & \bar{\eta}=0 \end{cases} \tag{44}$$

$\bar{h} = 0$ applies at the point where $h = h_{Y_2}$, since this is the intersection of the boundary lines. Now we seek the second value of $\bar{\eta}$ where $\bar{h} = 0$. Based on Eq. (34), we obtain:

$$\bar{h}=0 \text{ for } \begin{cases} \bar{\eta}=-\frac{3}{5}\Delta s \\ \bar{\eta}=\frac{\Delta s}{10\,\bar{\bar{s}}_0}\left(6-3\Delta s\sin^2\Theta_0-2\cos^2\Theta_0\right) \end{cases} \tag{45}$$

Even in the most disadvantageous case, both values of $\bar{\eta}$ are located far below 3. Consequently, a curve point can never be located on the boundary line $\bar{h} = 0$ when $\bar{\eta} \geq 3$. According to Eq. (44), there is no curve point on the straight line $\bar{\eta} = h/\sin\theta_0$ when $\bar{\eta} > 3$. The point $\bar{\eta} = 3$, $h = 3\sin\theta_0$ is the only curve point on the boundary line when $\bar{\eta} \geq 3$. Now, if we substitute $\bar{\eta} = +3$ in Eq. (34), we will obtain the following when we solve the system with respect to h: /108

$$\bar{h}_{1,2}(\bar{\eta}=+3)=\frac{1}{5}\sin\Theta_0\,\Delta s\pm\left(\frac{1}{25}\sin^2\Theta_0(\Delta s)^2-6\,\bar{\bar{s}}_0+\frac{2}{5}\Delta s\left(2+\sin^2\Theta_0\right)\right)^{1/2} \tag{46}$$

These two zero points of $\bar{\eta}(h) = 3$ are complex for the permissible region of the Δs, $\bar{\bar{s}}_0$-plane. The straight line $\bar{\eta} = 3$, consequently, is intersected at only one point in every instance.

After these preliminary steps, we are now ready to show that $\bar{\eta} > 3$ is impossible. First, the region between $\bar{h} = 0$ and $\bar{\eta} = h/\sin\theta_0$ is forbidden because of $(h - \bar{\eta}\sin\theta_0)/\bar{h} < 0$. There are no curve points on the boundary lines $\bar{h} = 0$ and $\bar{\eta} = 3$ as well as $\bar{\eta} = h/\sin\theta_0$, except for $h = 3\sin\theta_0$, that would be compatible with Eq. (34) when $\bar{\eta} \geq 3$. Since there is no pole in the region $\bar{\eta} > 3$, $\bar{h} < 0$, while it is impossible for any curve branch to be inbound from infinity because of Eq. (43), this region could contain a closed

curve only. Assuming that there is such a curve, the mean of two $\bar{\eta}$-values under a certain value of h on this curve would have to be greater than three. If we write Eq. (34) in the form

$$a\,\bar{\eta}^2 + b\,\bar{\eta} + c = 0 \tag{47}$$

it would have to apply, therefore, that $-b/2a > 3$. If we use the Eq. (34) to define a and b, we can easily show that the curve $-b/2a$ (h) is certainly not located within the region under consideration here. Consequently, no part of the curves described by Eq. (34) can be located within this region. There remains only the region where $\bar{\eta} > 3$ and $h > \bar{\eta} \sin \theta_0$, that is to the right of $\bar{\eta} = h/\sin \theta_0$. No part of any curve can extend from infinity into this region, because of Eq. (43). Nor is it possible, except via the point $\bar{\eta} = 3$, $h = 3 \sin \theta_0$ /109 that any curve branch could reach this region by passing through the boundary lines $\bar{\eta} = +3$ and $\bar{\eta} = h/\sin \theta_0$. It is impossible for any curve branch to reach this region via $\bar{\eta} = 3$, $h = 3 \sin \theta_0$ because in that case it could depart from this region only via $\bar{\eta} = 3$, $h = 3 \sin \theta_0$, and because Eq. (46) states that, where $h = 3 \sin \theta_0$, $\bar{\eta} = 3$, it is never possible for a double root of Eq. (34) to be oriented other than with a vertical tangent. As a result, we obtain the important inequation

$$-\infty \leq \frac{d\bar{\eta}}{dh}\left(h = 3 \sin \theta_0,\ \bar{\eta} = 3\right) \leq 0 \tag{48}$$

or

$$\frac{1}{\sin \theta_0} \leq \frac{d\bar{\eta}}{dh}\left(h = 3 \sin \theta_0,\ \bar{\eta} = 3\right) \leq +\infty$$

This formula states, in other words, that the curve branch incoming from $\bar{\eta} < 3$ and passing through $\bar{\eta} = 3$, $h = 3 \sin \theta_0$ must be originating in the permissible region. Therefore, the only remaining possibility for the region where $\bar{\eta} > 3$ and $h > \bar{\eta} \sin \theta_0$ is that of a closed curve. That such a curve is impossible can be shown by means of Vieta's root theorem. For this purpose, we rewrite Eq. (34) in order to obtain a determining equation for h under a given value of $\bar{\eta}$:

$$
\begin{aligned}
&\bar{h}^3 \\
&+ \bar{h}^2 \left(2 \sin\Theta_0 \left(1 - \tfrac{1}{5}\Delta\bar{s}\right) - \bar{\eta}\,\tfrac{5}{3}\sin\Theta_0\right) \\
&+ \bar{h}\left(\tfrac{2}{3}\bar{\eta}^2 - 2\left(1 - \bar{\bar{s}}_0\right)\bar{\eta} - \tfrac{4}{5}\Delta\bar{s}\,\cos^2\Theta_0\right) \\
&- 2\sin\Theta_0\left(\bar{\bar{s}}_0 - \tfrac{1}{5}\Delta\bar{s}\right)\bar{\eta}^2 - \tfrac{2}{5}\Delta\bar{s}\sin\Theta_0\cos^2\Theta_0\,\bar{\eta} = 0
\end{aligned}
\tag{49}
$$

Let $\bar{\eta}$ be a certain value on the assumed closed curve, and h_1, h_2, h_3 the associated h-values where $h_1 < h_2 < h_3$. h_1 must be located in the forbidden region. Since the curve is closed, it is impossible that only one real root exists. Consequently, all the roots must be real. According to Vieta's root theorem it applies that /110

$$
\bar{h}_1 + \bar{h}_2 + \bar{h}_3 = \sin\Theta_0\left\{\tfrac{5}{3}\bar{\eta} - 2 + \tfrac{2}{5}\Delta\bar{s}\right\}
$$

Consequently,

$$
\left(\bar{h}_1 + \tfrac{3}{5}\Delta\bar{s}\sin\Theta_0\right) + \left(\bar{h}_2 - \bar{\eta}\sin\Theta_0\right) + \left(\bar{h}_3 - \bar{\eta}\sin\Theta_0\right)
$$

$$
= \sin\Theta_0\left\{-\tfrac{1}{3}\bar{\eta} - 2 + \Delta\bar{s}\right\}
$$

Since there are no curve points in existence where $\bar{\eta} > 3$ and $\bar{h} \leq 0$, the first round bracket must be positive. The two other round brackets must be positive, too, since they are supposed to be located on the closed curve in the region where $h > \bar{\eta}\sin\theta_0$. Consequently, the entire left-hand side must be positive. On the other hand, because of $\bar{\eta} > 3$ and $\Delta s \leq 5/3$ the left-hand side is certain to be negative and smaller than $-4/3 \sin\theta_0$. This is a contradiction. It is impossible that a closed curve could exist in the region under consideration.

Hence, we have shown that $\bar{\eta} > 3$ is impossible because either the curve $\bar{\eta}(h)$ is located within the forbidden region or because there is no solution of Eq. (34) in the permissible regions. Moreover, Eqs. (36) through (39) show that /111 it applies for $h = 3\sin\theta_0$, $\bar{\eta} = 3$ that $\bar{Y} \approx +\infty$, $V_{n,1}/b_{n,1} = +\infty$, $V_{n,0}/b_{n,0} = +\infty$, $[u_n]/b_{n,1} = +\infty$, and that $[u_y]/b_{n,1} = 0$.

The next step is to vary the magnitudes Δs, $\bar{\bar{s}}_0$ and θ_0 and to determine when the curve branch passing through $h = 3 \sin \theta_0$, $\bar{\eta} = 3$ will have a vertical tangent. Obviously, this corresponds to the transition of the regions of the two inequalities (48).

According to Eq. (47), the following applies to $d\bar{\eta}/dh$:

$$\frac{d\bar{\eta}}{dh} = - \frac{\bar{\eta}^2 a' + \bar{\eta} b' + c'}{2\bar{\eta} a + b} \tag{50}$$

The prime marks denote derivatives with respect to h. Consequently, $d\bar{\eta}/dh = \pm\infty$ shall apply at the point where $h = 3 \sin \theta_0$, $\bar{\eta} = 3$. Hence, we obtain the equation $6 \cdot a(h = 3 \sin \theta_0) + n(h = 3 \sin \theta_0) = 0$. This equation will yield

$$\bar{\bar{s}}_0 = 1 - \frac{5}{2} \sin^2 \theta_0 + \Delta s \left(\frac{1}{3} + \frac{1}{15} \sin^2 \theta_0\right) \tag{51a}$$

This relationship is represented as a dotted curve in Figure 6 where it is plotted for different values of θ_0. Together with Eq. (48) we obtain, moreover,

$$-\infty < \frac{d\bar{\eta}}{dh}(\bar{\eta} = 3, h = 3 \sin \theta_0) \leq 0 \tag{51b}$$

where

$$\bar{\bar{s}}_0 < 1 - \frac{5}{2} \sin^2 \theta_0 + \Delta s \left(\frac{1}{3} + \frac{1}{15} \sin^2 \theta_0\right)$$

and

$$\frac{1}{\sin \theta_0} < \frac{d\bar{\eta}}{dh}(\bar{\eta} = +3, h = 3 \sin \theta_0) \leq +\infty \tag{51c}$$

where

$$\bar{\bar{s}}_0 \geq 1 - \frac{5}{2} \sin^2 \theta_0 + \Delta s \left(\frac{1}{3} + \frac{1}{15} \sin^2 \theta_0\right)$$

Similar to Bazer and Ericson [1958], we shall use these inequalities in Section 2.3. in order to classify the M_f shock waves.

Now, we shall clarify the further progress of the curve branch passing through $h = 3 \sin \theta_0$ and $\bar{\eta} = 3$ in the case where $\bar{\eta} < 3$. For this purpose, we start out by defining the zero points of $\bar{\eta}$. We substitute $\bar{\eta} = 0$ in Eq. (34) and obtain:

$$\bar{\eta} = 0$$

where

$$h_{01} = h_{Y_3} = 0 \tag{52}$$

$$h_{02} = -\sin\theta_0\left(1 - \frac{1}{5}\Delta s\right) - \sqrt{\sin^2\theta_0\left(1 - \frac{1}{5}\Delta s\right)^2 + \frac{4}{5}\Delta s\cos^2\theta_0}$$

$$h_{03} = -\sin\theta_0\left(1 - \frac{1}{5}\Delta s\right) + \sqrt{\sin^2\theta_0\left(1 - \frac{1}{5}\Delta s\right)^2 + \frac{4}{5}\Delta s\cos^2\theta_0}$$

Here it applies that $h_{03} \geq h_{02}$. We can see that in the case where $\Delta s > 0$ $h_{03} > h_{01} = 0 > h_{02}$ and where $\Delta s < 0$, it applies that $h_{02} < h_{03} < h_{01} = 0$, provided we make the additional assumption that $\theta_0 < 90°$. The zero points depend only on θ_0 and on the anisotropy parameter Δs. In the case where $\Delta s = 0$, it applies simply that $h_{01} = 0$, $h_{02} = -2 \sin\theta_0$ and that $h_{03} = 0$. Consequently, a double zero point is located where $h = 0$. Moreover, we determine the $\bar{\eta}$-values for $h = 0$: <113

$$h = 0$$

where

$$\bar{\eta}_{01} = 0 \tag{53a}$$

$$\bar{\eta}_{02} = -\frac{\Delta s\cos^2\theta_0}{5\bar{\varsigma}_0 - \Delta s}$$

Now, what is the slope of the curve branch where it passes through $h = 0$, $\bar{\eta} = 0$? Based on Eq. (50), we find that

$$\frac{d\bar{\eta}}{dh}(h=0,\ \bar{\eta}=0) = -\frac{2}{\sin\theta_0} \tag{53b}$$

This result is not contradicted by the result obtained for $\Delta s = 0$. For, if we allow Δs to shift toward zero, the vicinity of $h = 0$, $\bar{\eta} = 0$, where the behavior described by (53b) is predominant will become continuously smaller, while at some distance from $h = 0$, $\bar{\eta} = 0$, the behavior applicable to $\Delta s = 0$ already becomes visible, where two derivatives exist for $h = 0$, $\bar{\eta} = 0$ because two curve branches pass through the point.

Using the Eqs. (52) and (53), we can now describe the curve profile in the region where $0 \leq \bar{\eta} \leq 3$, $h > 0$. Only one point in addition to $\bar{\eta} = +3$, $h = 3 \sin \theta_0$ is located on the boundary of this region. Moreover, if we apply Vieta's root theorem to Eq. (49), we will find that in the case where $3 \geq \bar{\eta} > \bar{\eta}_{02}$ /114 only a value $h > 0$ can exist in the permissible region defined by Figure 7 where $(h - \bar{\eta} \sin \theta_0)/\bar{h} \geq 0$, in addition to a value $\bar{\eta}$. In the case where $\bar{\eta} \leq \bar{\eta}_{02}$, no value or two values of $h \geq 0$ can exist in addition to a value $\bar{\eta}$. Of course, due to $\bar{\eta} \geq 0$ this case can occur only where $\Delta s < 0$.

Consequently, we have the following curve profile. In the case where $\Delta s \leq 0$ and where the inequation (51c) is applicable, the curve $\bar{\eta}(h)$ will proceed from $h = 3 \sin \theta_0$, $\bar{\eta} = 3$ via $h_{Y_2} = -3/5\, \Delta s \sin \theta_0$, $\bar{\eta} = -3/5\, \Delta s$ to $h = 0$, $\bar{\eta} = \bar{\eta}_{02}$. A minimum of $\bar{\eta}$ can occur. In the case where $\Delta s \leq 0$ and where the inequation (51b) is applicable, h will initially rise from $h = 3 \sin \theta_0$, $\bar{\eta} = 3$ passing through a maximum. Subsequently, passing through h_{Y_2}, $\bar{\eta} = -3/5\, \Delta s$ and to $h = 0$, $\bar{\eta}_{02}$, the boundary of the region is reached again. In the case where $\Delta s > 0$, the curve proceeds from $h = 3 \sin \theta_0$, $\bar{\eta} = 3$ via h_{03}, $\bar{\eta} = 0$. Extremes of h can occur on the way.

The region where $-1 \leq \bar{\eta} \leq 0$ and where $h > 0$ shall be discussed next. In conjunction with Eq. (49), Vieta's root theorem will show that one, and only one, point exists where $h > 0$ and $\bar{\eta} = -1$. Moreover, Vieta's root theorem when applied to Eq. (49) will show that, where $\Delta s > 0$, any one

$$\bar{\eta} < -\frac{1}{5} \quad \frac{\cos^2 \theta_0 \, \Delta s}{\bar{\zeta}_0 - \frac{1}{5} \Delta s} = \bar{\eta}_{02}$$

is associated with one, and only one, h-value where $h > 0$. In the case where $\bar{\eta} > \bar{\eta}_{02}$, one value of $\bar{\eta}$ is associated with no value of h or with two values of h.

Consequently, the following curve profiles are obtained. Two possibilities exist in the case where $\Delta s > 0$. In the first of these, the curve branch originating from h_{03}, $\bar{\eta} = 0$ departs from the region via the point where $\bar{\eta} = -1$. /115 Moreover, a curve branch exists that originates from $h = 0$, $\bar{\eta} = 0$, achieves a maximum point at h, and departs from the region via $h = 0$, $\bar{\eta}_{02}$. In the second possibility, the curve branch originating from h_{03}, $\bar{\eta} = 0$ passes through a minimum at point $\bar{\eta}$ where $\bar{\eta} \geq \bar{\eta}_{02}$, and departs from the region via the point where $h = 0$, $\bar{\eta} = 0$. A second branch proceeds from $h = 0$, $\bar{\eta}_{02}$ to the point where

$\bar{\eta} = -1$. The transition from one case to the other is made via two intersecting curve branches. This requires that a relationship between $\bar{\bar{s}}_0$, Δs, and θ_0 is satisfied. In the case where $\Delta s \leq 0$, one curve branch proceeds monotonely from $h = 0$, $\bar{\eta} = 0$ to a point where $\bar{\eta} = -1$. That part of this curve branch where $h < -3/5\ \Delta s \sin \theta_0$ is excluded, according to Figure 7, because it must apply that $da(h - \bar{\eta} \sin \theta_0)/\bar{h} > 0$.

Now, we shall study the region where $h < 0$. We had already obtained the following results for the boundaries of this region. According to Eq. (43), it is impossible for any curve branch to be incoming from infinity between points $\bar{\eta} = -1$ and $\bar{\eta} = +3$. There is no curve point on the straight line $\bar{\eta} = +3$ when $h < 0$. There are two curve points on the vertical straight line where $h = 0$, one at point $\bar{\eta}_{02}$ according to Eq. (53a), and the other at point $\bar{\eta} = 0$. In the latter case, the slope will always be $d\bar{\eta}/dh = -2/\sin \theta_0$. In the case where $\Delta s = 0$, these two curve points will coincide with $h = 0$ so that two curve branches will pass through $h = 0$, $\bar{\eta} = 0$. The straight line $\bar{\eta} = -1$ can contain one or two curve points when $h < 0$ in the case where $\Delta s \geq 0$, this being h_{02}, unless it applies at the same time that $\theta_0 = 0°$ and $\Delta s = 0$. In the case where $\Delta s < 0$ and where $\theta_0 \neq 90°$, we have two zero points $h_{02} < h_{03} < 0$ or none at all.

In the case where $\Delta s > 0$ we obtain one curve branch when $h \leq 0$. This branch starts out with the slope $d\bar{\eta}/dh = -2/\sin \theta_0$ at point $h = 0$, $\bar{\eta} = 0$, achieves a maximum in $\bar{\eta}$, and then passes through $h = h_{02}$, $\bar{\eta} = 0$. Subsequently, ∠116
there are two possibilities: in the first case, the curve branch passes through a minimum in $\bar{\eta}$ and terminates at point $h = 0$, $\bar{\eta} = \bar{\eta}_{02}$. In the second possible case, the curve branch originating from $h = h_{02}$, $\bar{\eta} = 0$ will terminate on the straight line where $\bar{\eta} = -1$. Another curve branch starts closer to the straight line $h = 0$ where $\bar{\eta} = -1$, and terminates where $h = 0$, $\bar{\eta} = \bar{\eta}_{02}$.

Of course, there must be a minimum in h or a maximum in $|h|$. We designate this h_{min}. In the case of a large region of possible values of θ_0, Δ_s, and $\bar{\bar{s}}_0$, this minimum where $dh/d\bar{\eta} = 0$ is located between $\bar{\eta} = -1$ and $\bar{\eta} = +3$. In particular, the minimum can be located above or below the h-axis. In the boundary case it will be located near $h = h_{02}$. In that case, Eqs. (47) and (50) require that $b = 0$ and $c = 0$ apply at the same time. We obtain the following condition for the applicability of $dh/d\bar{\eta} = 0$ in the case where $h = h_{02}$, $\bar{\eta} = 0$:

$$\bar{\bar{s}}_o = 1 - \frac{7}{12}\sin^2\theta_*\left(1-\frac{1}{5}\Delta s\right)$$

$$-\frac{13}{12}\sin\theta_*\sqrt{\sin^2\theta_*\left(1-\frac{1}{5}\Delta s\right)^2+\frac{4}{5}\Delta s\,\cos^2\theta_*} \qquad (54a)$$

In particular, we find that

$$-\infty \le \bar{\eta}' \le 0 \quad \text{where} \quad h = h_{o2},\ \bar{\eta} = 0 \qquad (54b)$$

where

$$\bar{\bar{s}}_o \le 1 - \frac{7}{12}\sin^2\theta_*\left(1-\frac{1}{5}\Delta s\right)$$

$$-\frac{13}{12}\sin\theta_*\sqrt{\sin^2\theta_*\left(1-\frac{1}{5}\Delta s\right)^2+\frac{4}{5}\Delta s\,\cos^2\theta_*}$$

$$0 \le \bar{\eta}' < \infty \quad \text{where} \quad h = h_{o1},\ \bar{\eta} = 0 \qquad (54c)$$

/117

where

$$\bar{\bar{s}}_o > 1 - \frac{7}{12}\sin^2\theta_*\left(1-\frac{1}{5}\Delta s\right)$$

$$-\frac{13}{12}\sin\theta_*\sqrt{\sin^2\theta_*\left(1-\frac{1}{5}\Delta s\right)^2+\frac{4}{5}\Delta s\,\cos^2\theta_*}$$

We shall use these relationships for classification later on. The boundary relation (54a) is represented as dots and dashes in Figure 6, using different angles.

Finally, we can show that curves other than the curve branches described above cannot occur in the region $h < 0$, $-1 \le \bar{\eta} < 3$. Based on what we stated before, these could be closed curves only. Such a curve would have to satisfy $h < h_{min} \le h_{02}$. Let us assume the existence of such a closed curve. According to Figure 8, a line drawn from a point A of this curve to the zero point would intersect the closed curve once again at point B, and the curve passing through the zero point $h = 0$, $\bar{\eta} = 0$ which was described before will be intersected at at a point C. There must be a point C on the imaginary line because the tangent placed through $h = 0$, $\bar{\eta} = 0$ will intersect the straight line $\bar{\eta} = 3$ at a point

$$h_{T,1} = -\frac{3}{2}\sin\theta_* > h_{min}$$

Therefore, together with points A, B, C and the zero point there will be four points on the auxiliary line, which is impossible because of Eqs.(34) and (49), respectively. Therefore, another curve cannot exist. Finally, the requirement that $(h - \bar{\eta} \sin \theta_0)/\bar{h} \geq 0$ according to Figure 7 and Eq. (45) means that the curve branch with $\bar{\eta} \geq 0$ and $h > 3/5\ \Delta s \sin \theta_0$ is impossible. /118

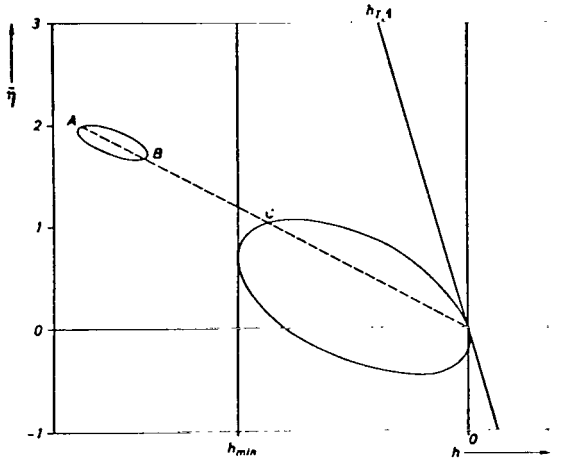

Figure 8. Sketch to prove that a closed curve $\bar{\eta}(h)$ cannot exist where $\Delta s \geq 0$ in the range $h < 0$.

Let us now turn to the case where $\Delta s < 0$. This is somewhat more complicated than the case where $\Delta s > 0$. We start out with the behavior of the curve branch which passes through the zero point $h = 0$, $\bar{\eta} = 0$, and has the slope $d\bar{\eta}/dh = -2/\sin \theta_0$. In order to study this situation, we first determine the location of the curve point of the tangent in the zero point which is represented in Figure 8. As a rule, such a curve point where $h \neq 0$ must exist because of the form of Eqs. (34) and (49), respectively. We substitute the tangential equation $\bar{\eta} = -2/\sin \theta_0 \cdot h$ in Eq. (34), we obtain /119

$$h_{T,2}\left(\frac{13}{3}\sin^2\theta_0 + \frac{8}{3}\right) = 12 \sin\theta_0\left(\frac{\bar{s}_0}{5} - \frac{1}{3} - \frac{2}{15}\Delta s - \frac{1}{6}\sin^2\theta_0\left(1 - \frac{1}{5}\Delta s\right)\right) \tag{55a}$$

In the boundary case where $h_{T,2} = 0$, it applies, except for $\theta_0 = 0$ that

$$\bar{\bar{s}}_{0,T} = \frac{1}{3} + \frac{1}{6}\sin^2\Theta_0\left(1 - \frac{1}{5}\Delta s\right) + \frac{2}{15}\Delta s \qquad (55b)$$

This relationship is shown by a dotted curve in Figure 9 where Eq. (55b) was also used for $\theta_0 = 0$.

Consequently, we have the following curve profile: where $\bar{\bar{s}}_0 \geq \bar{\bar{s}}_{0,T}$, it applies that $\bar{\eta}'' \geq 0$ where $h = 0$, $\bar{\eta} = 0$, and the curve which is incoming from $h = 0$, $\bar{\eta} = 0$ continues to increase its slope, reaching a minimum in h, and then reaches the point where $h = 0$, $\bar{\eta} = \bar{\eta}_{02} > 0$. In addition, a closed curve or a curve branch terminating at two points where $\bar{\eta} = -1$ can exist in the region $h < 0$. A <u>sufficient</u> condition for the existence of such a curve is the presence of two curve points where $\bar{\eta} = 0$ and $h < 0$, or of the boundary case of one tangent point. In that case, Eq. (52) demands that $\sin^2\theta_0(1 - 1/5\,\Delta s)^2 + 4/5\,\Delta s \cos^2\theta_0 \geq 0$ be satisfied for the radicand. Consequently, $\Delta s \geq (\Delta s)_{crit}$ must apply, where /121

$$(\Delta s)_{crit} = 5\left\{1 - 2\,\mathrm{tg}^2\Theta_0 + 2\frac{\mathrm{tg}\,\Theta_0}{\sin\Theta_0}\sqrt{\cos 2\Theta_0}\right\} \qquad (56)$$

Since $(\Delta s)_{crit}$ is independent of $\bar{\bar{s}}_0$, the curves $\Delta s = (\Delta s)_{crit}$ in Figure 6 are vertical lines which are located at the end of the dot-dashed curves that correspond to Eq. (54a). Of course, the significance of the dot-dashed lines is the same for $\Delta s < 0$ as for $\Delta s > 0$. They represent the boundary where h_{min} still has a positive or negative $\bar{\eta}$. In the case of value triplets θ_0, Δs, $\bar{\bar{s}}_0$ on the dot-dashed boundary curve the slope at point $h = h_{02}$, $\bar{\eta} = 0$ will be infinite. Of course, the criterion of infinite slope at the extreme zero point of $\bar{\eta}(h)$ h_{02} can be used only where h_{02} exists as a real number. Consequently, the dot-dashed lines must terminate at $\Delta s = (\Delta s)_{crit}$. The terminal point of such a line in the Δs, $\bar{\bar{s}}_0$-plane is remarkable insofar as the closed curve degenerates into a point where suitable value triplets θ_0, Δs, $\bar{\bar{s}}_0$ exist. Therefore, this point at the same time represents the point of maximum Δs on the boundary curve of the region Δs, $\bar{\bar{s}}_0$, within which it is impossible for closed curves $\bar{\eta}(h)$ with $\bar{\bar{s}}_0 \geq \bar{\bar{s}}_{0,T}$ to exist. However, the conditions that $\bar{\bar{s}}_0 \geq \bar{\bar{s}}_{0,T}$ and $\Delta s \geq (\Delta s)_{crit}$ are merely a sufficient set of conditions for the existence of a closed curve or of a curve branch that terminates in two points where $\bar{\eta} = -1$. Moreover, partial areas exist in the region where $\bar{\bar{s}}_0 \geq \bar{\bar{s}}_{0,T}$ and $\Delta s < (\Delta s)_{crit}$ which contain closed curves below or above the h-axis.

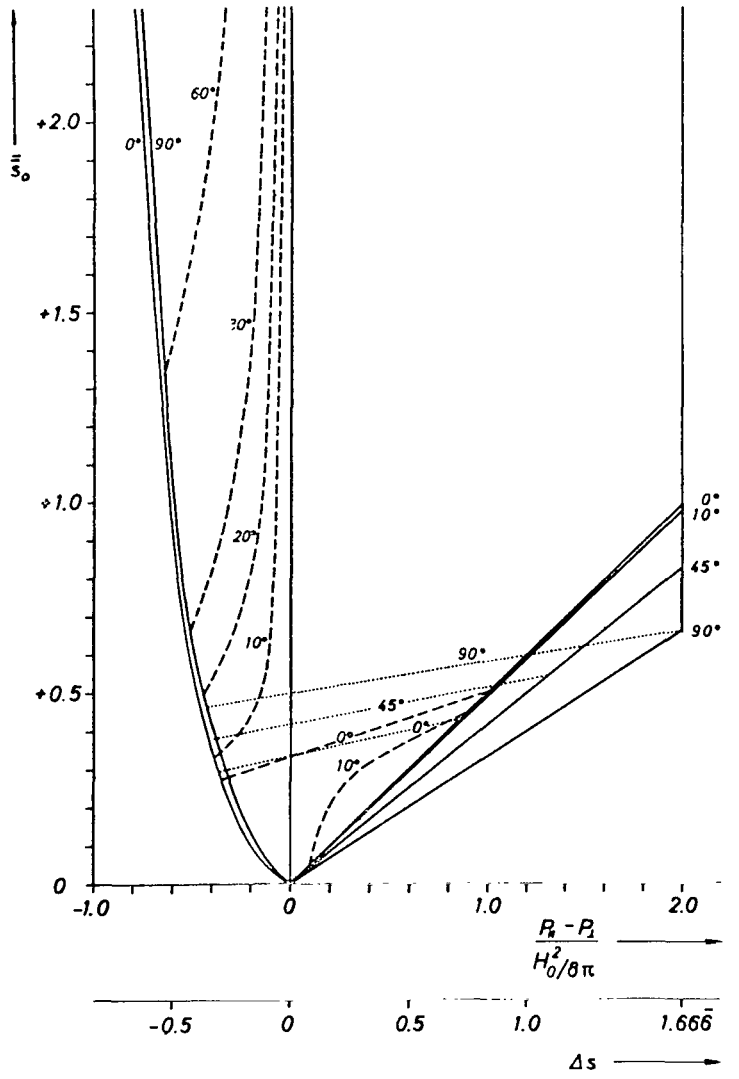

Figure 9. Boundary lines for the existence of Alfvén shock waves (dashed) and for the sign of $h_{T,2}$ (dotted) within the permissible region of the Δs, $\bar{\bar{s}}_0$-plane. The curve parameters are values of θ_0.

In the case where $\bar{\bar{s}}_0 < \bar{\bar{s}}_{0,T}$, one curve branch with $\bar{\eta}' = -2/\sin\theta_0$ and $\bar{\eta}'' < 0$ starts at $h = 0$, $\bar{\eta} = 0$. When $\Delta s > (\Delta s)_{crit}$, this branch passes through $h = h_{03}$, $\bar{\eta} = 0$, reaches positive values of $\bar{\eta}$ again after passing through $h = h_{02}$, $\bar{\eta} = 0$, passes through $h = h_{T,2}$, $\bar{\eta} = -2/\sin\theta_0 \cdot h_{T,2}$, and finally reaches the point $h = 0$, $\bar{\eta} = \bar{\eta}_{02}$. Another possibility is that the curve branch terminates at $\bar{\eta} = -1$ and that a new curve branch, incoming from $\bar{\eta} = -1$, passes through $h = h_{02}$, $\bar{\eta} = 0$ and $h = h_{T,2}$, $\bar{\eta} = -2/\sin\theta_0 \cdot h_{T,2}$, and reaches the point $h = 0$, $\bar{\eta} = \bar{\eta}_{02}$. In the case where $\Delta s < (\Delta s)_{crit}$, one curve starts out from $h = 0$, $\bar{\eta} = 0$, reaches a minimum at $h\ h_{min} < h_{T,2}$, passes through $h = h_{T,2}$, $\bar{\eta} = -2/\sin\theta_0 \cdot h_{T,2}$, and reaches the point $h = 0$, $\bar{\eta} = \bar{\eta}_{02}$. Moreover, in the case of $\bar{\bar{s}}_0 \leq \bar{\bar{s}}_{0,T}$ a closed curve profile or a profile cut off at $\bar{\eta} = -1$ can exist in addition to the curve branch or branches passing through $h = 0$, $\bar{\eta} = 0$ and $h = 0$, $\bar{\eta} = \bar{\eta}_{02}$. ∠122

3.2.2. In the Limiting Cases $\theta_0 \to 90°$ and $\theta_0 \to 0°$

To this point of our discussion, we were frequently forced to exclude the cases where $\theta_0 = 0°$ and $\theta_0 = 90°$ in order to prevent deviations. We shall now discuss these cases where it is best to generate the shock waves with parallel magnetic field vector and $\underline{n}$-vector by the boundary transition $\theta_0 \to 0°$ and the shock waves with vertically oriented $\underline{H}$-vector and $\underline{n}$-vector by the boundary transition $\theta_0 \to 90°$. In both cases, the effect of anisotropy is only small because the pressure tensor components P_{yx} and P_{xy} disappear.

We start out with $\theta_0 = 90°$. In the $h, \bar{\eta}$-plane, we have a straight line passing from $h = -1$, $\bar{\eta} = -1$ to $h = 3$, $\bar{\eta} = 3$.

$$\bar{\eta} = h \tag{57a}$$

and the curve ∠123

$$\bar{\zeta} = \frac{3}{2}\, h\, \frac{h + 2\left(1 - \frac{1}{5}\Delta s\right)}{h - 3\left(\bar{\bar{s}}_0 - \frac{1}{5}\Delta s\right)} \cdot \tag{57b}$$

The latter starts at $h = -4/3 + \sqrt{16/9 + 4\,\bar{\bar{s}}_0}$, $\bar{\zeta} = -1$, passes through $h = 0$, $\bar{\eta} = 0$ with a slope of -2, reaches a maximum, passes through point $h = -2$, $\bar{\eta} = 0$ and finally arrives the point $h = -4/3 - \sqrt{16/9 + 4\,\bar{\bar{s}}_0}$, $\bar{\zeta} = -1$. In the case of $\bar{Y}$, we obtain an indefinite expression of the form 0/0 for $\theta_0 = 90°$ if we use Eq. (36). In the case of the boundary transition $\theta_0 \to 90°$,

we obtain the following for $\bar{Y}$:

$$\bar{Y} = \frac{5}{3}\,\frac{h + \frac{h^3}{6 s_0} + \frac{\Delta s}{5 s_0}(1+h)}{1 - \frac{h}{3}} \qquad \text{for } \bar{\eta} = h. \tag{57c}$$

Since $b_n = 0$ where $\theta_0 = 90°$, it follows from Eqs. (37) and (38) that the curve branch (57b) represents special tangential discontinuities with $V_{n,1} = V_{n,0} = [u_n] = 0$ and

$$[u_y] = b_0\,\bar{h}\left(\frac{h}{(1+\bar{\eta})} - \frac{\bar{\eta}}{\bar{h}}\right)^{1/2}$$

where

$$b_0 = \frac{|\underline{H}_0|}{\sqrt{4\pi\rho_0}}$$

Moreover, it applies that

$$\left[p + \frac{H_y^2}{8\pi}\right] = 0$$

The following applies to the velocities of branch (57a), using the reference velocity b_0:

$$V_{n,1} = \frac{V_{n,0}}{1+h} = b_0\left(\frac{s_0 + 1 + h/6 + \frac{\Delta s}{5}\,\frac{1+h}{h}}{(1-\frac{h}{3})(1+h)}\right)^{1/2} \tag{57d}$$

$$[u_n] = -\,b_0 \cdot h\left(\frac{s_0 + 1 + \frac{h}{6} + \frac{\Delta s}{5}\,\frac{1+h}{h}}{(1-\frac{h}{3})(1+h)}\right)^{1/2} \tag{57e}$$

$$[u_y] = 0 \tag{57f}$$

Now we shall discuss the shock wave solutions that result from the boundary transition $\theta_0 \to 0°$. In the $h, \bar{\eta}$-plane, these boundary curves are generally composed of pieces of the $\bar{\eta}$-axis and that part of the ellipse

$$h^2 + \frac{\left(\bar{\eta} - \frac{3}{2}(1 - \bar{\bar{s}}_0)\right)^2}{3/2} = \frac{3}{2}(1 - \bar{\bar{s}}_0)^2 + \frac{4}{5}\,\Delta s \tag{58a}$$

where $\bar{\eta} \geq -1$. In the individual cases of boundary transitions, we must keep the condition $(h - \bar{\eta}\sin\theta_0)/\bar{h}$ in mind.

We can give the parts with $h = 0$ the designation G_{St} as a generalization

of the collision relationships for shock waves in gas dynamics. The parts with $h \neq 0$ on the ellipse must be considered switch-on shock waves S_W (for the English switch-on). The other jump functions of the S_W-parts can be calculated directly with the aid of Eqs. (36) through (39). The G_{St}-parts require the solution of indefinite expressions. We obtain

$$\bar{Y} = -\frac{\Delta s}{s_o} + \frac{5}{3}\,\frac{\left(\bar{\eta} + \frac{3}{5}\Delta s\right)\left(\bar{\eta} - \frac{3}{5}\,\frac{\Delta s}{s_o}\,\bar{\eta} + \frac{1}{5}\,\frac{\Delta s}{s_o}\right)}{-\frac{1}{3}\,\bar{\eta}^2 + \bar{\eta}\left(1 - \frac{1}{5}\Delta s\right) + \frac{3}{5}\Delta s} \tag{58b}$$

The other jump functions read

$$\frac{V_{n,1}}{b_{n,1}} = \frac{V_{n,o}}{b_{n,o}}\,(1+\bar{\eta})^{-1/2} \tag{58c}$$

$$= \left(\begin{array}{c} \bar{\eta}^2\left(s_o - \frac{2}{5}\Delta s\right) + \frac{3}{5}\Delta s\left(s_o - \frac{2}{5}\Delta s - \frac{2}{3}\right)\bar{\eta} - \frac{6}{25}(\Delta s)^2 \\ \bar{\eta}\left(-\frac{1}{3}\,\bar{\eta}^2 + \bar{\eta}\left(1 - \frac{1}{5}\Delta s\right) + \frac{3}{5}\Delta s\right) \end{array} \right)^{1/2}$$

$$\frac{[u_n]}{b_{n,1}} = -\bar{\eta}\,\frac{V_{n,1}}{b_{n,1}} \tag{58d}$$

$$\frac{[u_y]}{b_{n,1}} = 0 \tag{58e}$$

According to Eq. (58a), an S_W-solution will not exist when /126

$$\frac{3}{2}\left(1 - \bar{\bar{s}}_o\right)^2 + \frac{4}{5}\Delta s < 0$$

This holds true within the parabola

$$\Delta s = -\frac{15}{8}\left(1 - \bar{\bar{s}}_o\right)^2 \leq 0$$

whose apex is located in the Δs, $\bar{\bar{s}}_o$-plane at $\Delta s = 0$, $\bar{\bar{s}}_o = 1$, and which opens to the left. At least part of the ellipse exists outside the inside area of the parabola in the Δs, $\bar{\bar{s}}_o$-diagram, in the region $-1 \leq \bar{\eta} \leq +3$ of the h, $\bar{\eta}$-plane. The center of the ellipse for $\bar{\eta}_M = 3/2(1 - \bar{\bar{s}}_o)$ below the h-axis when $\bar{\bar{s}}_o > 1$, and above it when $\bar{\bar{s}}_o < 1$. In the case where $\Delta s > 0$, intersections of the ellipse with the h-axis exist which merge into a tangent point in the boundary case where $\Delta s = 0$. In the case where $\Delta s < 0$, the ellipses are located either above or below the h-axis. The extremes of $\bar{\eta}$ on the ellipse within $-1 \leq \bar{\eta} \leq +3$

are designated $\bar{\bar{\eta}}_{max}$ and $\bar{\bar{\eta}}_{min}$.

In addition to that part of the ellipse where $\bar{\bar{\eta}} \geq -1$, we usually have parts of the $\bar{\bar{\eta}}$-axis as G_{St}-parts of the boundary curves for $\theta_0 \to 0°$. We shall compile the results for the G_{St}-parts in tabular form, where the individual partial sections can overlap. A distinction must be made between the G_{St}-parts that result from curves with $h \leq 0$ and with $h \geq 0$. We designate this by a - or by a + sign:

TABLE 4.

/127

h	Δs	Additional conditions	G_{St} - parts
+0	>0	$\bar{\bar{s}}_0 \leq \bar{\bar{s}}_{0,T}(\theta_0 \to 0') = \frac{1}{3} + \frac{2}{15}\Delta s$	$\bar{\eta}_{max} \leq \bar{\eta} \leq +3$ $\bar{\eta}_{min} \leq \bar{\eta} \leq 0$ $-1 \leq \bar{\eta} \leq \bar{\eta}_{02}(\theta_0 \to 0') = -\frac{1}{5}\frac{\Delta s}{\bar{\bar{s}}_0 - \frac{1}{5}\Delta s}$
0	>0	$\bar{\bar{s}}_0 \geq \bar{\bar{s}}_{0,T}(\theta_0 \to 0')$ $\bar{\eta}_{min} \geq \bar{\eta}_{02}$	$\bar{\eta}_{max} \leq \bar{\eta} \leq +3$ $\bar{\eta}_{min} \leq \bar{\eta} \leq 0$ $-1 \leq \bar{\eta} \leq \bar{\eta}_{02}$
0	>0	$\bar{\bar{s}}_0 \geq \bar{\bar{s}}_{0,T}$ $\bar{\eta}_{min} \leq \bar{\eta}_{02}$	$\bar{\eta}_{max} \leq \bar{\eta} \leq +3$ $\bar{\eta}_{02} \leq \bar{\eta} \leq 0$ $-1 \leq \bar{\eta} \leq \bar{\eta}_{min}$ $\frac{2}{5}\frac{\Delta s}{\bar{\bar{s}}_0} \leq \bar{\eta} \leq \bar{\eta}_{max}$
-0	>0	$\bar{\bar{s}}_0 \leq \bar{\bar{s}}_{0,T}$	$\bar{\eta}_{02} \leq \bar{\eta} \leq \bar{\eta}_{min}$ $\frac{2}{5}\frac{\Delta s}{\bar{\bar{s}}_0} \leq \bar{\eta} \leq \bar{\eta}_{max}$
-0	>0	$\bar{\bar{s}}_0 \geq \bar{\bar{s}}_{0,T}$ $\bar{\eta}_{min} \geq \bar{\eta}_{02}$	$\bar{\eta}_{02} \leq \bar{\eta} \leq \bar{\eta}_{min}$ $\frac{2}{5}\frac{\Delta s}{\bar{\bar{s}}_0} \leq \bar{\eta} \leq \bar{\eta}_{max}$
		$\bar{\bar{s}}_0 \geq \bar{\bar{s}}_{0,T}$ $\bar{\eta}_{min} \leq \bar{\eta}_{02}$	$\bar{\eta}_{min} \leq \bar{\eta} \leq \bar{\eta}_{02}$
+0	<0	$0 \leq \bar{\bar{s}}_0 \leq 1 - \sqrt{-\frac{8}{15}\Delta s}$	$\bar{\eta}_{max} \leq \bar{\eta} \leq +3$ $Min(\bar{\eta}_{min}, \bar{\eta}_{02}) \leq \bar{\eta} \leq Max(\bar{\eta}_{min}, \bar{\eta}_{02})$ $-1 \leq \bar{\eta} \leq +\frac{2}{5}\frac{\Delta s}{\bar{\bar{s}}_0}$

TABLE 4 (continued)

/128

$\bar{h}$	Δs	Additional conditions	G_{St} -parts
			$\bar{\eta}_{02} \leq \bar{\eta} \leq +3$
$+0$	<0	$1-\sqrt{-\frac{8}{15}\Delta s} \leq \bar{\bar{s}}_0 \leq 1+\sqrt{-\frac{8}{15}\Delta s}$	$-1 \leq \bar{\eta} \leq +\frac{2}{5}\frac{\Delta s}{\bar{\bar{s}}_0}$
			$\bar{\eta}_{02} \leq \bar{\eta} \leq +3$
$+0$	<0	$1+\sqrt{-\frac{8}{15}\Delta s} \leq \bar{\bar{s}}_0$	$\bar{\eta}_{max} \leq \bar{\eta} \leq \frac{2}{5}\frac{\Delta s}{\bar{\bar{s}}_0}$
			$-1 \leq \bar{\eta} \leq \bar{\eta}_{min}$
-0	<0	$0 \leq \bar{\bar{s}}_0 \leq \bar{\bar{s}}_{0,T}$	$\bar{\eta}_{02} \leq \bar{\eta} \leq \bar{\eta}_{max}$
			$0 \leq \bar{\eta} \leq \bar{\eta}_{min}$
		$\bar{\bar{s}}_{0,T} \leq \bar{\bar{s}}_0 \leq 1-\sqrt{-\frac{8}{15}\Delta s}$	$\bar{\eta}_{min} \leq \bar{\eta} \leq \bar{\eta}_{max}$
		$\bar{\eta}_{02} \leq \bar{\eta}_{min}$	$0 \leq \bar{\eta} \leq \bar{\eta}_{02}$
-0	<0	$\bar{\bar{s}}_{0,T} \leq \bar{\bar{s}}_0 \leq 1-\sqrt{-\frac{8}{15}\Delta s}$	$\bar{\eta}_{02} \leq \bar{\eta} \leq \bar{\eta}_{max}$
		$\bar{\eta}_{02} \geq \bar{\eta}_{min}$	$0 \leq \bar{\eta} \leq \bar{\eta}_{min}$
-0	<0	$1-\sqrt{-\frac{8}{15}\Delta s} \leq \bar{\bar{s}}_0 \leq 1+\sqrt{-\frac{8}{15}\Delta s}$	$0 \leq \bar{\eta} \leq \bar{\eta}_{02}$
			$0 \leq \bar{\eta} \leq \bar{\eta}_{02}$
-0	<0	$1+\sqrt{-\frac{8}{15}\Delta s} \leq \bar{\bar{s}}_0$	$\bar{\eta}_{min} \leq \bar{\eta} \leq \bar{\eta}_{max}$

The results compiled in Table 4 are useful in conjunction with Figures 6 and 7 where it is desired to make a rapid determination of the approximate profile of a shock wave curve for small angles. /129

The limiting case where $\Delta s \to 0$ was mentioned briefly once before, in conjunction with the behavior near $h = 0$, $\bar{\eta} = 0$. Since the results of Bazer and Ericson [1958] are available, we shall dispense with a special discussion

here. Formulas 35 through 39 merge into the formulas of Bazer and Ericson without complications.

3.2.3. Collinear Alfvén Shock Waves

In Para. 2.5.2., we studied Alfvén shock waves that are not collinear as a rule but can be collinear. We had seen that the rotational angle of the transverse field $\underline{H}_{tr}$ is not contained in the conservation equations. Therefore, we can use the algebraically simple case of the collinear Alfvén shock wave in order to study some additional characteristics of this shock wave type. An Alfvén shock wave with isotropic pressure in its rear will be present, and only then, when it applies that $\bar{\eta} = -3/5\ \Delta s$ and that $[\underline{u}_{tr}] \neq 0$. We substitute $\bar{\eta} = -3/5\ \Delta s$ in Eq. (49) and obtain one or three real solutions for h. The solution that $\bar{h} = 0$ is forbidden because of $[u_y] = 0$. The two other solutions read:

$$h_{A,1} = -\sin\theta_0 + \sqrt{\sin^2\theta_0 - \Delta s\left(\frac{6}{25}\Delta s + \frac{2}{5}\cos^2\theta_0 - \frac{6}{5}\bar{\bar{s}}_0\right)} \tag{59a}$$

$$h_{A,2} = -\sin\theta_0 - \sqrt{\sin^2\theta_0 - \Delta s\left(\frac{6}{25}\Delta s + \frac{2}{5}\cos^2\theta_0 - \frac{6}{5}\bar{\bar{s}}_0\right)}$$

These solutions will exist only when the radicand of the root is not negative. We obtain the following boundary curve in the Δs, $\bar{\bar{s}}_0$-plane: /130

$$\bar{\bar{s}}_{0,lim} = \frac{1}{3} - \frac{1}{3}\sin^2\theta_0 + \frac{1}{5}\Delta s - \frac{5}{6}\frac{\sin^2\theta_0}{\Delta s} \tag{59b}$$

This function $\bar{\bar{s}}_{0,\,lim}(\Delta s,\ \theta_0)$ is represented by a dotted curve in Figure 9 for different values of θ_0. Alfvén shock waves are possible when it applies that $\Delta s > 0$ and $\bar{\bar{s}}_0 > \bar{\bar{s}}_{0,lim}$ or that $\Delta s < 0$ and $\bar{\bar{s}}_0 < \bar{\bar{s}}_{0,lim}$.

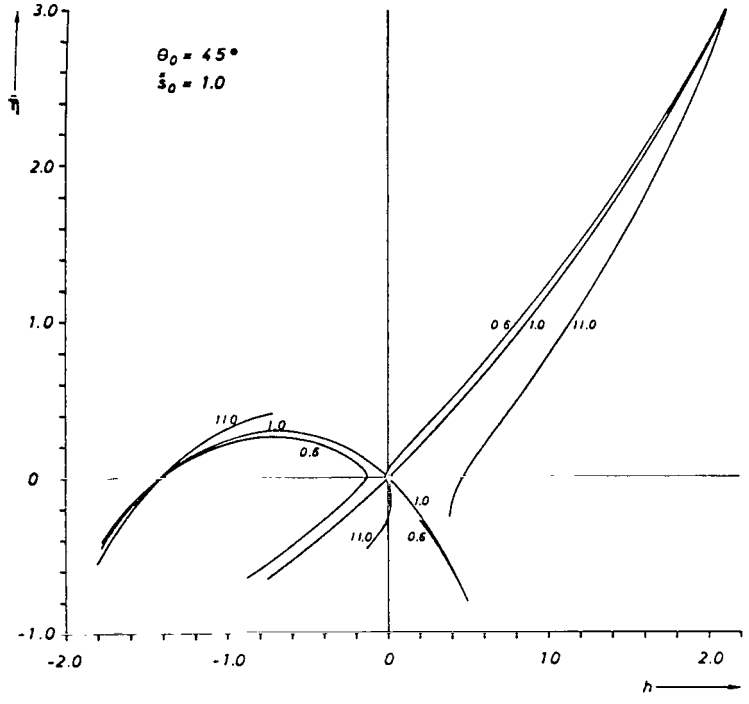

Figure 10. Jump functions $\bar{\eta}(h)$ for $\bar{\bar{s}}_0 = 1.0$, $\theta_0 = 45°$

The numerals at the curves indicate $P_{\parallel}/P_{\perp}$. The values of $P_{\parallel}/P_{\perp} = 0.6$, 1.0 and 11.0 correspond to the values of $\Delta s = -0.5$, 0, 5/3.

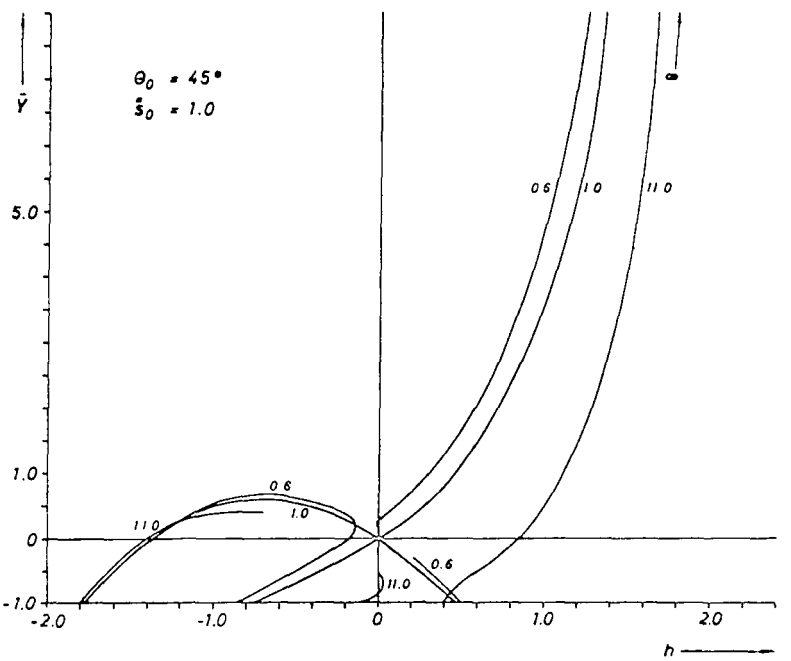

Figure 11. Jump functions $\bar{Y}(h)$ for $\bar{\bar{s}}_0 = 1.0$, $\theta_0 = 45°$.

The numerals at the curves indicate $P_{\parallel}/P_{\perp}$. The values of $P_{\parallel}/P_{\perp} = 0.6$, 1.0 and 11.0 correspond to the values of $\Delta s = -0.5$, 0, 5/3.

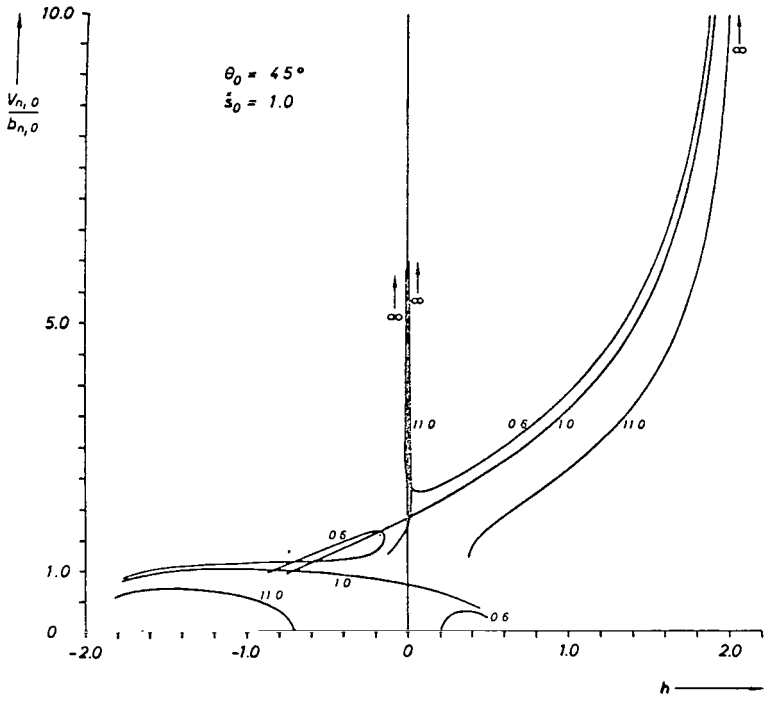

Figure 12. Jump functions $V_{n,0}/b_{n,0}$ for $\bar{\bar{s}}_0 = 1.0$, $\theta_0 = 45°$.

The numerals at the curves indicate $P_{\shortparallel}/P_{\perp}$.
The values of $P_{\shortparallel}/P_{\perp} = 0.6$, 1.0 and 11.0 correspond to the values of $\Delta s = -0.5$, 0, 5/3.

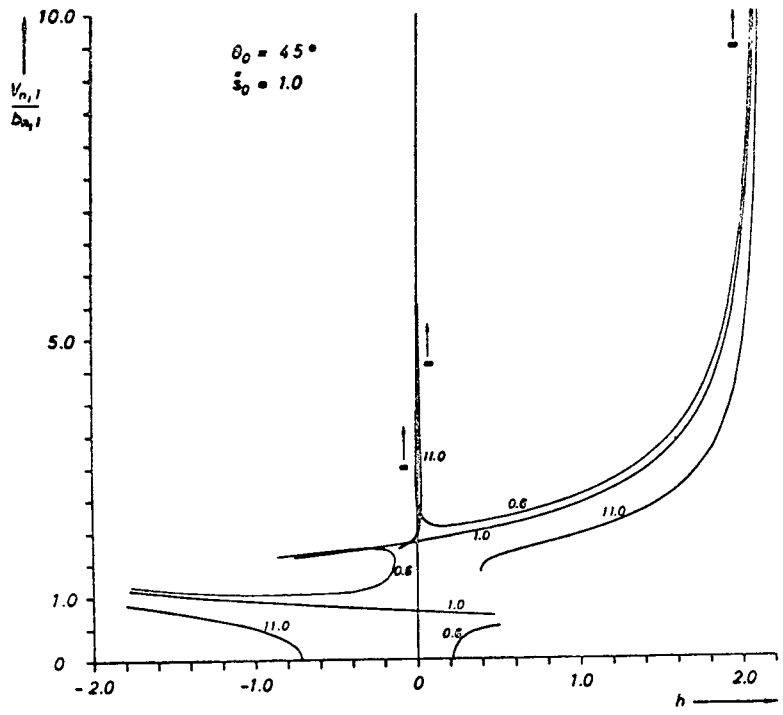

Figure 13. Jump functions $V_{n,1}/b_{n,1}$ for $\bar{\bar{s}}_0 = 1.0$, $\theta_0 = 45°$.

The numerals at the curves indicate $P_{//}/P_{\perp}$.
The values of $P_{//}/P_{\perp} = 0.6$, 1.0 and 11.0 correspond to the values of $\Delta s = -0.5$, 0, 5/3.

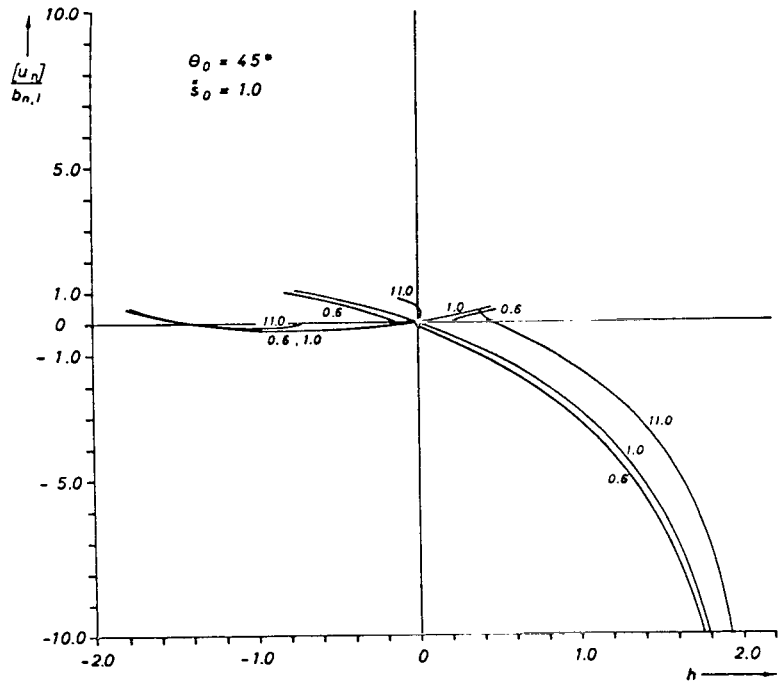

Figure 14. Jump functions $[u_n]/b_{n,1}$ for $\bar{\bar{s}}_0 = 1.0$, $\theta_0 = 45°$.

The numerals at the curves indicate $P_{11}/P_{\perp}$.
The values of $P_{11}/P_{\perp}$ = 0.6, 1.0 and 11.0
correspond to the values of Δs = -0.5, 0, 5/3.

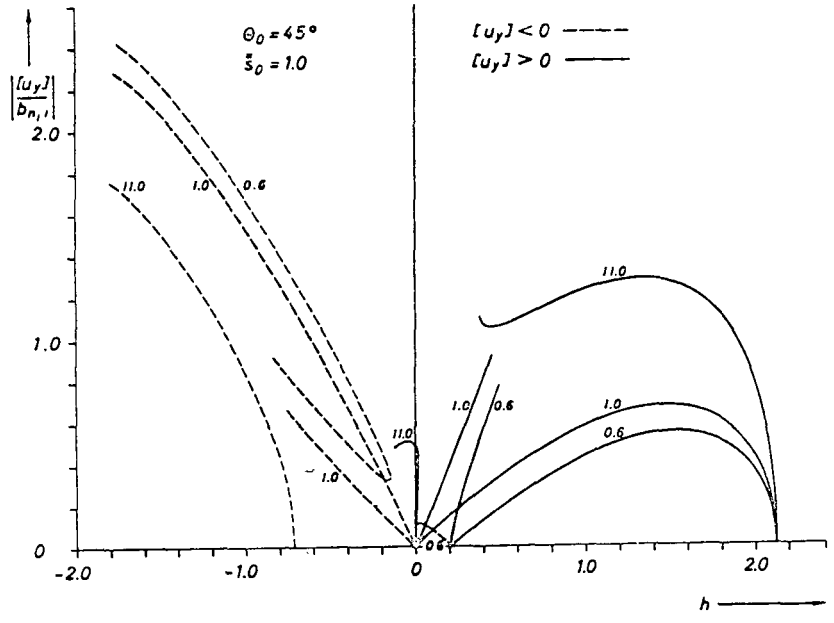

Figure 15. Jump functions $|[u_y]|/b_{n,1}$ for $\bar{\bar{s}}_0 = 1.0$, $\theta_0 = 45°$.

The numerals at the curves indicate $P_{\parallel}/P_{\perp}$.
The values of $P_{\parallel}/P_{\perp} = 0.6$, 1.0 and 11.0
correspond to the values of $\Delta s = -0.5$, 0, 5/3.

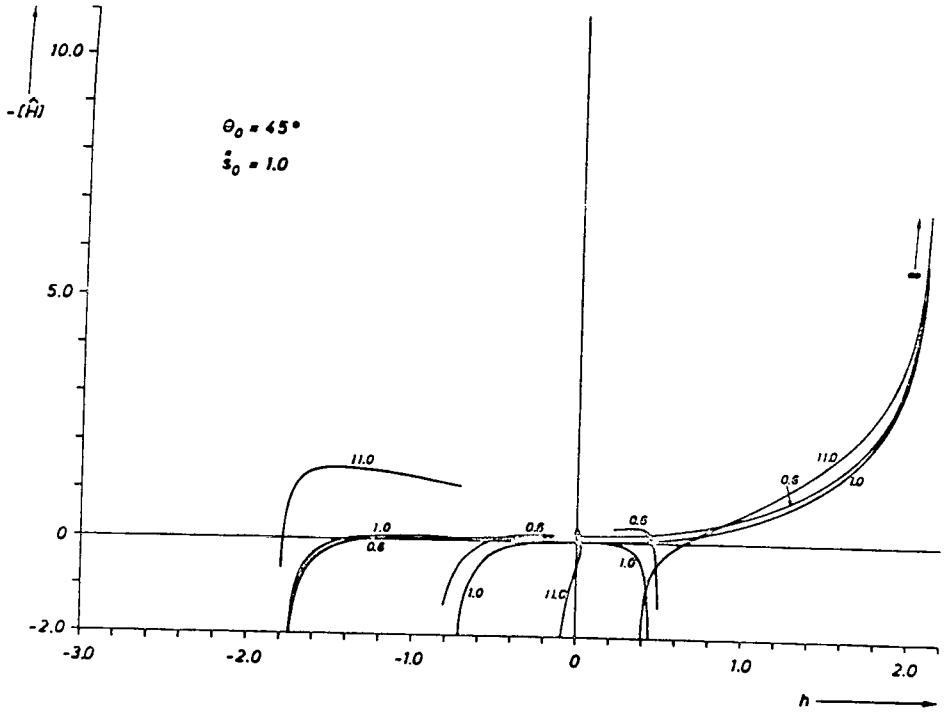

Figure 16. Jump functions $-[\hat{H}]$ for $\bar{\bar{s}}_0 = 1.0$, $\theta_0 = 45°$.

The numerals at the curves indicate $P_{//}/P_{\perp}$. The values of $P_{//}/P_{\perp} = 0.6$, 1.0 and 11.0 correspond to the values of $\Delta s = -0.5$, 0, 5/3.

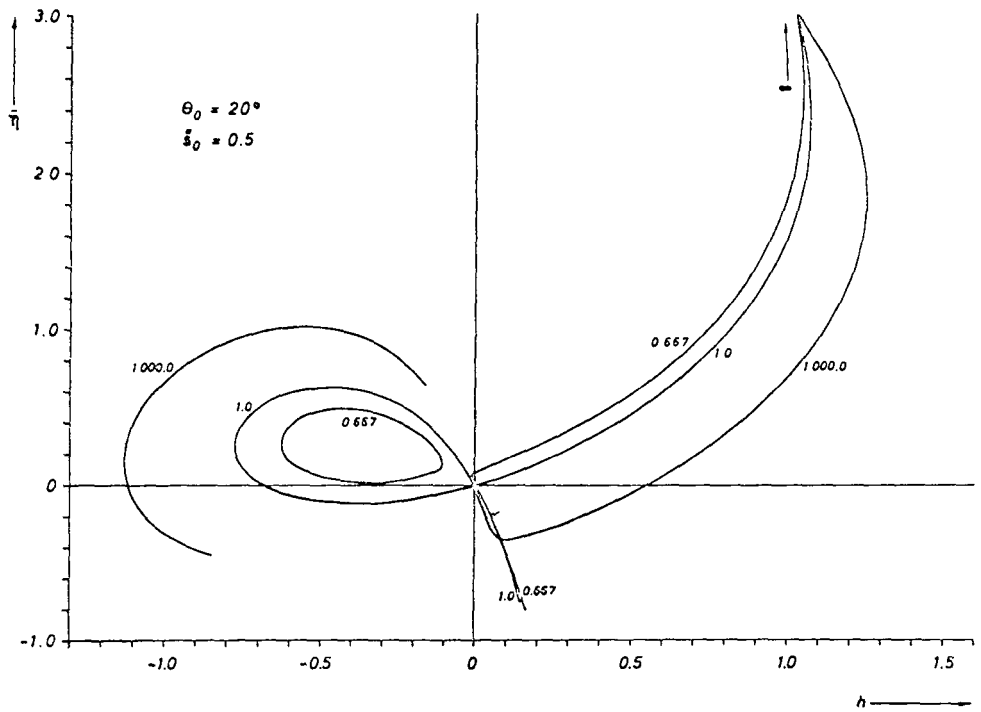

Figure 17. Jump functions $\bar{\eta}(h)$ for $\bar{s}_0 = 0.5$, $\theta_0 = 20°$.

The numerals at the curves indicate $P_{\parallel}/P_{\perp}$. The values of $P_{\parallel}/P_{\perp} = 0.667$, 1.0 and 1000.0 correspond to the values of $\Delta s = -0.2061$, 1.0 and +0.8656.

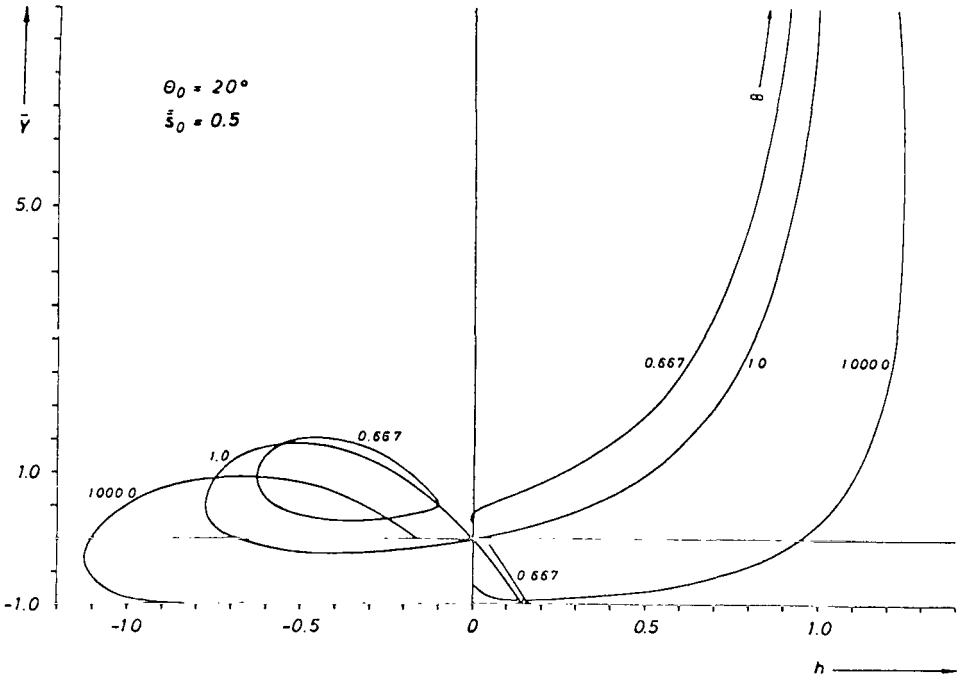

Figure 18. Jump functions $\bar{Y}(h)$ for $\bar{\bar{s}}_0 = 0.5$, $\theta_0 = 20°$.

The numerals at the curves indicate $P_{//}/P_{\perp}$. The values of $P_{//}/P_{\perp} = 0.667$, 1.0 and 1000.0 correspond to the values of $\Delta s = -0.2061$, 1.0 and +0.8656.

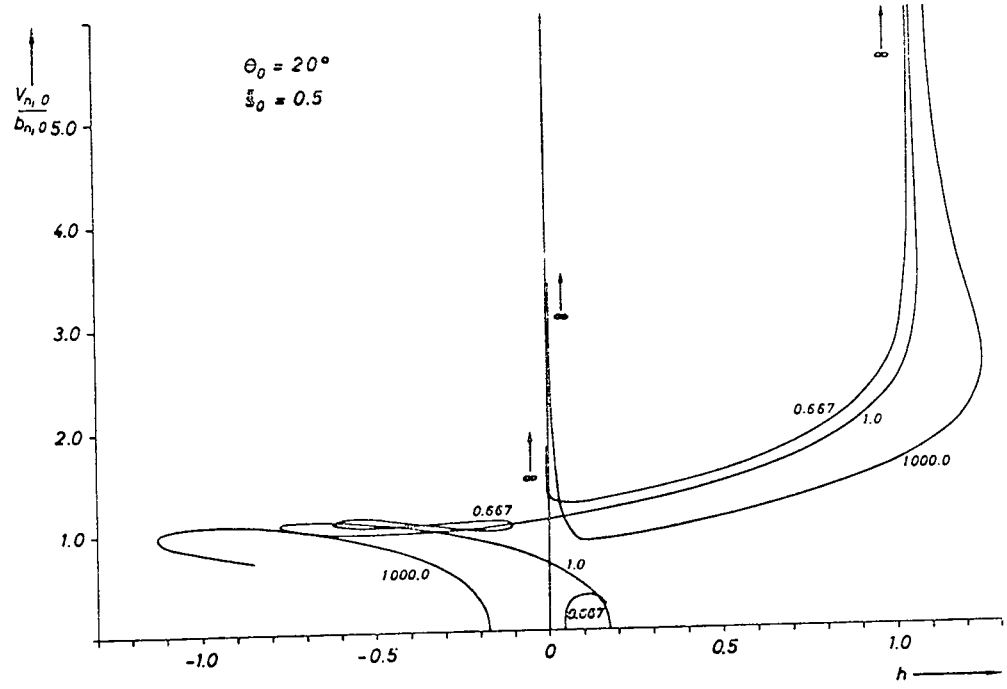

Figure 19. Jump functions $V_{n,0}/b_{n,0}$ for $\bar{\bar{s}}_0 = 0.5$, $\theta_0 = 20°$.

The numerals at the curves indicate $P_{\parallel}/P_{\perp}$. The values of $P_{\parallel}/P_{\perp} = 0.667$, 1.0 and 1000.0 correspond to the values of $\Delta s = -0.2061$, 1.0 and +0.8656.

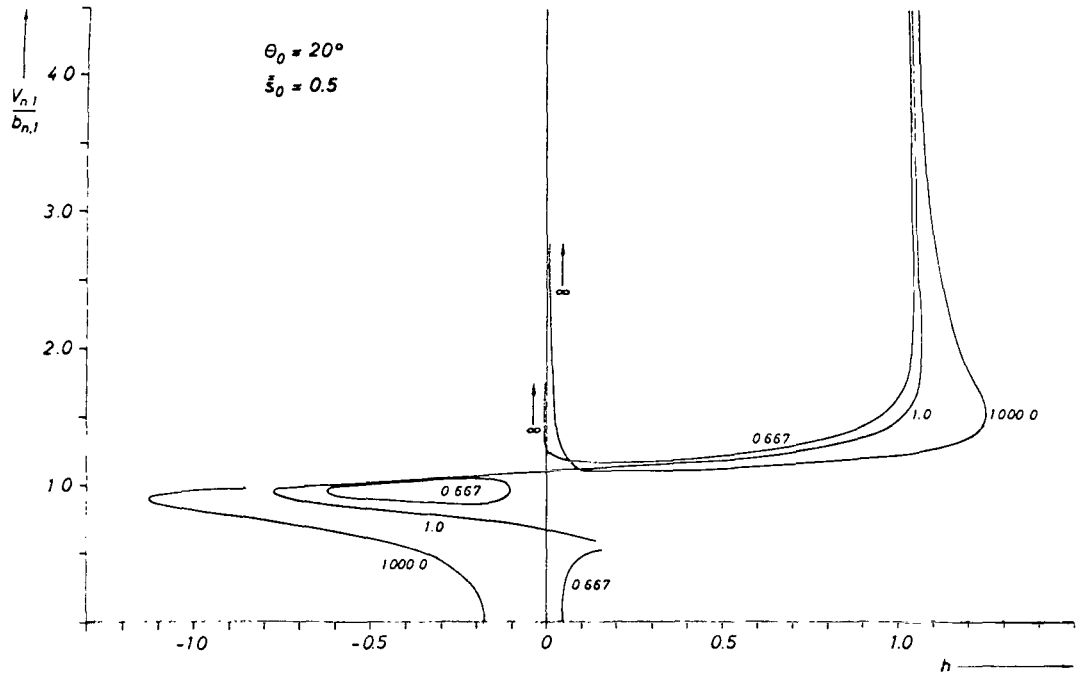

Figure 20. Jump functions $V_{n,1}/b_{n,1} = \bar{\bar{s}}_0 = 0.5$, $\theta_0 = 20°$.

The numerals at the curves indicate $P_{\parallel}/P_{\perp}$. The values of $P_{\parallel}/P_{\perp} = 0.667$, 1.0 and 1000.0 correspond to the values of $\Delta s = -0.2061$, 1.0 and +0.8656.

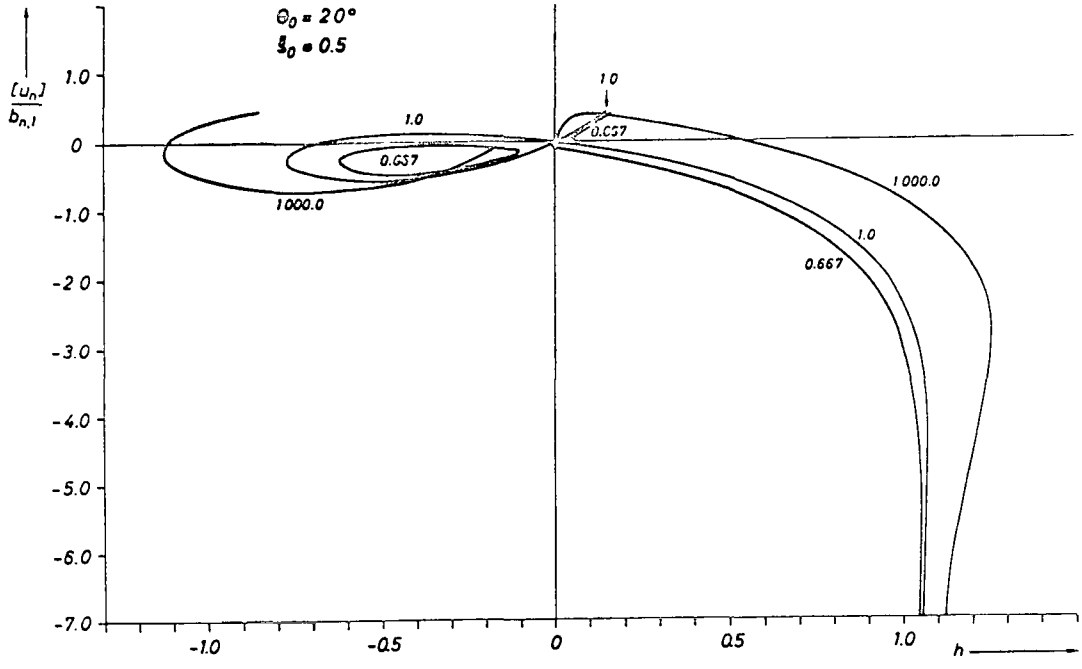

Figure 21. Jump functions $[u_n]/b_{n,1}$ for $\bar{\bar{s}}_0 = 0.5$, $\theta_0 = 20°$.

The numerals at the curves indicate $P_{//}/P_{\perp}$. The values of $P_{//}/P_{\perp} = 0.667$, 1.0 and 1000.0 correspond to the values of $\Delta s = -0.2061$, 1.0 and +0.8656.

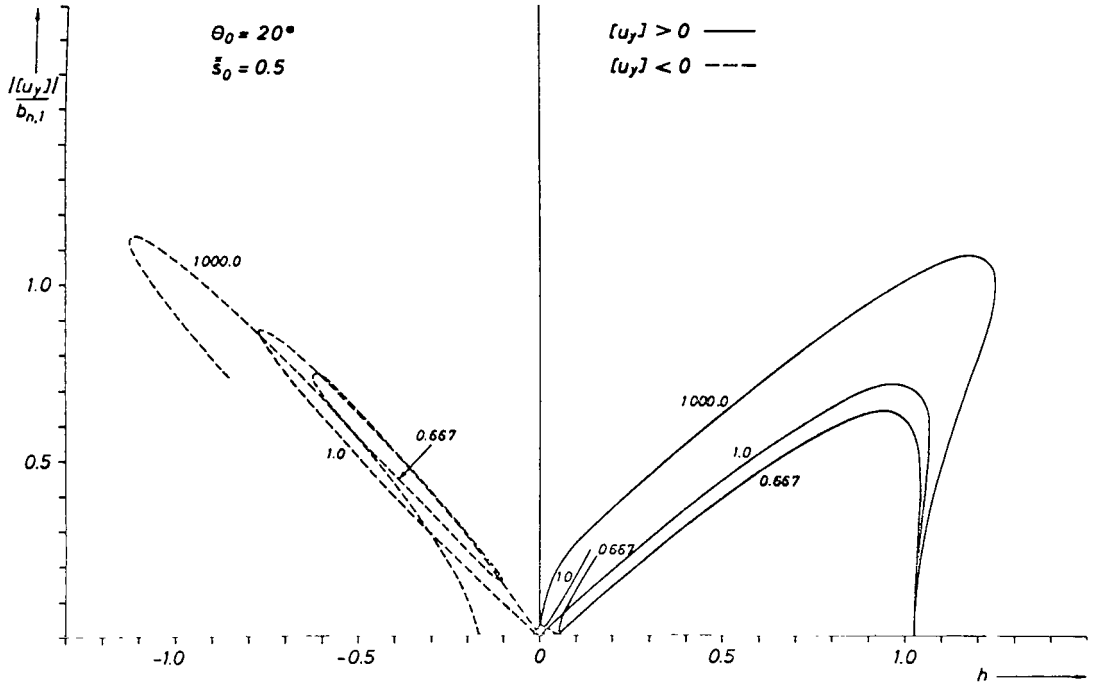

Figure 22. Jump functions $\left| [u_y] \right| / b_{n,1}$ for $\bar{\bar{s}}_0 = 0.5$ $\theta_0 = 20°$.

The numerals at the curves indicate $P_{\parallel}/P_{\perp}$. The values of $P_{\parallel}/P_{\perp} = 0.667$, 1.0 and 1000.0 correspond to the values of $\Delta s = -0.2061$, 1.0 and +0.8656.

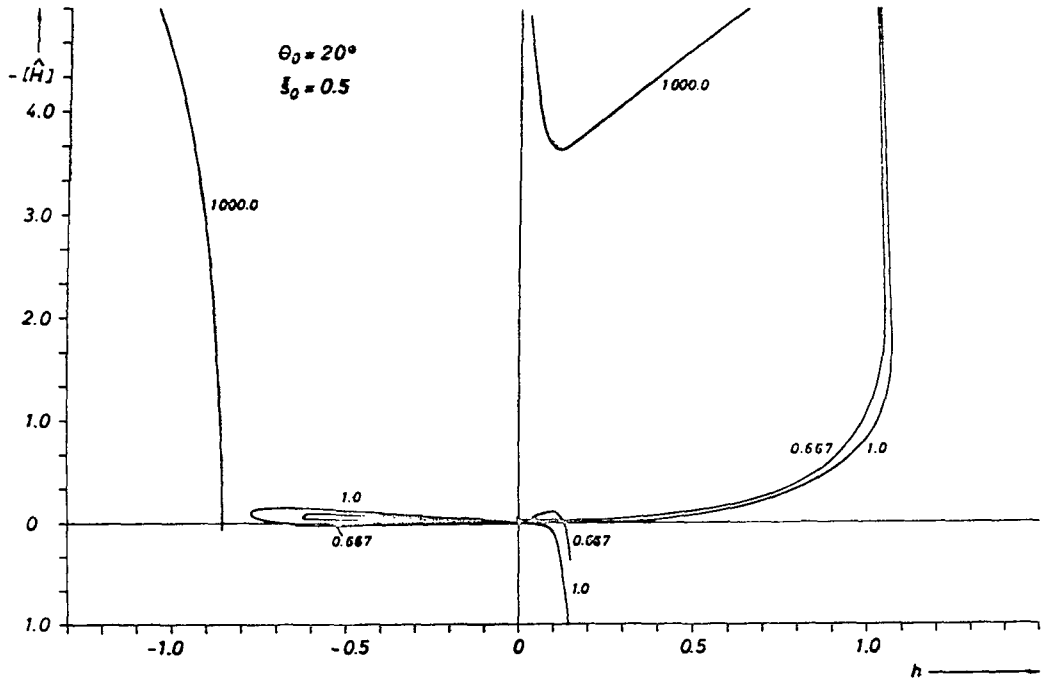

Figure 23. Jump functions $-[\hat{H}]$ for $\bar{\bar{s}}_0 = 0.5$, $\theta_0 = 20°$. The numerals at the curves indicate $P_{\parallel}/P_{\perp}$. The values of $P_{\parallel}/P_{\perp} = 0.667$, 1.0 and 1000.0 correspond to the values of $\Delta s = -0.2061$, 1.0 and +0.8656.

3.3. Classification and Physical Discussion of Collinear Shock Waves

/145

3.3.1. Classification System

We shall implement a classification of shock waves in this section. The guiding principle shall be that any definition of a shock wave type for $\Delta s \to 0$ will transform into the corresponding definition by Bazer and Ericson [1958]. Moreover, each shock wave type shall differ markedly from all the other types. We shall define six types of shock waves. The criteria for their occurrence are the following:

TABLE 5.

$M_f^{(1)}$ $\quad \bar{\bar{s}}_0 \geq 1 - 5/2 \sin^2\theta_0 + \Delta s(1/3 + 1/15 \sin^2\theta_0)$

(according to inequality 51c)

$M_f^{(2)}$ $\quad \bar{\bar{s}}_0 < 1 - 5/2 \sin^2\theta_0 + \Delta s(1/3 + 1/15 \sin^2\theta_0)$

(according to inequality 51b)

$M_s^{(1)}$ $\quad \bar{\bar{s}}_0 \geq 1 - 7/12 \sin^2\theta_0(1-1/5\,\Delta s) - 13/12 \sin\theta_0 \cdot$

$\cdot \sqrt{\sin^2\theta_0(1-1/5\,\Delta s)^2 + 4/5\,\Delta s \cos^2\theta_0}$

(according to inequality 54b)

and $\Delta s \geq (\Delta s)_{crit}$ (according to Eq. (56)

$M_s^{(2)}$ $\quad \bar{\bar{s}}_0 < 1 - 7/12 \sin^2\theta_0(1-1/5\,\Delta s) - 13/12 \sin\theta_0 \cdot$

$\cdot \sqrt{\sin^2\theta_0(1-1/5\,\Delta s)^2 + 4/5\,\Delta s \cos^2\theta_0}$

(according to inequality 54c)

and $\Delta s \geq (\Delta s)_{crit}$ (according to Eq. (56)

$M_s^{(3)}$ $\quad \Delta s < (\Delta s)_{crit}$ (according to Eq. (56)

/146

Some of the individual shock wave types are mutually exclusive because any one triplet of values θ_0, $\bar{\bar{s}}_0$, Δ_s is associated with only one M_f-shock wave and one M_s-shock wave. The types in $M_f^{(1)}$, $M_f^{(2)}$, $M_s^{(1)}$, and $M_s^{(2)}$ transform into the corresponding types by Bazer and Ericson [1958] when $\Delta s \to 0$. $M_s^{(3)}$-type shock waves exist only in the case of sufficiently strong negative anisotropy.

We shall now describe the individual shock wave types, using primarily physical aspects. We shall use not only $\Delta s = 5/3 \frac{P_{\parallel} - P_{\perp}}{H_0^2/4\pi}$ but also the ratio $P_{\parallel}/P_{\perp}$ as the measure of antropy.

3.3.2. M_f-Type Shock Waves

We shall start out by considering the M_f-type shock waves. These are defined as the shock wave solutions where $h \geq 0$. The point where $h = 0$, $\bar{\eta} = 0$ is excluded only for $\Delta s < 0$. Consequently, the curve segments where $h \geq 0$ are M_f-type shock waves. It applies generally for this shock wave type, with the exception of the case when $h = 0$, that the field lines of the magnetic field are "broken off" by the shock wave normal. The quantity of the magnetic field behind the shock wave, $|\underline{H}_1|$, is always greater than it is in front of the shock wave, with the exception of $h = 0$. The transverse part of the magnetic field, $\underline{H}_{tr}$, retains its orientation. Currents are required in order to change the magnetic field. Their area current density according to the geometry shown in Figure 2 is

$$\underline{j}_F = -\frac{h\,|H_0|}{2\pi}\,\hat{z}$$

where $\hat{z}$ is the unit vector in the z-direction. In the case of the M_f-type shock waves the force $\underline{j} \times \underline{H}$ (since $\underline{H}$ is equal to $\underline{B}$) will cause a retardation of the velocity component u_n and an acceleration of u_y. This means that expansive shock waves of type $M_f(\bar{\eta} \leq 0)$ where the plasma on the average accelerates $(V_{n,1} \geq V_{n,0})$ must be accelerated by the pressure $P_0 - P_1$ if it applies that $h > 0$. This will result in $\bar{Y} < 0$ where $h > 0$ even in the case of weakly compressive shock waves. For instance, we can see in Figures 17 and 18 that the shock wave with $P_{\parallel}/P_{\perp} = 1000$ has a $\bar{Y} \geq 0$ only for $\bar{\eta} \geq 0.56$. $\bar{Y}$ in Figure 11 will become zero at a ratio $P_{\parallel}/P_{\perp} = 11.0$ only if it already applies that $\bar{\eta} = +0.53$ according to Figure 10.

The index f for "fast" applied to the M_f-type shock waves implies another important characteristic. In the case where $\bar{\eta} \geq -3/5\ \Delta s$ and $h \geq \max(-3/5\ \Delta s \sin\theta_0, 0)$ the velocity components $V_{n,1}$ and $V_{n,0}$ are greater than or at most equal to the associated generalized Alfvén wave velocities in the direction of $\underline{n}$, which is $\bar{b}_{n,1} = b_{n,1}$ and $\bar{b}_{n,0}$. In this sense they are fast. Consequently, we can see that even weakly expansive M_f-type shock waves can be fast when there is positive anisotropy. If we introduce the classical entropy condition in the form

$$\log\left(\frac{p_1}{p_0}\right)^{3/2}\left(\frac{\rho_0}{\rho_1}\right)^{5/2} \geq 0$$

and implement the boundary transition $\Delta s \to 0$, we will find in agreement with Bazer and Ericson [1958] that the velocity component $V_{n,0}$ of the M_f-type shock waves is greater than or at least equal to the velocity of fast magnetoacoustical waves in the $\underline{n}$-direction on the front side. Now, in the anisotropic case, we can state that the generally applicable entropy condition prefers large compression ratios $1 + \bar{\eta} = \rho_1/\rho_0$. Therefore, it is also meaningful from the point of the boundary case where $\Delta s \to 0$, that classification by velocities be made using the region $\bar{\eta} \geq -3/5\ \Delta s$ and not $\bar{\eta} < -3/5\ \Delta s$. Another characteristic is that the velocity jump $[u_n]$ can grow beyond all bounds ($\to -\infty$) only in the case of the M_f-type shock waves. /148

Moreover, the region $\bar{\eta} \geq -3/5\ \Delta s$ is interesting because it includes the shock waves which develop in the event of very strong to infinitely strong perturbations where the relative pressure jump $\bar{Y}$, the velocities $V_{n,1}$, $V_{n,0}$, $[u_n]$, and the magnitude $-[\hat{H}]$ can grow without bound. $\bar{Y} = \infty$, $V_{n,1} = \infty$, $V_{n,0} = \infty$, $[u_n] = -\infty$ and $-[\hat{H}] = \infty$ are reached when $\bar{\eta} = +3$, which also describes the maximum density jump of $\rho_1 - \rho_0 = 3\ \rho_0$ that can take place. $\bar{\eta} = +3$ corresponds to the known boundary value of $2/(\gamma - 1)$ for a medium where the ratio between the specific heat values in the rear of the shock wave is $\gamma = 5/3$. This boundary value of $\bar{\eta} = +3$ is independent of $\bar{\bar{s}}_0$, Δs and θ_0 because, in the case of infinitely strong shock waves, the flow energy of the plasma in front of the shock wave is infinitely great compared to the thermal energy and the magnetic field energy whose characteristics are reflected by this triplet of values. Since the ratio of thermal energy to flow energy in the rear of the shock wave tends toward a finite boundary value if $\bar{\eta} \to +3$, the characteristics of the

special interrelationship existing between pressure and energy are contained in the boundary value $\bar{\eta} = 2/(\gamma - 1)$.

On the other hand, the magnetic field in the rear of the shock wave remains finite. In the case where $\bar{\eta} \to +3$, it applies that $h \to 3 \sin \theta_0$. In that case, the definition used for h requires that $H_{y,1} = 4\, H_{y,0}$ applies to the transverse components of the magnetic field. Moreover, since $[H_n] = 0$, we encounter the greatest magnetic energy density ratio $\underline{H}_1^2/8\pi / \underline{H}_0^2/8\pi$ of 16 for infinitely strong shock waves in the case where $\theta_0 = 90°$, that is for transverse shock waves.

The change in the transverse velocity component where $\bar{\eta} \to +3$ will decrease continuously so that $[u_y] = 0$ applies to $\bar{\eta} = +3$. This is due to the fact that, where $\bar{\eta} \to +3$, the mass which must be accelerated per unit of time by the transverse component of the force $\underline{j} \times \underline{H}$ and of the anisotropy force, continues to increase so that $[u_y] \to 0$ applies to the velocity change. /149

The jump function branch which, in the case where $\bar{\eta} \to +3$, leads to $\bar{Y} \to +\infty$, $V_n \to \infty$, etc., can be seen from Figures 10 through 23 where it is shown for two different triplets of values and for the different step functions. We can observe a quite variable behavior. In the case where $\bar{\bar{s}}_0 = 1.0$ and $\theta_0 = 45°$ represented in Figures 10 through 16, $\bar{\eta}$, $\bar{Y}$, $V_{n,1}$, $V_{n,0}$ and $-[\hat{H}]$ increase, while $+[u_n]$, $|[u_y]|$ decrease monotonely with increasing h, starting from a certain value of h and ending at $h = 3 \sin \theta_0$. In Figures 17 through 23 where $\bar{\bar{s}}_0 = 0.5$ and $\theta_0 = 20°$, a value of $h_{max} = 1.25 > 3 \sin \theta_0 = 1.025$ is reached. From that point, $\bar{\eta}$, $\bar{Y}$, $V_{n,1}$, $V_{n,0}$ and $-[\hat{H}]$ increase, while $[u_n]$, $|[u_y]|$ decrease with decreasing h until finally, at point $h = 3 \sin \theta_0$, $+3$, $+\infty$, $+\infty$, $+\infty$, $+\infty$, as well as $-\infty$ and 0 are reached consecutively. These two cases characterize the difference between types $M_f^{(1)}$ and $M_f^{(2)}$ shock waves. In the case of the $M_f^{(1)}$-type shock waves, the slopes $d\bar{\eta}/dh$, $d\bar{Y}/dh$, $d/dh\,(V_{n,1}/b_{n,1})$, $d/dh\,(V_{n,0}/b_{n,0})$, $-d/dh\,[H]$ for $h = 3 \sin \theta_0$, $\bar{\eta} = +3$ are positive, while $d/dh\,([u_n]/b_{n,1})$ and $d/dh\,(|[u_y]|/b_{n,1})$ are negative. In the generally applicable case, these signs do not apply to all values of h along the curve branch. In the case of the $M_f^{(2)}$-type shock waves, the slopes at point $h = 3 \sin \theta_0$, $\bar{\eta} = +3$ have exactly the opposite signs. The boundaries of types $M_f^{(1)}$ and $M_f^{(2)}$ are represented for different angles by the dotted curves in Figure 6. This agrees with Figures 10 through 23, where

we can see that, in the case where $\bar{\bar{s}}_0 = 1.0$, $\theta_0 = 45°$, we are dealing with $M_f^{(1)}$-type shock waves, and where $\bar{\bar{s}}_0 = 0.5$, $\theta_0 = 20°$, with $M_f^{(2)}$-type shock waves. Moreover, we can see from Figure 6 that $M_f^{(2)}$-type shock waves can exist only where $\theta_0 \lesssim 39.2°$. Reduction of this angle will enlarge the permissible region in the Δs, $\bar{\bar{s}}_0$-plane. If θ_0 and $\bar{\bar{s}}_0$ are maintained constant, we can increase Δs to move from the $M_f^{(1)}$-region into the $M_f^{(2)}$-region, unless we reach the instability limit first, or unless $P_\perp = 0$. In any event, only $M_f^{(1)}$-type shock waves exist above $\bar{\bar{s}}_0 = 14/9$. In the case of very small values of $\bar{\bar{s}}_0$, we have $M_f^{(2)}$-type shock waves where $\theta_0 \lesssim 39.2°$, and $M_f^{(1)}$-type shock waves where $\theta_0 > 39.2°$. ∠150

In the case of the M_f-type shock waves, we studied in special detail the behavior where $\bar{\eta} \to +3$. Among other aspects there, we had $V_{n,0} \to +\infty$ and $V_{n,1} \to +\infty$. When there is positive anisotropy, another possibility for M_f-type shock waves to reach $V_{n,0} \to +\infty$ or $V_{n,1} \to +\infty$ exists. The only requirement is that $-2/3\ \Delta s/s_0 \cos^2 \theta_0 \geq -1$ be satisfied. In that case, where $h \to 0$ and $\bar{\eta} \to 0$, we obtain $\bar{Y} \to -2/3\ \Delta s/s_0 \cos^2\theta_0$, $[u_n] \to 0$, $[u_y] \to 0$ and $[\hat{H}] \to$ finite value. Moreover, a finite value is achieved by $\rho_0 V_{n,0}^2 - \rho_1 V_{n,1}^2$ with $-2/3\ \Delta s/s_0 \cos^2 \theta_0$. In the case where Δs is too small, the isotropy-producing processes will become too weak so that the formulas used here will lose their validity near $h = 0$, $\bar{\eta} = 0$. Here, in the vicinity of $h = 0$, we have shock waves that are expansive so that a pressure reduction results. In the case where $h \to 0$ and $\bar{\eta} \to 0$, respectively, only the pressure reduction and especially the isotropization remains. These waves are either located on the same curve branch as the infinitely strong shock waves (cf. Figures 17 through 23) or on a curve branch that will reach only small values of h (cf. Figures 10 through 16). Moreover, some of the curve branches can be absent because of $\bar{Y} < -1$. However, the transition between these two possibilities does not correspond to the transition from $M_f^{(1)}$-type to $M_f^{(2)}$-type shock waves. If we discuss the M_s-type shock waves, we will find a compressive counterpart to these shock waves which are predominantly anisotropy-destroying only.

In addition to the shock waves just described there can be other M_f-type shock waves, all of which are expansive so that $\bar{Y} < 0$. In the case of positive anisotropy these start at $h = 0$ and $\frac{\rho_1 - \rho_0}{\rho_0} = \bar{\eta} = -\frac{1}{5} \cdot \frac{\Delta s}{\bar{s}_0} \cdot \frac{\cos^2 \theta_0}{1 - \frac{1}{5} \Delta s}$. $\bar{\eta}$ decreases ∠151

monotonely after reaching some maximum. These shock waves do not exist under the conditions of the examples in Figures 10 through 23 where $\Delta s > 0$. They can exist in the presence of smaller positive anisotropy, as we can see from the curve segments where $P_{\parallel}/P_{\perp} = 1.0$ which start out from $h = 0$, $\bar{\eta} = 0$. Similar shock wave types can also exist in the presence of negative anisotropy, as in Figures 10 through 13. However, these begin at a point where $h = -3/5\ \Delta s \sin \theta_0$.

Examination of the magnitude $-[\hat{H}]$ shows that at least partial segments of all shock wave curves under consideration exist under the specific stipulations made for $-[\hat{H}]$. Consequently, all the compressive M_f-type shock waves with negative anisotropy shown in the examples in Figures 10 through 23 can exist. When there is positive anisotropy with $P_{\parallel}/P_{\perp} = 11.0$, the compressive shock waves with $\bar{\bar{s}}_0 = 1.0$, $\theta_0 = 45°$ can exist where $\bar{\eta} > +0.27$. All M_f-type shock waves are permissible in the case where $\bar{\bar{s}}_0 = 0.5$, $\theta_0 = 20°$ and $P_{\parallel}/P_{\perp} = 1000$, although $\bar{\eta}$ is sometimes located very close to -1. This is due to the extreme selection of $P_{\parallel}/P_{\perp}$.

3.3.3. M_s-Type Shock Waves

We now turn to the M_s-type shock waves. These represent the shock wave solutions where $h < 0$. In addition we shall also consider the shock wave where $h = 0$, $\bar{\eta} = 0$ as being an M_s-type shock wave.

The index s denotes "slow" and describes the characteristic of M_s-type shock waves that, in the case where $\bar{\eta} \geq -3/5\ \Delta s$, the shock waves are always slow in the sense of $V_{n,0} \leq \bar{b}_{n,0}$ and $V_{n,1} \leq \bar{b}_{n,1}$. Again, the region of compressive and expansive shock waves with $\bar{\eta} \geq -3/5\ \Delta s$ is used for classification instead of the region where $\bar{\eta} < 3/5\ \Delta s$ because it is preferred by the generalized entropy condition, as we can see from Figures 16 and 23. Another characteristic that justifies the designation slow is the limitation of the velocity jump $[u_n]$. This characteristic can be seen from Figures 14 and 21 for the examples where $\bar{\bar{s}}_0 = 1.0$, $\theta_0 = 45°$ and $\bar{\bar{s}}_0 = 0.5$, $\theta_0 = 20°$. /152

In the case of the M_s-type shock waves, $\bar{\eta}$, $\bar{Y}$, $[u_y]$, $-[\hat{H}]$ are limited, too. The maximum relative density jump is smaller than three.

$H_{y,1} \leq H_{y,0}$ applies because the M_s-type shock waves are defined by $h < 0$ with the one exception where $h = 0$. The definition of h according to the set

of defining Eqs. (32) means that $\left| \underline{H}_1 \right| \leq \left| \underline{H}_0 \right|$ in the region $-2 \sin \theta_0 \leq h \leq 0$. Again, the magnetic field increases when $h < -2 \sin \theta_0$. Using similar reasoning as used in the case of the M_f-type shock waves, we conclude from these circumstances that the velocity component u_n of compressive M_s-type shock waves with $-2 \sin \theta_0 \leq h \leq 0$ must be retarded by a positive $\bar{Y}$. Conversely, expansive M_s-type shock waves with $h < -2 \sin \theta_0$ must be accelerated by a negative $\bar{Y}$. In the case where $-2 \sin \theta_0 \leq h \leq 0$, the pressure change $P_1 - P_0 = 0$ occurs in the expansive region, and for $h < -2 \sin \theta_0$ in the compressive region. Moreover, where $\bar{\eta} = 0$ in the case of $h = -2 \sin \theta_0$, it applies that $\bar{Y} = 0$. One curve branch passes through this point when $\theta_0 = 45°$. Finally, we note that the case where $h = -\sin \theta_0$ corresponds to a switch-off shock wave which, consequently, is always an M_s-type shock wave.

What are the distinguishing features of the individual shock wave types, $M_s^{(1)}$, $M_s^{(2)}$, and $M_s^{(3)}$? First, we must reiterate that these three types are mutually exclusive. In the event that a situation existing in front of the shock wave and described by $\bar{\bar{s}}_0$, Δs, θ_0 satisfies the condition $\Delta s < (\Delta s)_{crit}$ for $M_s^{(3)}$-type shock waves, a shock wave without density change cannot exist except for $h = 0$. Consequently, the shock wave solutions $M_s^{(3)}$ do not permit any reduction of H_y without a density change or a change of $[u_n]$. This is in contradiction with the M_s-type shock waves in an isotropic plasma where $h = -2 \sin \theta_0$, $\bar{\eta} = 0$ is a solution. The $M_s^{(3)}$-states are located in the Δs, $\bar{\bar{s}}_0$-plane to the left of the vertical line which passes through the terminal point of the dot-dashed curve in Figure 6 which is designated by the θ_0-value in question. For instance, in the case of $\theta_0 = 20°$ and $\Delta s < -0.2$, we are dealing with $M_s^{(3)}$-type shock waves. The terminal points of the dot-dashed curves are connected by a solid line which coincides, within the scope of drawing accuracy, with the continuation of the dotted line designated 0° in the direction of negative Δs. Since $(\Delta s)_{crit} = -5/6$ applies where $\theta_0 \approx 42°$, $M_s^{(3)}$-type shock waves can exist only for $\theta_0 < 42°$. Examples of $M_s^{(3)}$-type shock waves are the solutions with $h < 0$ and $h = 0$, $\bar{\eta} = 0$ for $\bar{\bar{s}}_0 = 0.5$, $\theta_0 = 20°$ and $P_{\parallel}/P_{\perp} = 0.667$ that are represented in Figures 17 through 23. We can see two curve segments there. A characteristical feature is the closed curve. If we permit $\bar{\bar{s}}_0$ to grow from 0.5 on, maintaining θ_0 and Δs constant, the closed curve will shrink and will finally disappear.

153

If we continue to increase $\bar{\bar{s}}_0$, a new closed curve will grow from a point, and this curve will contain only expansive shock waves. This curve will grow in circumference until growing curve segments are cut off by the $\bar{\eta} = -1$ line and $\bar{Y} = -1$ line. The boundary lines in the Δs, $\bar{\bar{s}}_0$-plane which in the case of a certain θ_0 correspond to the situations where the closed curve degenerate into a point, are obtained from the equations

$$h^2 R = 0$$

and

$$\frac{d}{dh}(h^2 R) = 0$$

These boundary lines are curves opening to the left which reach their maximum $\Delta s = (\Delta s)_{crit}$ at the terminal points of the dot-dashed curves in Figure 6. Consequently, these terminal points on the solid line in Figure 6 correspond to the boundary cases of closed curves in the h, $\bar{\eta}$-plane which are points on the h-axis that have just stopped being $M_s^{(3)}$-type shock waves. Of course, the diagrams with the other step functions include corresponding isolated points, too. In the case where $\theta_0 = 0$, the boundary line in the Δs, $\bar{\bar{s}}_0$-plane can be stated simply as follows:

$$\Delta s = -\frac{15}{8}(1 - \bar{\bar{s}}_0)^2$$

The dotted boundary curves for Alfvén shock waves in Figure 9 are useful for the determination of the topology of the M_s-type shock waves and especially of the $M_s^{(3)}$-type shock waves. By way of example, we shall consider a shock wave with $\theta_0 = 20°$ whose Δs and $\bar{\bar{s}}_0$-values are located on the intersection between the Alfvén shock wave boundary curve and the straight line $\Delta s = (\Delta s)_{crit}$, which is at $\bar{\bar{s}}_0 = 0.76$ and $\Delta s = -0.19$. In this case a closed curve exists which is tangent to the h-axis $\bar{\eta} = 0$ and the straight line $\bar{\eta} = -3/5\,\Delta s = +0.115$.

If we permit $\bar{\bar{s}}_0$ to become smaller than $\bar{\bar{s}}_{0,T}$, maintaining $\Delta s < (\Delta s)_{crit}$, which means that we drop below the dotted curve in Figure 9 that is associated with the angle θ_0 in question, it can happen that the closed curve opens to the right and reaches the $\bar{\eta}$-axis at $h = 0$, $\bar{\eta} = 0$ and $h = 0$, $\bar{\eta} = \bar{\eta}_{02}$.

All M_s-type shock waves with negative anisotropy, and especially the $M_s^{(3)}$-type shock waves, are associated with a shock wave branch which begins at $h = 0$,

$\bar{\eta} = \bar{\eta}_{02} > 0$, $\bar{Y} = -\Delta s/s_0 \cos^2 \theta_0$, etc., on the edge of the M_f region, passes through a minimum in h, and reaches $h = 0$, $\bar{\eta} = 0$. In the case where $\bar{\bar{s}}_0 > \bar{\bar{s}}_{0,T}$, this branch is located in the h, $\bar{\eta}$-plane to the right of the tangent at $h = 0$, $\bar{\eta} = 0$. Upon passage to the limit $h \to 0$, $\bar{\eta} \to 0$, we obtain the compressive counterpart to the expansive shock waves described in conjunction with the M_f-type shock waves under positive anisotropy, which reach an infinite velocity where $h \to 0$, $\bar{\eta} \to 0$. The same formulas apply in both cases. In both instances, the significant effect of such a shock wave in the vicinity of $h = 0$ is the isotropization of the plasma and a pressure change of $\bar{Y} = -2/3 \Delta s/s_0 \cos^2 \theta_0 > 0$. In the case of excessively small values of $|\Delta s|$ near $h = 0$, $\bar{\eta} = 0$, the formulas used here will lose their validity again as isotropy is established in the rear of the shock wave.

We now turn to the $M_s^{(1)}$ and $M_s^{(2)}$-type shock waves which transform into the corresponding types of Bazer and Ericson [1958] when $\Delta s \to 0$. In the case of a triplet of values Δs, $\bar{\bar{s}}_0$, θ_0, which corresponds to an $M_s^{(1)}$-type or $M_s^{(2)}$-type shock wave, there are always two shock wave solutions which make $H_{y,1}$ smaller than $H_{y,0} > 0$ without density change. This is the significant difference between these and the $M_s^{(3)}$-type shock wave. In the case of negative anisotropy and $\bar{\bar{s}}_0 \geq \bar{\bar{s}}_{0,T}$, the shock wave solutions are not subject to density change and are located on a curve which would <u>always</u> be closed if we incorporate the curve segments where $\bar{Y} < -1$ and $\bar{\eta} < -1$. This curve contains a shock wave solution that corresponds to a maximum $|h|$ or minimum $h = h_{min}$. When this shock wave is compressive, we call it an $M_s^{(2)}$-type shock wave along with all other M_s-type shock waves associated with the same triplet of values Δs, $\bar{\bar{s}}_0$, θ_0. If this shock wave is expansive, the shock waves are called $M_s^{(1)}$-type shock waves. The boundary between the two types is represented by dot-dashed curves for each θ_0 in Figure 6. It is seen that $M_s^{(2)}$-type shock waves cannot exist above $\bar{\bar{s}}_0 = 1$. Moreover, $M_s^{(2)}$-type shock waves cannot exist above $50.8^\circ = \arcsin \sqrt{3/5}$. Figures 10 through 16 contain the step functions of $M_s^{(1)}$-type shock waves with $\bar{\bar{s}}_0 = 1.0$, $\theta_0 = 45^\circ$ as well as $P_{\parallel}/P_{\perp} = 0.6$, 1.0 and 11.0. Figures 17 through 23 contain two $M_s^{(2)}$-type shock waves with $\bar{\bar{s}}_0 = 0.5$, $\theta_0 = 20^\circ$, $P_{\parallel}/P_{\perp} = 1000.0$ and 1.0. It was already mentioned at the end of the description of the $M_s^{(3)}$-type shock waves that, in the presence of negative anisotropy and $\bar{\bar{s}}_0 \geq \bar{\bar{s}}_{0,T}$ there is always one shock wave branch which is located in the h, $\bar{\eta}$-plane to the

/156

right of the tangent placed through the zero point, reaches only small values of h, and contains a shock wave of infinite velocity when $h = 0$, $\bar{\eta} = 0$. This branch can merge into the closed curve when $\bar{\bar{s}}_0 < \bar{\bar{s}}_{0,T}$. In the case of positive anisotropy, and if we were to disregard the inequalities $\bar{\eta} \geq -1$ and $\bar{Y} \geq -1$, but took into consideration that $(h - \bar{\eta} \sin \theta_0)/\bar{h} \geq 0$, we would obtain a shock wave curve which starts at $h = -3/5 \cdot \Delta s \sin \theta_0$ and $\bar{\eta} = (\Delta s/10\bar{\bar{s}}_0)(6 - 3\Delta s \sin^2\theta_0 - 2\cos^2\theta_0)$ intersects the h-axis, passes through $h = -3/5\ \Delta s \sin \theta_0$, $\bar{\eta} = -3/5\ \Delta s$, and terminates at the $\bar{\eta}$-axis. Part of this curve is cut off as a result of the conditions $\bar{Y} \geq -1$, $\bar{\eta} \geq -1$, which can be seen from Figures 10 and 17.

Examination of the $-[\hat{H}]$ curves in Figure 16 will show that the $M_s^{(1)}$-type shock wave with $\theta_0 = 45°$, $\bar{\bar{s}}_0 = 1.0$ and $P_{\parallel}/P_{\perp} = 11.0$ is still permissible even far into the expansive region. The region of the $M_s^{(1)}$-type shock wave with negative anisotropy $P_{\parallel}/P_{\perp} = 0.6$ is constrained in comparison to the isotropic case. Almost all anisotropic shock wave solutions are permissible in the case where $\bar{\bar{s}}_0 = 0.5$, $\theta_0 = 20°$ $P_{\parallel}/P_{\perp} = 1000$.

Eq. 39 in addition to Figures 15 and 22 show that sign $[u_y]$ = sign $\bar{h}$ applies. Consequently, $\bar{h}$ determines the sign of the impulse change in the y-direction which the plasma undergoes upon passing through the shock wave region. The forces acting in the y-direction are the y-component of the current force $\underline{j} \times \underline{H}$ and the y-component of $-\nabla \cdot \underline{\underline{P}}$. /157

3.3.4. Shock Waves with Very Great and Very Small Values of $\bar{\bar{s}}_0$

We shall now discuss briefly the shock waves with greatly predominant thermal energy ($\bar{\bar{s}}_0 \gg 1$) and greatly predominant magnetic field energy ($\bar{\bar{s}}_0 \ll 1$).

In the case where $\bar{\bar{s}}_0 \gg 1$, the instability limits have the result that $P_{\parallel}/P_{\perp}$ is located within an interval about 1 which progressively narrow down Apart from fine details the dynamic behavior will be determined only by the particle pressure components and velocities. Consequently, we can expect that the dependence of $\bar{Y}$ (and of the velocities $V_{n,0}$ and $V_{n,1}$ of $\bar{\eta}$ that are referred to the sonic velocity $a_0 = \left(\frac{5}{3} p_0/\rho_0\right)^{1/2}$) on $\bar{\bar{s}}_0$ will decrease progressively as $\bar{\bar{s}}_0 \to \infty$. (Here we must usually consider the sonic velocity a_0 as being a numerical magnitude which describes the thermic velocities). In the case of a large value of $\bar{\bar{s}}_0$, these functions will differ only little from the corresponding functions for shock waves in gas dynamics where $\gamma = 5/3$.

We shall note down these functions $\bar{\Upsilon}(\bar{\eta})$, $V_{n,0}/a_0$, $V_{n,1}/a_1$ for shock waves in gas dynamics using $P_{\parallel}/P_{\perp} = 1$.

$$\bar{\Upsilon}(\bar{\eta}) = \frac{5}{3}\,\frac{\bar{\eta}}{1-\bar{\eta}/3} \tag{60a}$$

$$\frac{V_{n,0}^2}{a_0^2} = \frac{1+\bar{\eta}}{1-\bar{\eta}/3} \tag{60b}$$

$$\frac{V_{n,1}^2}{a_1^2} = \frac{1}{1+\frac{4}{3}\bar{\eta}} \tag{60c}$$

$$a_i^2 = \frac{5}{3}\,\frac{P_i}{\rho_i} \qquad i = 0,1 \qquad\qquad a_0^2 = s_0 b_{n,0}^2 \tag{60d}$$

/158

The behavior of a residual magnetic field will then be dominated primarily by the particles without having any appreciable reaction on particle motion.

Of course, as far as any measurements are concerned, the magnetic field is still an important indicator for the behavior of matter. Therefore, we shall consider briefly the behavior of the shock wave functions in their dependence on h under large values of $\bar{\bar{s}}_0$. In that case we have only $M_f^{(1)}$, $M_s^{(1)}$ and $M_s^{(3)}$-types of shock waves. In the case where $|b| \lesssim 3$, the shock wave curves in the h, $\bar{\eta}$-plane are located in the vicinity of $\bar{\eta} = h/\sin\theta_0$ and $\bar{\eta} = 0$. One shock wave curve starts out from $h = 3\sin\theta_0$, $\bar{\eta} = 3$, proceeds along the straight line $\bar{\eta} = h/\sin\theta_0$, and reaches a sharp minimum in h near negative $h(\Delta s < 0)$ or positive $h(\Delta s > 0)$ depending on the sign Δs.

In the case of negative anisotropy, the curve proceeds from $h = 0$, $\bar{\eta} = 0$, with a small value of $|\bar{\eta}| \ll 1$ and a shallow decline toward positive values of h. Moreover, another curve of slightly expansive shock waves proceeds with a weakly rising slope from the direction of negative h-values to a point where $h = h_{02}$, $\bar{\eta} = 0$, passes through a weak maximum, turns negative again with a shallow negative slope at point $h = h_{03}$, performs a downward bend, and proceeds approximately along the straight line $\bar{\eta} = h/\sin\theta_0$. This was the $M_s^{(1)}$ case. In the $M_s^{(3)}$ case, the maximum is still reached under very slight expansion. /159

In the case of positive anisotropy, there is also a curve which proceeds from negative n-values at a slight rise and slightly negative $\bar{\eta}$, becomes positive

at $h = h_{02}$, reaches a weak maximum, passes $h = 0$, $\bar{\bar{\eta}} = 0$ and a maximum in h, and turns downward again alongside $\bar{\bar{\eta}} = h/\sin\theta_0$.

It is important in the case of $\bar{\bar{s}}_0 \gg 1$ that fairly strong compressive shock waves are located near $\bar{\bar{\eta}} = h/\sin\theta_0$ where $h \gtrsim 0$. At best the M_s-type shock waves will reach very weakly positive $\bar{\bar{\eta}}$-values so that they will never be slow in the sense of $V_{n,1} < b_{n,1}$ in the presence of negative, fairly strong anisotropy. Large values of $|h|$ can be achieved only under very unrealistic stipulations with respect to the H-theorem in the inequality (33g).

The case where $\bar{\bar{s}}_0 \gg 1$ is interesting for still another reason. We had shown with the aid of Eq. (46) that, within the limits imposed by fire hose instability and reflection instability, $\bar{\bar{\eta}} = +3$ can be reached only where $h = 3\sin\theta_0$. This was one of the auxiliary theorems for the proof that $\bar{\bar{\eta}} = +3$ can be the maximum density change. If we limit the stability requirement and if the values of $\bar{\bar{s}}_0$ are large, density changes with $\bar{\bar{\eta}} > 3$ are possible as well. For instance, in the case where $\theta_0 = 90°$ and $\Delta s > 0$, this will be possible when $\bar{\bar{s}}_0 > 44$. The absolute minimum of Δs is 110, while the limit of fire hose instability is located near 5/3. In any event, the instability will be very great. However, it is still possible that the characteristic length $L_F \geq V_{n,0}/f_{ci}$ which is associated with the fire hose instability will satisfy the condition $L_S/L_F \ll 1$, where we made use of the fact that the fire hose instability is stabilized below the ion gyro frequency f_{ci} as a result of the effect of the finite gyro radius, /160 and that the growth constant of instability is $< f_{ci}$. The lower boundary of L_F depends only on $|\underline{H}|$. Using the value acquired from the measurements of Heppner et al. [1967] and Wolfe et al. [1968], $L_S \approx 1000\, V_A/\omega_{ci}$, and extrapolating the validity range toward large values of $\bar{\bar{s}}_0$, we will find $L_S/L_F \lesssim 1000(V_A\,\omega_{ci})/(\omega_{ci}\cdot V_{n,o}) = 1000\cdot V_A/V_{n,o}$. When the Alfvén Mach number is very great, L_S/L_F can become very small compared to one. In that case the plasma will be quasistable for the purpose of the theory implemented here, unless other types of instabilities become effective. It is admitted that the expressions L_F and L_S cited above are very rough approximations. However, they are used merely as illustrations for the physical concept that the instability limits are not absolute boundaries.

At the end of this section we shall discuss briefly the case where $\bar{\bar{s}}_0 \ll 1$. Since this will also imply $\Delta s \ll 1$, we can see immediately from Eq. (34) that $\bar{\bar{s}}_0$ and Δs can be disregarded, except for a small region about h = 0. This will also apply to Eqs.(36) through (39), if we merely keep in mind that

$$\frac{s_0 \bar{Y}}{5/3} = \frac{P_1 - P_0}{H_0^2/4\pi}$$

The disappearance of $\bar{\bar{s}}_0$ and Δs from Eqs. (34) through (39) is not surprising since only the magnetic field H_0 and the density ρ_0 have a decisive effect on the step functions if $\bar{\bar{s}}_0 \ll 1$. The shock wave solutions in the vicinity of h = 0 can be acquired easily from the discussions in Paras. 3.3.2. and 3.3.3. In particular, it applies again that the shock waves with infinite velocities but finite $\bar{Y}$ and $[u_y] = 0$ as well as $[u_n] = 0$ are possible where h = 0, $\bar{\eta} = 0$.

Consequently, the step functions for $\bar{\bar{s}}_0 \ll 1$ are independent of Δs, except in close proximity to h = 0. Yet the anisotropy can have a strong effect in that, based on the classical entropy condition and via the H-theorem according to inequation (33g), forbidden shock waves can be permissible and vice versa. /161

The discussion in this section has shown that the effect of anisotropy is generally small for both, large and small values of $\bar{\bar{s}}_0$. In fact, the effect of anisotropy is greatest in the vicinity of $\bar{\bar{s}}_0 = 1$ in the Δs, $\bar{\bar{s}}_0$-plane.

3.3.5. Some Supplementary Considerations on the Effect of Anisotropy

We have already seen the great effect of anisotropy on the shock wave functions in many instances in Chapter 3. A discussion of the behavior of these functions under constant θ_0 and $\bar{\bar{s}}_0$ and variable Δs would be of additional interest. However, we would again have to make a distinction between a large number of cases in order to make the discussion complete. Therefore, we shall be content with some special cases.

First, we consider $\frac{\partial h}{\partial \Delta s}$ under constant $\bar{\eta}$:

$$\left.\frac{\partial h}{\partial \Delta s}\right|_{\bar{\eta}} = - \frac{\left.\frac{\partial \bar{\eta}}{\partial \Delta s}\right|_h}{\left.\frac{\partial \bar{\eta}}{\partial h}\right|_{\Delta s}}$$

Moreover, the following relationship is obtained with Eq. (34):

$$\left.\frac{\partial h}{\partial \Delta s}\right|_{\bar{\eta}} = -\frac{2}{5}\sin\theta_0 \frac{\bar{\eta}^2 - \bar{\eta}\cos^2\theta_0 - h^2 - 2h\frac{\cos^2\theta_0}{\sin\theta_0}}{(2\bar{\eta}a + b)\left.\frac{\partial \bar{\eta}}{\partial h}\right|_{\Delta s}} \tag{61}$$

$$\left.\frac{\partial h}{\partial \Delta s}\right|_{\bar{\eta}} = 0, \text{ applies when} \tag{62}$$

$$\bar{\eta}^2 - \bar{\eta}\cos^2\theta_0 - h^2 - 2h\frac{\cos^2\theta_0}{\sin\theta_0} = 0$$

is satisfied. Eq. (62) describes a hyperbola in the h, $\bar{\eta}$-plane whose vertices are located near

$$\bar{\eta} = \frac{1}{2}\cos^2\theta_0$$

$$h = -\frac{\cos^2\theta_0}{\sin\theta_0} \pm \frac{\cos^2\theta_0}{\sin\theta_0}\sqrt{1 - \frac{1}{4}\sin^2\theta_0}$$

This hyperbola is very important. For, if we have found a curve point for a certain triplet of values θ_0, $\bar{\bar{s}}_0$, Δs which satisfies Eqs. (34) and (62) equally well, this curve point will satisfy Eq. (34) under any value of Δs with constant θ_0 and $\bar{\bar{s}}_0$. This is seen most easily from Eq. (34). Figures 10 and 17 contain several such points. First, the already known point $h = 0$, $\bar{\eta} = 0$ and the point $h = 3\sin\theta_0$, $\bar{\eta} = 3$ which corresponds to the case of the infinitely strong shock wave, are solutions of Eq. (34), independently of Δs and $\bar{\bar{s}}_0$. In Figure 10 another point which is independent of anisotropy is located near $h = -2\sin\theta_0$, $\bar{\eta} = 0$, or $h = -1.414$, $\bar{\eta} = 0$. If the curves were not limited by the condition that $\bar{Y} \geq -1$, we would have still another common point near $h \approx 0.55$, $\bar{\eta} \approx -0.9$. Still another point which is not dependent on anisotropy is located near $h \approx 0.17$ and $\bar{\eta} \approx -0.36$ in Figure 17.

Now, the question arises immediately whether there are also some compressive M_f type shock wave solutions with $0 < \bar{\eta} < 3$ where, for given $\bar{\eta}$, h is not dependent on Δs. It is easily seen from the general profile of $\bar{\eta}(h)$ where $\Delta s = 0$ and from the profile of the hyperbola according to Eq. (62) that, in the region where $h \geq 0$, $3 > \bar{\eta} > 0$, a point in the h, $\bar{\eta}$-plane which is independent

of anisotropy could never be possible. This circumstance, and the rise $\left.\frac{\partial\bar{\eta}}{\partial h}\right|_{\Delta s}$ at $h = 3 \sin\theta_0$, $\bar{\eta} = 3$, finally yield the following important statement. Let $\bar{\eta}_1(h)$ and $\bar{\eta}_2(h)$ be the compressive M_f-type shock waves in the h, $\bar{\eta}$-plane that are associated with the same θ_0 and $\bar{\bar{s}}_0$ but with different values of Δs, these being $(\Delta s)_1$ and $(\Delta s)_2$. In that case, $\bar{\eta}_1$ and $\bar{\eta}_2$ will proceed so that the two curves do not intersect in the region where $h \geq 0$ and $0 \leq \bar{\eta} < 3$, and that $\bar{\eta}_2$ with $(\Delta s)_2 > (\Delta s)_1$ is located near $h = 3 \sin\theta_0$, $\bar{\eta} = 3$ on the way toward lower values of $\bar{\eta}$, to the right of $\bar{\eta}_1$. Except for negative anisotropy, small angles θ_0 and not excessively great values of $\bar{\bar{s}}_0$, points with $\frac{\partial\bar{\eta}}{\partial h} = 0$ will not occur. In that case the above statement can be summarized into the inequality

$$\frac{\partial \bar{\ell}}{\partial \Delta s} > 0$$

where $\bar{\ell} \geq 0$ and $0 < \bar{\tau} < 3$

This characteristic can be seen in Figures 10 and 17. As Δs increases, the h associated with a constant $\bar{\eta}$ continues to grow.

The relationships for the other shock wave functions are not as simple as they are for $\bar{\eta}(h; \bar{\bar{s}}_0, \Delta s, \theta_0)$. It is seen from these examples that the above statement on $\bar{\eta}(h)$ is also valid for $\bar{Y}$, $V_{n,0}$ and $V_{n,1}$, provided that the shock waves are sufficiently strong.

4. Conclusion

/164

The shock wave relationships for an anisotropic plasma with magnetic field were derived for the nonrelativistic case in Chapters 2 and 3, and discussed in great detail. For this purpose, we started out by deriving the conservation equations via several stages from the basic equations by Klimontovich and Dupree. Some weak assumptions were made that establish the applicability range of the calculations within very wide limits.

Subsequently, we used the theories on the structure of shock waves in an anisotropic plasma, observations acquired from the earth's shock wave, and other physical considerations for an attempt to justify the assumption of the existence of an isotropic plasma in the rear of the shock wave region. This included considerations of a more general nature on the generalization of the classical

entropy condition. Finally, we derived the shock wave relations and discussed their implications under a variety of mathematical and physical aspects. We emphasize again, that it is not possible to make any quantitative statement as to the existence of the shock wave solutions which were discussed. Also, in the case of the classical magnetohydrodynamic shock waves the investigations of structure and stability sometimes took place considerably later than the investigations of the shock wave relations.

We shall now enumerate the most important results. We shall start with the commonalities existing between the classical hydromagnetic shock waves and the solutions discussed here.

1. The density cannot increase by more than a factor of four during a shock wave transition (cf. Para. 3.3.4.).

2. The magnetic field can change only by a finite quantity during a shock wave transition. /165

3. Except for the special case of the Alfvén shock waves where $(\rho_1 - \rho_0)/\rho_0 = (P_\perp - P_\parallel)/\frac{H_0^2}{4\pi}$ and $[u_y] \neq 0$, the transverse portions of the magnetic field in front of the shock wave and in its rear are collinear, meaning that the plane formed of the magnetic field vectors in front of the shock wave region and in its rear is oriented perpendicularly to the shock front. The normal component of the magnetic field does not change.

Apart from the fact that the jump functions are sometimes changed considerably as a result of anisotropy, we can next enumerate some especially important points.

4. The effect of anisotropy is strongest in the case of a plasma state in front of the shock wave where the magnetic energy density and the thermal energy density of the plasma have approximately the same order of magnitude.

5. When there is negative anisotropy of adequate strength, that is, where $\Delta s < (\Delta s)_{crit}$, accompanied by a low energy density of the magnetic field as compared to the thermal energy density of the plasma, there will be no compressive shock waves whose magnetic field decreases by a major amount (meaning that $h > -1/4$ applies where $\bar{\eta} > 0$).

6. The generalized entropy condition may also allow expansive shock waves, and this not only when the collisionless plasma in front of the shock wave is anisotropic.

7. A shock wave type is possible in the presence of anisotropy whose velocity can grow beyond all bounds, while the density jump, magnetic field jump, and pressure jump tend toward zero. This shock wave type is expansive under positive anisotropy and compressive under negative anisotropy (this type corresponds to a small neighborhood of $h = 0$, $\bar{\eta} = 0$). Its effect is primarily one of anisotropy destruction. /166

8. In the case of compressive shock waves associated with an increase of the magnetic field transverse component (meaning that $H_{y,1} > H_{y,0}$ or that $h > 0$), this increase cannot drop below a certain value if the anisotropy is positive. In the case of negative anisotropy, compressive shock waves with increasing transverse component of the magnetic field cannot exist below a minimum pressure jump which differs from zero.

At the present time, it is difficult to effect a comparison of the calculations with experimental results. This would require simultaneously acquired magnetic field and plasma measurements that cover all the important particle types and have such a high resolution that the anisotropy can be determined. The following Table 6 lists all the authors who have reported on plasma and magnetic field measurements acquired from the same shock wave transition in solar wind.

TABLE 6.

Authors and year of publication	Type of shock wave	Measured magnitudes
Sonett, et al., [1964]	Interplanetary shock wave	Magnetic field, ion energy spectra without directional resolution.
Van Allen and Ness, [1967]	Interplanetary shock wave	Magnetic field
Sugiura et al., [1968] (Original measurements by Lazarus and Binsack, [1968])		Numerical ion density and mass velocities are cited in the paper by Sugiura, et al.
Ness et al., [1966]	Earth's shock wave	Magnetic field
Wolfe et al., [1968]		Ion and electron measurements with approximate citation of the anisotropy for the ions.

/167

Moreover, there is a large number of observation data where, unfortunately, the magnetic field measurements and plasma measurements on both sides of the earth's shock wave were not acquired simultaneously. Finally, the paper by Gosling et al. [1968], contains plasma observations of interplanetary shock waves. However, even the measurements cited in Table 6 cannot be used for testing the shock wave relations. In the first cited instance, the measurements lack the directional resolution and the measurements of the electron distribution which should play a significant role, according to the observations by Montgomery [1968]. In the second instance, the complete measurements acquired by Lazarus and Binsack were not available when this thesis was being completed. The third cited case is the most advantageous under the circumstances. However, the condition that $L_S/L \ll 1$ is not satisfied for the earth's shock wave. Moreover, the error limits are very great, especially for the temperature measurements behind the shock wave, but also for the derivation of the ion pressure anisotropy in front of the earth's shock wave. In addition, there is a lack of information on the electron pressure anisotropy which is due to the great difficulties involved in measuring electron spectra in solar wind. It is true that we can make suitable stipulations on the electron pressure anisotropy in order to effect a comparison between theory and experiment which will yield

/168

better results than the classical theory on MHD shock waves. However, this is more due to the fact that we have an additional parameter available in the form of Δs which can be varied within the measuring limits in order to adapt the theory to the experiment. Therefore, the numerical computations associated with this comparison shall not be cited.

We conclude this discussion with the statement that we must wait for more exact plasma and magnetic field measurements before we can investigate the agreement between theory and experiment.

1. Abraham-Shrauner, B., "Propagation of Hydromagnetic Waves Through an Anisotropic Plasma," J. Plasma Physics, 1, 1967a, pp. 361-378.

2. Abraham-Shrauner, B., "Shock Jump Conditions for an Anisotropic Plasma," J. Plasma Physics, 1, 1967b, pp. 370-381.

3. Allen, J. A. van, Ness, N. F., "Observed Particle Effects of an Interplanetary Shock Wave on July 8, 1966," J. Geophys. Res., 72, 1967, pp. 935-942.

4. Anderson, J. E., Magnetohydrodynamic Shock Waves, The M.I.T. Press, Cambridge, Mass., 1963.

5. Argo, H. V., Asbridge, I. R., Bame, S. J., Hundhausen, A. J., Strong, I. B., "Observation of Solar Wind Plasma Characteristics Across the Bow Shock," J. Geophys. Res., 47, 1966, p. 142.

6. Asbridge, J. R., Bame, S. J., Felthauser, H. E., Strong, I. B., "Electrons in the Transition Region Between the Bow and Shock and the Magnetosphere," Trans. Am. Geophys. Union, 47, 1966, p. 142.

7. Asbridge, J. R., Bame, S. J., Strong, I. B., "Outward Flow of Protons from the Earth's Bow Shock," J. Geophys. Res., 73, 1968, pp. 5777-5782.

8. Auer, P. L., Hurwitz, H., Jr., Kilb, R. W., "Low Mach Number Magnetic Compression Waves in a Collision-Free Plasma," Phys. Fluids, 4, 1961, pp. 1105-1121.

9. Auer, P. L., Hurwitz, H., Jr., Kilb, R. W., "Large-Amplitude Magnetic Compression of a Collision-Free Plasma, II. Development of a Thermalized Plasma," Phys. Fluids, 5, 1962, pp. 298-316.

10. Barnes, A., "Collisionless Damping of Hydromagnetic Waves," Phys. Fluids, 9, 1966, pp. 1483-1495.

11. Bazer, J., Ericson, W. B., "Hydromagnetic Shocks," Ap. J., 129, 1958, pp. 758-785. /170

12. Camac, M., Kantrowitz, A. R., Litvak, M. M., Patrick, R. M., Petschek, H. E., "Shock Waves in Collision-Free Plasmas," Nucl. Fusion: 1962 Suppl., Part 2, pp. 423-445.

13. Chew, G. F., Goldberger, M. L., Low, F. E., "The Boltzmann Equation and the One-Fluid Hydromagnetic Equations in the Absence of Particle Collisions," Proc. Roy. Soc., A 245, 1956, pp. 112-118.

14. Colgate, S. A., Hartman, C. W.,"Collisionless Electrostatic Shocks," Phys. Fluids, 10, 1967, pp. 1288-1297.

15. Davis, L., Lüst, R., Schlüter, A., "The Structure of Hydromagnetic Shock Waves, I. Nonlinear Hydromagnetic Waves in a Cold Plasma," Z. Naturf., 13a, 1958, pp. 916-936.

16. Dupree, T. H., "Dynamics of Ionized Gases," Phys. Fluids, 4, 1961, pp. 696-702.

17. Dupree, T. H., "Kinetic Theory of Plasma and the Electromagnetic Field," Phys. Fluids, 6, 1963, pp. 1714-1729.

18. Eviatar, A., "The Role of Electrostatic Plasma Oscillations in Electron Scattering in the Earth's Outer Magnetosphere," J. Geophys. Res., 71, 1966, pp. 2715-2728.

19. Eviatar, A., "Scattering of Particles by Waves in the Presence of a Magnetic Field," J. Geophys. Res., 72, 1967, pp. 5997-6012.

20. Fishman, F. J., Kantrowitz, A. R., Petschek, H. E., "Magnetohydrodynamic Shock Wave in a Collision-Free Plasma," Rev. Mod. Phys., 32, 1960, pp. 959-966.

21. Fried, B. D., Gould, R. W., "Longitudinal Ion Oscillations in a Hot Plasma," Phys. Fluids, 4, 1961, pp. 139-147.

22. Gardner, C. S., Goertzel, H., Grad, H., Morawetz, C. S., Rose, M. H., Rubins, H., "Hydromagnetic Shock Waves in High Temperature Plasmas," IN: Proc. 2nd U.N. Intern. Conf. on Peaceful Uses of Atomic Energy, 31, 1958, pp. 230-237.

23. Gosling, J. T., Asbridge, J. R., Bame, S. J., Hundhausen, A. J., Strong, I. B., "Satellite Observations of Interplanetary Shock Waves, J. Geophys. Res., 73, 1968, pp. 43-50. /171

24. Greenstadt, E. W., Green, I. M., Inouye, G. T., Hundhausen, A. J., Bame, S. J., Strong, I. B., "Correlated Magnetic Field and Plasma Observations of the Earth's Bow Shock," J. Geophys. Res., 73, 1968, pp. 51-60.

25. Helfer, H. L.. "Magnetohydrodynamic Shock Waves," Astrophys. J., 117, 1953, p. 177.

26. Heppner, J. P., Sugiura, M., Skillman, T. L., Ledley, B. G., Campbell, M., "OGO- A Magnetic Field Observations," J. Geophys. Res., 72, 1967, pp. 5417-5472.

27. Hoffmann, F. De., Teller, E., "Magnetohydrodynamic Shocks," Phys. Rev., 80/2. 1950, pp. 692-703.

28. Holzer, R. E., McLeod, M. G., Smith, E. J., "Preliminary Results from the OGO-1 Search Coil Magnetometer: Boundary Positions and Magnetic Noise Spectra," J. Geophys. Res., 71, 1966, pp. 1481-1486.

29. Hundhausen, A. J., Asbridge, J. R., Bame, S. J., Strong, I. B., Vela Satellite Observations of Solar Winde Ions, Book of Abstracts: The Inter-Union Symposium on Solar-Terrestrial Physics, Belgrade, 1966, A 21.

30. Hundhausen, A. J., Asbridge, J. R., Bame, S. J., Gilbert, H. E., Strong, I. B., "Vela 3 Satellite Observations of Solar Wind Ions: A Preliminary Report," J. Geophys. Res., 72, 1967, pp. 87-100.

31. Hundhausen, A. J., Bame, S. J., Ness, N. F., "Solar Wind Thermal Anisotropies: Vela 3 and IMP 3," J. Geophys. Res., 72, 1967, pp. 5265-5274.

32. Joyce, G., Montgomery D., Roqué, C., "Deflection of Charged Particles by a Current-Carrying Plasma," Phys. Fluids, 10, 1967, pp. 2399-2404.

33. Kadomtsev, B. B., Plasma Turbulence, Academic Press, London-New York, 1965.

34. Kennel, C. F., Petschek, H. E., "Limit on Stably Trapped Particle Fluxes," J. Geophys. Res., 71, 1966, pp. 1-28.

35. Kennel, C. F., Engelmann, F., "Velocity Space Diffusion from Weak Plasma Turbulence in a Magnetic Field, Phys. Fluids, 9, 1966, pp. 2377-2388. /172

36. Kennel, C. F., Sagdeev, R. Z., "Collisionless Shock Waves in High β Plasmas," 1, J. Geophys. Res., 72, 1967, pp. 3303-3326.

37. Kennel, C. F., Sagdeev, R. Z., "Collisionless Shock Waves in High β Plasmas," 2, J. Geophys. Res., 72, 1967, pp. 3327-3342.

38. Klimontovich, I. u. L., "On the Method of Second Quantization in Phase Space," Sov. Phys. JEPT, 6, 1958, pp. 753-760.

39. Kovrijnykh, L. M., Contribution à la théorie de l'interaction non linéaire des ondes dans un plasma [Contribution to the Theory of Nonlinear Wave Interaction in a Plasma], S.T.G.I., EUR-CEA-FC, 1964.

40. Litvak, M. M., A Transport Equation for Magnetohydrodynamic Waves, Avco Everett Res. Lab. Report 92, 1960.

41. Lüst, R., "Magnetohydrodynamic Shock Waves in a Plasma of Infinite Conductivity," Z. Naturf., 8a, 1953, pp. 277-284.

42. Lynn, Y. M.,"Discontinuities in an Anisotropic Plasma," Phys. Fluids, 10, 1967, pp. 2278-2279.

43. McLeod, M. G., Holzer, R. E., Smith, E. J., "Spectra, Direction of Propagation, and Polarization of Waves in the Magnetosheath in the Frequency Range from 0.01 Hz to 140 Hz," Trans. Am. Geophys. Union, 49, 1968, p. 277.

44. Moiseev, S. S., Sagdeev, R. Z., "Collisionless Shock Waves in a Plasma in a Weak Magnetic Field, Plasma Phys. (J. Nucl. Energy, Part C), 5, 1963, pp. 43-47.

45. Montomery, M. D., Bame, S. J., Hundhausen, A. J., "Solar Wind Electrons: Vela 4 Measurements," J. Geophys. Res., 73, 1968, pp. 4999-5003.

46. Montgomery, D. C., Tidman, D. A., Plasma Kinetic Theory, McGraw Hill, New York, San Francisco, Toronto and London, 1964.

47. Morawetz, C. S., "Magnetohydrodynamic Shock Structure Without Collisions," Phys. Fluids, 4, 1961, pp. 988-1006.

48. Morawetz, C. S., "Modification for Magnetohydrodynamic Shock Structure Without Collisions," Phys. Fluids, 5, 1962, pp. 1447-1450. /173

49. Morton, K. W., "Finite Amplitude Compression Waves in a Collision-Free Plasma," Phys. Fluids, 7, 1964, pp. 1800-1815.

50. Ness, N. F., Scearce and Cantarano, S., "Preliminary Results from the Pioneer 6 Magnetic Field Experiment," J. Geophys. Res., 71, 1966, pp. 3305-3314.

51. Ness, N. F., Direct Measurements of Interplanetary Magnetic Field and Plasma, GSFC Report No. X-612-67-293, 1967.

52. Neugebauer, M., Snyder, C. W., "Mariner 2 Observations of the Solar Wind, 1, Average Properties," J. Geophys. Res., 71, 1966, pp. 4469-4484.

53. Olbert, S., Egidi, A., Moreno, G., Pai, L. G., "Summary of Fimal Results from the M.I.T. Plasma Experiment on IMP 1: (2) Average Properties in the Transition Region," Trans. Am. Geophys. Union, 48, 1967, p. 177.

54. Olson, J. V., McLeod, M. G., Holzer, R. E., Smith E. J., "High Frequency Magnetic Fluctuations Associated with the Earth's Bow Shock," Trans. Am. Geophys. Union, 49, 1968, p. 277.

55. Parker, E. N., "Dynamics of the Interplanetary Gas and Magnetic Fields," Astrophys. J., 128, 1958, pp. 664-676.

56. Parker, E. N., Coherent Electron Oscillations in Nonuniform Plasmas and Their Interaction with Electromagnetic Fields. IV. Shock Fronts. U. of Chicago. Enrico Fermi Inst. for Nucl. Stud. EF INS-59-1, 1959.

57. Parker, E. N., " A Quasilinear Model of Plasma Shock Structure in a Longitudinal Magnetic Field," J. Nucl. Energy, C, 2, 1961, pp. 146-153.

58. Parker, E. N., Interplanetary Dynamical Processes, Interscience Publishers, New York and London, 1963.

59. Rosenbluth, M., McDonald, W. M., Judd, D. L., "Fokker-Planck Equation for an Inverse-Square Force, Phys. Rev., 107/1, 1957, pp. 1-6.

60. Rossow, V., "Magnetic Compression of Collision-Free Plasmas with Charge-Separation, Phys. Fluids, 8, 1965, pp. 358-365. /174

61. Rossow, V., "Magnetic Compression Waves in Collisionless Plasma-Oblique Ambient Magnetic Field, Phys. Fluids, 10, 1967, pp. 1056-1062.

62. Sagdeev, R. Z., "Cooperative Phenomena and Shock Waves in Collisionless Plasmas," Rev. Plasma Phys., 4, 1966, pp. 23-91.

63. Scarf, F. L., Wolfe, J. H., Silva, R. W., "A Plasma Instability Associated with Thermal Anisotropies in the Solar Wind," J. Geophys. Res., 3, 1967, pp. 993-1006.

64. Shapiro, V. D., Shevchenko, V. I., "Quasilinear Theory of Instability of a Plasma with an Anisotropic Ion Velocity Distribution," Soviet Phys. JETP, 18, 1964, pp. 1109-1116.

65. Siscoe, G. L., Davis, L., Jr., Smith, E. J., Coleman, Jr., P. J., Jones, D.E., "Magnetic Fluctuations in the Magnetosheath Mariner 4," J. Geophys. Res., 72, 1967, pp. 1-18.

66. Smith, E. J., Holzer, R. E., McLeod, M., Russel, C. T., "Magnetic Noise in the Magnetosheath in the Frequency Range 3 - 300 Hz," J. Geophys. Res., 72, 1967, pp. 4803-4814.

67. Sonett, C. P.,Colburn, D. S., Davis, Jr., L., Smith, E. J., Coleman, Jr., P. J., "Evidence for a Collision-Free Magnetohydrodynamic Shock in Interplanetary Space," Phys. Rev. Letters, 13, 1964, pp. 153-156.

68. Sugiura, M., Skillman, T. L., Ledley, B. G., Heppner, J. P., "Propagation of Sudden Commencement of July 8, 1966, to the Magnetotail," J. Geophys. Res., 73, 1968, pp. 6699-6710.

69. Tidman, D. A., Eviatar, A., "Scattering of a Test-Particle by Enhanced Plasma Fluctuations," Phys. Fluids, 8, 1965, pp. 2059-2065.

70. Tidman, D. A., "Turbulent Shock Waves in Plasmas, " Phys. Fluids, 10, 1967a, pp. 547-564.

71. Tidman, D. A., "The Earth's Bow Shock Wave," J. Geophys. Res., 72, 1967b, pp. 1799-1808.

72. Tidman, D. A., Northrop, T. G., "Emission of Plasma Waves by the Earth's Bow Shock," J. Geophys Res., 73, 1968, pp. 1543-1554. /175

73. Tolman, R. C., The Principles of Statistical Mechanics, Oxford University Press, 1950.

74. Wolfe, J. H., Silva, R. W., McKibbin, D. D., Matson, R. H., "The Compositional, Anisotropic, and Nonradial Flow Characteristics of the Solar Wind," J. Geophys. Res., 71, 1966, pp. 3329-3336.

75. Wolfe, J. H., Silva, R. W., Myers, M. A., "Preliminary Results from the Ames Research Center Plasma Probe Observations of the Solar-Wind-Geomagnetic Field Interaction Region on IMP - II and OGO - I," Space Res., 6, 1966.

76. Wolfe, J. H., McKibbin, D. D., "Pioneer 6 Observations of a Steady-State Magnetosheath," Plan. Sp. Sci., 16, 1968, pp. 953-969.

"The aeronautical and space activities of the United States shall be conducted so as to contribute . . . to the expansion of human knowledge of phenomena in the atmosphere and space. The Administration shall provide for the widest practicable and appropriate dissemination of information concerning its activities and the results thereof."

— NATIONAL AERONAUTICS AND SPACE ACT OF 1958

NASA SCIENTIFIC AND TECHNICAL PUBLICATIONS

TECHNICAL REPORTS: Scientific and technical information considered important, complete, and a lasting contribution to existing knowledge.

TECHNICAL NOTES: Information less broad in scope but nevertheless of importance as a contribution to existing knowledge.

TECHNICAL MEMORANDUMS: Information receiving limited distribution because of preliminary data, security classification, or other reasons.

CONTRACTOR REPORTS: Scientific and technical information generated under a NASA contract or grant and considered an important contribution to existing knowledge.

TECHNICAL TRANSLATIONS: Information published in a foreign language considered to merit NASA distribution in English.

SPECIAL PUBLICATIONS: Information derived from or of value to NASA activities. Publications include conference proceedings, monographs, data compilations, handbooks, sourcebooks, and special bibliographies.

TECHNOLOGY UTILIZATION PUBLICATIONS: Information on technology used by NASA that may be of particular interest in commercial and other non-aerospace applications. Publications include Tech Briefs, Technology Utilization Reports and Technology Surveys.

Details on the availability of these publications may be obtained from:

SCIENTIFIC AND TECHNICAL INFORMATION OFFICE

NATIONAL AERONAUTICS AND SPACE ADMINISTRATION

Washington, D.C. 20546